Theses   Electronic Theses and Dissertations

2009

Polymeric Nanofibrous Media for Enhanced Ground Water Filtration

Bothaina Abdulla Al Shamsi

Follow this and additional works at: https://scholarworks.uaeu.ac.ae/all_theses

Part of the Environmental Sciences Commons

United Arab Emirates University

College of Science

M. Sc. Program in Environmental Sciences

POLYMERIC NANOFIBROUS MEDIA FOR ENHANCED

GROUND WATER FILTRATION

By

Bothaina Abdulla Al Shamsi

A thesis

Submitted to

United Arab Emirates University

In partial fulfillment of the requirements

For the Degree of M. Sc. in Environmental Sciences

2009

United Arab Emirates University

College of Science

M. Sc. Program in Environmental Science

POLYMERIC NANOFIBROUS MEDIA FOR ENHANCED GROUND WATER FILTRATION

By

Bothaina Abdulla Al Shamsi

A thesis

Submitted to

United Arab Emirates University

In partial fulfillment of the requirements

For the Degree of M. Sc. in Environmental Sciences

Supervisors

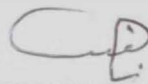| Dr. Yaser E. Greish	Dr. Mohammed A. Meetani	Dr. Eisa A. Al Matroushi
Assistant Professor	Assistant Professor	Assistant Professor
Department of Chemistry	Department of Chemistry	Department of Chemical
Faculty of Science	Faculty of Science	Engineering
UAE University	UAE University	Faculty of Engineering
		UAE University

2008-2009

The Thesis of **Bothaina Abdulla Al Shamsi** for the Degree of Master of Science in Environmental is approved.
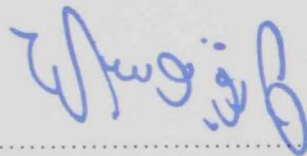
Examining Committee Member, **Dr. Yaser Afifi Greish**

Examining Committee Member, **Dr. Ashraf Al-Hinai**

Examining Committee Member, **Dr. Nayef Ghasem**

Program Director, **Dr. Tarek Youssef**

Acting Dean, College of Science, **Prof. Mohammed N. Anwar**

United Arab Emirates University
2008/2009

Acknowledgments

Abstract

Water is one of the bulk transportation media for transmission of particulate contaminants. These contaminants are complex mixtures of particles; most of them are usually smaller than 1000 μm in diameter. Chemical and biological aerosols (particulates) are frequently in the range of 1-10 μm. The particulate matters may carry some adsorbed gaseous contaminants. The removal of particulate and biological contaminants is thus an important step in water purification process. Particulate contaminants if not removed tend to foul reverse osmosis membranes and severely reduce the throughput of the final purification step. The filtration industry is looking for more efficient high performance filters for filtration of particles smaller than 0.3 μm and adsorbed toxic gases. Nanofibrous media have low basis weight, high permeability and small pore size that make the appropriate for a wide range of filtration applications. In addition, nanofiber membrane offers unique properties such as high surface area (ranging from 1-35 m^2/g depending on the diameter of fibers), good interconnectivity of pores and potential to incorporate active chemistry or functionality on nanoscale.

The current study investigated the formation of nanofibrous membranes, from a cellulose precursor; cellulose acetate, for water filtration. Membranes were prepared by an electrospinning technique that was based on the use of a high voltage power supply to force polymeric droplets to be sprayed in the form of fibers with different aspect ratios, depending on the process parameters. Different parameters affecting the structure, morphology and physical properties of the membranes were studied in details in order to optimize them. Characterization of the membranes was carried out at every stage of the

electrospinning process by infrared spectroscopy (IR) and scanning electron microscopy (SEM). Physical properties of the membranes such as density, porosity, BET surface area, pore size distribution, viscosity and surface tension were determined. Thermal treatment effects on the structure and morphology of the membranes were studied. Regeneration of cellulose was attempted by treatment of the membranes in alkaline media. Optimization of the alkali treatment process was also reached. Preliminary evaluation of the nanofibrous membranes for removing solid particulates from simulated solutions was also carried out. Filtration efficiency results were compared to those obtained with two commercially available membranes.

Results showed the possibility of obtaining nanofibrous membranes from solutions containing different concentrations of cellulose acetate, and showed a wide range of fiber and pore size distribution. Optimization of the electrospinning parameters led to the formation of highly porous membranes (with porosity approaching 94%) together with homogeneous fiber and pore size distributions. Structure instability was observed with the thermal treatment of these membranes and was found to be dependent on the membrane thickness. Treatment of the CA membranes in 0.5M NaOH solutions yielded a fully regenerated cellulose after 10 hours, without affecting the morphology of the nanofibers nor the pore size and its distribution. Efficiency of the nanofibrous membranes prepared in the current study showed superiority over the commercially available membranes.

Table of Contents

List of Tables

List of Figures

Figure 21: Fiber-size distribution obtained by an image analysis of the SEM micrographs of the CA nanofibrous membranes prepared from solutions containing A) 10, B) 12, C) 15, D) 17 and E) 20 wt % of CA in a solvent mixture of acetone and DMAc (2:1).

Figure 22: Viscosity curves of CA solutions as a function of shear rate.

Figure 23: Shear stress curves of CA solutions as a function of shear rate.

Figure 24: Effect of CA concentration on the surface tension of the prepared solutions.

Figure 25: SEM micrographs of CA nanofibrous membranes prepared from a 12 wt% solution, at a flow rate of A) 5, B) 10, C) 25, D) 50 and E) 100 mL/hr.

Figure 26: Fiber-size distribution obtained by an image analysis of the SEM micrographs of the CA nanofibrous membranes prepared from a 12 wt% solution, at a flow rate of A) 5, B) 10, C) 25, and D) 50. No fibers were observed in the sample prepared at a flow rate of 100 mL/hr.

Figure 27: SEM micrographs of CA nanofibrous membranes prepared from a 12 wt% solution, at a flow rate of A) 5, B) 10, C) 15, D) 20 and E) 25 mL/hr.

Figure 28: Fiber-size distribution obtained by an image analysis of the SEM micrographs of the CA nanofibrous membranes prepared from a 12 wt% solution, at a flow rate of A) 5, B) 10, C) 15, D) 20 and E) 25 mL/hr.

Figure 29: SEM micrographs of CA nanofibrous membranes prepared from a 12 wt% solution, at a flow rate of 5 mL/hr and a distance of A) 12, B) 14, C) 16, D) 18 and E) 20 cm from the collector.

Chapter I
Introduction

I. Introduction

I.1 Water Pollution:

Comprising over 70% of the Earth's surface, water is undoubtedly the most precious natural resource that exists on our planet. Without the seemingly invaluable compound comprised of hydrogen and oxygen, life on Earth would be non-existent: it is essential for everything on our planet to grow and prosper. Water is not only used by all creatures on earth in their routine daily life, but is also used in a wide range of industries. Water exists in oceans, seas, lakes, rivers, ..etc. All these water storage areas are, however, connected to each other through the natural water cycle that involves rain as well. Although we as humans recognize these facts, we disregard them by polluting our rivers, lakes, and oceans. Subsequently, we are slowly but surely harming our planet to the point where organisms are dying at a very alarming rate. In addition to innocent organisms dying off, our drinking water has become greatly affected as is our ability to use water for recreational purposes. In order to combat water pollution, we must understand the problems and become part of the solution [1].

Water pollution is a major problem in the global context. It has been suggested that it is the leading worldwide cause of deaths and diseases [2,3], and that it accounts for the deaths of more than 14,000 people daily [3]. In addition to the acute problems of water pollution in developing countries, industrialized countries continue to struggle with pollution problems as well. In the most recent national report on water quality in the United States, 45 % of assessed stream miles, 47 % of assessed lake acres, and 32 % of assessed bay and estuarine square miles were classified as polluted [4]. Water pollution occurs when a body of water is adversely affected due to the addition of large amounts of materials to the water. When it is unfit for its intended use, water is considered

2

polluted. Water pollution is also defined as "The alteration in composition or condition of surface water, either directly or indirectly as the result of the activities of man, which initiates the modification of ecological systems, hazards to human health and renders the stream less acceptable to downstream users" [5]. Two types of water pollutants exist; point source and nonpoint source. Point source pollution refers to contaminants that enter a waterway through a discrete conveyance, such as a pipe or ditch. Examples of sources in this category include discharges from a sewage treatment plant, a factory, or a city storm drain. The U.S. Clean Water Act (CWA) defines point source for regulatory enforcement purposes [6]. Non-point source (NPS) pollution refers to diffuse contamination that does not originate from a single discrete source. NPS pollution is often a cumulative effect of small amounts of contaminants gathered from a large area. Nutrient runoff in stormwater from "sheet flow" over an agricultural field or a forest are sometimes cited as examples of NPS pollution. Contaminated storm water washed off of parking lots, roads and highways, called urban runoff, is sometimes included under the category of NPS pollution. However, this runoff is typically channeled into storm drain systems and discharged through pipes to local surface waters, and is a point source. The CWA definition of point source was amended in 1987 to include municipal storm sewer systems, as well as industrial storm water, such as from construction sites [7]. Other sources of water pollution include agricultural runoff, urban runoff, construction runoff, mining runoff, septic systems, sewage treatment plants and industrial facilities [8]. Nonpoint sources are much more difficult to control. Pollution arising from nonpoint sources accounts for a majority of the contaminants in streams and lakes.

Pollution is also caused when silt and other suspended solids, such as soil, washoff plowed fields, construction and logging sites, urban areas, and eroded river banks when it rains. Under natural conditions, lakes, rivers, and other water bodies undergo

3

Eutrophication, an aging process that slowly fills in the water body with sediment and organic matter. When these sediments enter various bodies of water, fish respiration becomes impaired, plant productivity and water depth become reduced, and aquatic organisms and their environments become suffocated [1]. In UAE and similar countries where desert usually surrounds cities, sand pollution of both open and underground water is a common problem. Very fine sand particulates pollute water collected from wells and cannot be easily separated from water by traditional filtration systems. Sand Particulates with sub-micrometer (sub-μm) size usually pass through most common filters to drinking water, and is eventually settle and accumulate in certain body organs, causing health problems.

I.2 Water Purification:

Polluted water should be treated in a process called water purification. This process removes undesirable chemical and biological contaminants, both soluble and insoluble, from raw water. The aim of this process is to provide water that is fit for a specific purpose such as human consumption. The water purification methods can be categorized into two main areas; physical methods and chemical methods. Methods such as heat treatment, reverse osmosis, distillation, filtration and sedimentation are considered physical methods, while methods such as chlorination, coagulation/flocculation agents, ozonation and the use of electromagnetic radiation such as UV light, are classified as chemical methods. Heat treatment can be carried out by boiling water for a long period of time to purify it of all pathogens. After reaching a rolling boil, boiling is normally maintained for some time (about 5-10 minutes) in order to inactivate bacterial spores which can survive boiling. Reverse osmosis uses mechanical pressure that forces water to pass through a membrane that is impermeable to most contaminants. The water produced

by reverse osmosis lacks minerals and is close in purity to what is known as "distilled water". Therefore, minerals are normally added to this water in certain pre-calculated amounts to make it suitable for human consumption. The distillation process is another method of water purification, in which water is boiled to produce water vapor that is free of mostly physical contaminants. This water vapor is then allowed to condense on cool surfaces. The major disadvantage of this process is the inability to remove chemical contaminants, especially the soluble ones. These contaminants condense with the collected water. In the sedimentation process, the polluted water slowly enters a large tank, allowing solid contaminants (floc) to settle at the bottom. The filtration process is usually performed after separating most floc, and is considered the last step to remove remaining suspended particles and unsettled floc. However, the main disadvantage of this combined process is the inability to remove the dissolved substances in the water such as heavy metal ions and soluble organics. In the chlorination process, as a chemical method, chlorine is usually used to kill many harmful organisms. The disadvantage of using chlorine in this technique, however, is that it reacts with natural organic pollutants in water forming more harmful by-products such as trichloromethanes, which is a carcinogenic agent [5]. Coagulation/flocculation is another chemical method in which turbidity and color are removed from water to make it clear and colorless. In this process, a coagulant is used to collect all turbidity and color pollutants, causing them to precipitate in the form very small particles. After stirring, these small particles stick together and form bigger particles that can be removed by simple physical methods such as filtration. This process removes most of the suspended matter in water. A major result of removing particles using this method is that it reduces the levels of pathogens, that are usually shielded from chemical and thermal destruction by these solid particles [5]. In the ozonation process, ozone (O_3), which is a powerful disinfectant, is used because of its

5

toxic effect to most waterborne pathogens. Ozonation process is widely used in Europe to purify water. Using UV light in purifying water is a very effective way to kill pathogens if water is exposed to UV radiation for a long time. The efficiency of this technique depends on the water turbidity, where solid particulates are known to distract the incident UV radiation [5, 9, 10]

1.3 Water Filtration:

Filtration process is a common practice that is used in a large scale for the removal of solid particulate contaminants present in different types of waters. These contaminants are complex mixtures of particles; most of them are usually smaller than 1000 μm in diameter. Chemical and biological aerosols (particulates) are frequently in the range of 1-10 μm. Moreover, solid particulates may carry some adsorbed gaseous contaminants [11]. The removal of particulate and biological contaminants is thus an important step in water purification process. If not removed from water, these particulate contaminants tend to foul reverse osmosis membranes and severely reduce the throughput of the final purification step. Therefore, filtration is highly recommended as a pre-reverse osmosis step, and is an important step in the series of steps used for the purification of water in industry [11].

Commercially available filters are based on membranes or activated carbon beads. In the later type, activated carbon particles, or beads, are packed in a column, through which water passes. Filtration in this case is based on the separation of the solid particles by being trapped in the interstices created between the packed carbon beads. Moreover, being activated, these carbon beads provide the possibility of adsorbing bad odors and gasses from solution on their surfaces. The disadvantage of this type of filtration system,

6

however, is that the available porosity is still bigger than the possible wide range of tiny solid particulates and is thus limited to the separation of big particles only. In the membrane-type of filters, the physical and mechanical interlocking between the fibers making them provide networks or meshes with limited porosity to block solid particulates, hence separating them from aqueous media. The available porosity in this regard makes it more efficient than the activated carbon column filtration systems. Commercially available fibrous membranes are made of synthetic polymers such as polypropylene, Nylon, cellulose, and polystyrene. The common feature of all these fibrous membranes is their morphology in terms of the size of the fibers and the porosity provided for the filtration process as a result of the interlocking of these fibers. In most commercially available membranes, fibers are in the μm-mm range and the available porosity can thus filter certain size range of particles; usually above 100 μm. The filtration industry is looking for more efficient high performance filters for filtration of particles smaller than 100 μm [11]. Nanofibrous media have low basis weight, high permeability and small pore size that make it appropriate for a wide range of filtration applications. In addition, nanofiber membrane offers unique properties such as high surface area (ranging from 1-35 m^2/g depending on the diameter of fibers), good interconnectivity of the interstitial space, and above all, the nano-scaled fiber diameter which give rise to an increased surface area as compared with the conventional nonwoven filter media composed of currently available textile fibers with typical diameters of several microns [12].

1.4 Methods of making nanofibers:

Different techniques are used to make polymeric nanofibers. These include drawing [13], template synthesis [14], phase separation [15], melt fibrillation [16], island-

in-sea [17], gas jet [18], nanolithography [19], self-assembly [20] and electrospinning [21]. Each of these techniques has its own advantages and disadvantages. The usefulness of these techniques is limited by combinations of restricted material ranges, possible fiber assembly, cost, and production rate [22]. Electrospinning is considered by many researchers the most convenient of these techniques, to make polymeric nanofibers [23-28]. It has received a significant interest as a simple, versatile, very effective, and low-cost way to produce nanofibers. This technique was first studied by Zeleny in 1914 [29], was first patented by Formhals in 1934 [30], while the physics of the process was first studied by Taylor in 1964 [31]. Interest in this process was low for the following forty years and was then re-gained in the last decade. In this process, a high voltage power supply is used to charge polymer droplets that emerge from a nozzle [28]. Under the effect of the applied high voltage, droplets elongate, get stretched and accelerated towards a grounded collecting substrate [28]. Depending on the grounded geometry and mechanics of the grounded collector, woven or non-woven fibrous mats can be fabricated. Figure 1 shows schematics of two electrospinning setups in which woven and non-woven nanofibrous mats could be produced. As shown in both schematics, a typical electrospinning standard setup consists of four main components: a spinneret with metallic needle, high voltage power supply, syringe pump and grounded collecting plate (collector) [32-33]. In both types of setups shown in Figure 1, the alignments of the syringe with respect to the grounded collector can be vertical or horizontal. In the former setup, the ejected polymer stream is also influenced by an additional force; gravity [33]. Studies have shown, however, that this additional force does not influence the morphology nor the properties of the produced nanofibers. In fact, variables such as operating voltage, type of polymer, type of solvent, concentration of the polymer solution, flow rate, distance between needle tip and collector, needle gauge, and spinning

8
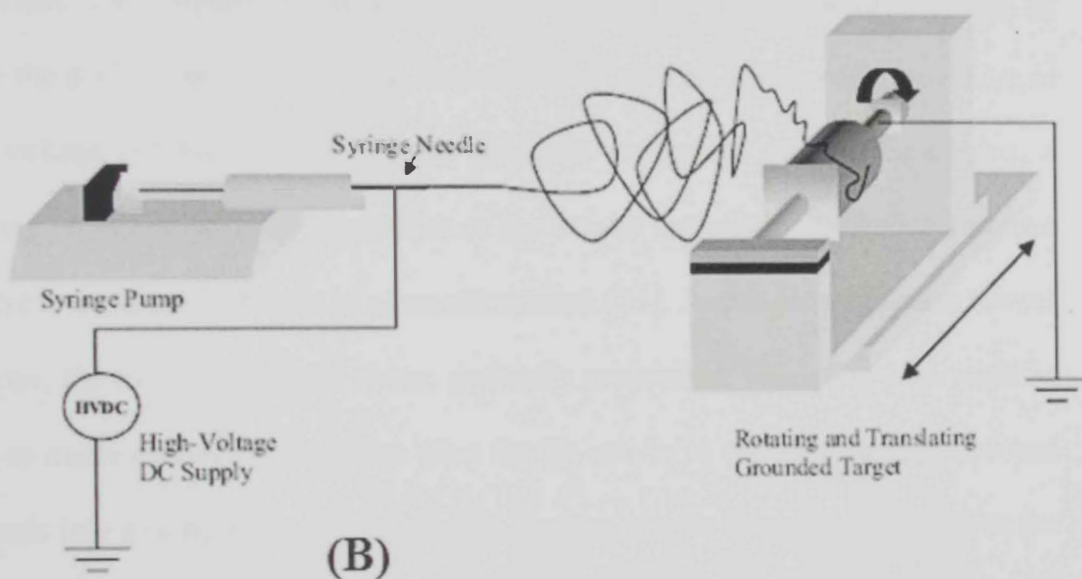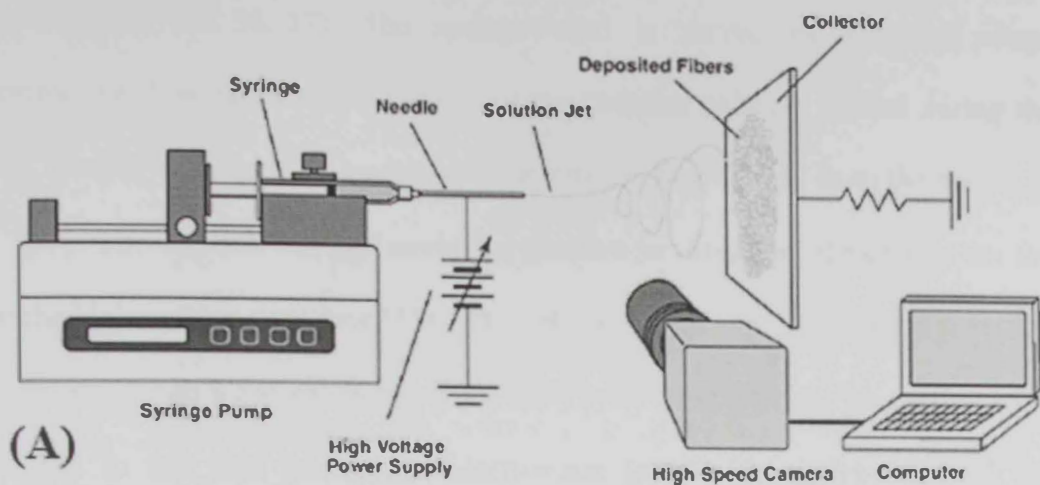
Figure 1. Schematic diagram of the electrospinning setup for the production of A: non-woven [32], and B: woven nanofibrous media [33]

atmosphere do indeed affect the morphology of the deposited fibers as well as the intra-fibrous porosity [27, 28, 36, 37]. The syringe used is driven by a syringe pump, which controls the flow rate and the volume of the polymer solution ejected during the experiment. The polymer solution loaded into a syringe is first ejected from the needle as a droplet [38]. The applied voltage could be positive or negative, depending on the polarity of the high voltage generator [38]. When this voltage is applied to the needle, the droplet is deformed into a conical shape called the Taylor cone after the pioneering work of Taylor [31]. In this case the applied electrostatic force is in equilibrium with the surface tension of the droplet. This cone is unstable and the charged jet seeks a path to the ground. Then, the polymer solution is charged to high voltage that is sufficient to overcome the surface tension forces of the polymer. When the electrostatic force (due to the high voltage potential of the polymer solution) overcomes the surface tension, a charged tiny jet is ejected from the surface of the droplet towards the grounded collector plate where it deposits randomly as a nanofiber mesh [31]. As the jet propagates toward the collector, the solvent in the jet stream gradually evaporates. This allows the jet to be stretched to nanometer-scale diameters (first the jet moves in a nearly straight line and then it bends into a complex path) and produce the non-woven fibers. Figure 2 shows the process of Taylor cone formation and the elongation of the charged polymeric stream afterwards. After the solvent evaporates solid nanofibers are left [40-43].

Electrospinning process has been investigated on polymer solutions [45-54] as well as polymer melts [55, 56]. In the later case, polymer is continuously heated to a temperature just above the melting temperature of the polymer in order to achieve and maintain the proper viscosity desired for spinning the polymer. Moreover, the distance
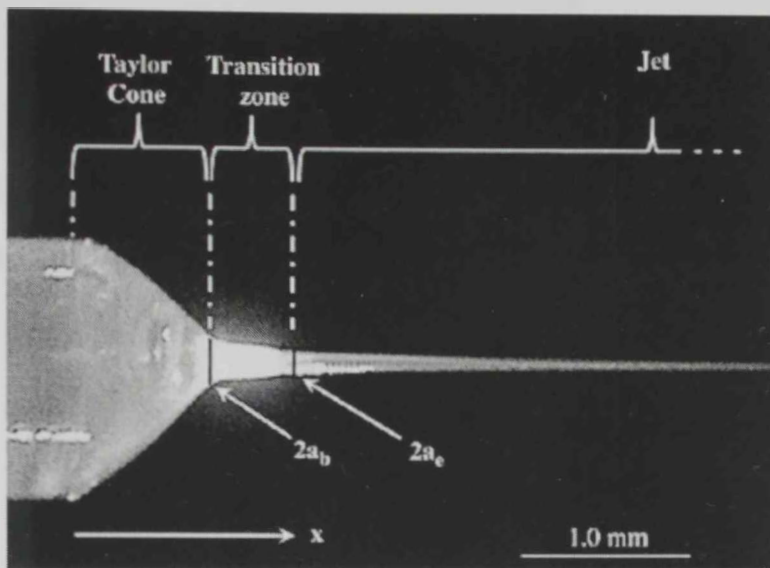
Figure 2. An actual photograph taken by a high speed camera showing the process
of Taylor cone formation and the stretching of the charged polymer
stream forming nanofibers [44]

between the needle that contains the molten polymer and the grounded collector is shorter and a higher voltage is used, for the spinning of molten polymers [57].

I.5 Applications of nanofibers:

Polymeric nanofibers produced by electrospinning have shown great potential for a wide range of applications in healthcare, biotechnology, environmental engineering, defense, security and energy generation [22, 50]. By having the ability to mass-produce nanofibers, electrospinning can become one of the most significant nanotechnologies of this century [22]. Electrospun fibers have shown potential applications in high performance air filters [58], protective textiles [59-61], sensors [62,63], advanced composites [64-66], photovoltaic cells [67], wound dressing [68,69] and as scaffolds in tissue engineering [70-74] and more recently as membranes in separation technology [75-80]. Electrospun polymeric nanofibers are either used as produced or further processed to other structural materials. As an example of the later case, pre-ceramic polymers containing silicon (Si) were successfully electrospun into nanofibers that were further thermally treated in reducing atmospheres, producing Silicon Carbide (SiC) nanofibers for a wide range of advanced structural applications [81]. Ultrasensitive chemiresistors were made of electrospun titanium oxide (TiO_2) nanofibers by loading oragno-Ti compounds onto a poly (vinyl acetate), which in turn was electrospun into fibers [82]. Controlled burning of these nanofibers yielded the TiO_2 chemiresistors [82]. Moreover, biodegradable polymeric solutions were pre-loaded with drugs and electrospun into nanofibers carrying these drugs [83-85]. These were used to deliver these drugs on a controlled basis to sites inside the human body where targeted treatment is required. On the other hand, and because of the similarity between the morphology of the non-woven nanofibrous mesh and the extracellular matrix (ECM), biocompatible nanofibrous

12

scaffolds were used in tissue engineering, specifically for the successful regeneration of bone and other hard tissues as well as other related tissue engineering applications [86, 87]. Electrospun nanofibers were also used in the fabrication of protective clothing for the safety of soldiers to capture and neutralize the chemical and biological warfare agents that are harmful for the soldiers without impedance of the air and water vapor permeability to the clothing [88-90]. Polymeric nanofibers have also been used for the production of a novel clean generation energy [45, 91-93].

I.5.1 Environmental applications of nanofibers:

In the field of environmental engineering, a high efficiency filtration is always required for an efficient air and liquid purification. It was estimated that the future filtration market would be up to US $700 billion by the year 2020 [94]. Nanofibrous media, especially those produced by electrospinning, have many properties which make them the best media for filtration applications [11]. They have been used as filters to filter moisture, dusts and bacteria. Some important properties make the nanofiber webs an excellent material for making filter media. These include high porosity, interconnectivity, microscale interstitial space and large surface-to-volume ratio in addition to high filtration efficiency and low air-blowing resistance [11, 39]. Especially designed affinity membranes with tailored surface chemistry that can capture specific target molecule (or ligates) on the membrane surface, have been studied. These permit the purification of molecules according to the physical/chemical properties or biological function in which they are different from the conventional filtration that depends on the molecular weight/size [94]. These affinity membranes were produced by chemically immobilizing certain chelating (capturing) agents (or ligands) onto the membrane nanofibrous surfaces [95-96]. These membranes have been used for the removal of organic waste heavy metal

pollutants from water. As an example, electrospun polyamide nanofibers on a sub-micron glass fiber substrate in order to provide the mechanical strength for the filter. The resulting modified filter showed an enhanced capability of capturing oil droplets with 210 nm diameter very effectively [97, 98]. Using a nanofibrous membrane for the remove of solid particles from air, Gibson et. al. proved that the nanofiber membrane was an extremely effective removal for the particles in the air with diameters ranging between 1 μm and 5 μm by physical trapping and adsorption [59, 99]. Similarly, Steffens et. al. successfully used a nanofibrous polyester filter to remove nano-sized aerosol particles [100]. A commercially available automobile air filter, called AMSOIL, is made of cellulose microfibers on which polymeric nanofibers were deposited via electrospinning, as shown in Figure 3A. This modified air filter is claimed to last for more than 100,000 miles due to its extraordinary properties and enhanced efficiency of air filtration to remove tiny particles in air [101]. Figure 3B shows a comparison between the unmodified filter versus the modified one in terms of their efficiency of air filtration. Gopal et. al. developed polysulfone nanofibrous pre-filters and used them for the removal of micro-particles from solution [102]. Their studies showed that these membranes were able to remove above 99% of 10, 8 and 7 μm particles without any permanent fouling [102]. Kaur et. al. used ligands immobilized on nanofibrous media for the removal of organic wastes, such as phenolphthalein, from water [103]. Similarly, Saeed et. al. chemically modified polyacrylonitrile (PAN) nanofibers and used them for the adsorption of metal ions from solutions [104]. Their studies showed the ability to adsorb Cu(II) and Pb(II) ions from aqueous media. Gopal *et al*. successfully produced polyvinylidene fluoride nanofibers in the form of non-woven membranes and were used for the separation of 1, 5 and 10 μm polystyrene particles from simulated aqueous media [102]. These membranes
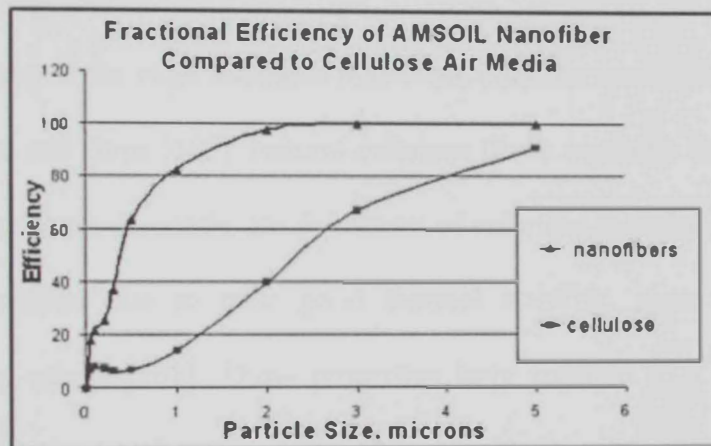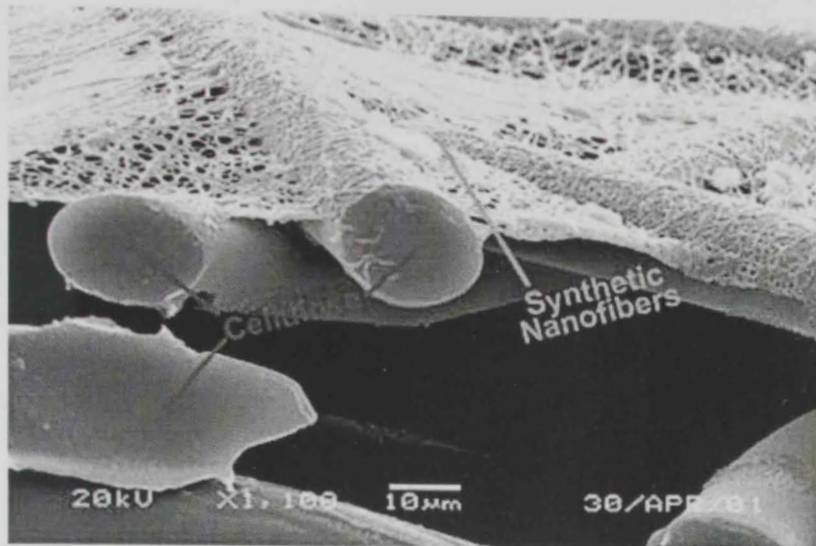
Figure 3. A. A scanning electron micrograph of an air filter modified by nanofibers; AMSOIL. B. A comparison between the efficiency of the unmodified to the modified air filters [101]

were found successful in rejecting more than 90% of the micro-particles from solution [102].

The above mentioned citations suggest that the use of nanofibers in making membranes for the filtration of air and water were found to dramatically enhance the filtration efficiency of these membranes for most types of pollutants. As well be mentioned in the objectives of the current study, nanofibrous filtration media made of cellulose will be tested for their efficiency for the removal of solid particulates from water compared to commercially available water filters.

I.6 Cellulose Nanofibers:

Cellulose is one of the most abundant renewable polymer resources, and has been widely used for fibers and films [105]. Natural cellulose fibers normally have dimensions within the micrometer scale. Recently, the formation of cellulose nanofibers has attracted a great deal of attention due to their good thermal stability, chemical resistance, biodegradability, and others [105]. These properties have resulted in a wide range of applications in affinity membranes, biosensors, chemosensors, protective cloths, reinforced nanocomposites, and others [105]. In addition, cellulose has been investigated for the manufacturing of filtration membranes [106]. The molecular structure of cellulose as a carbohydrate polymer, as shown in Figure 4, comprises of repeating β-D-glucopyranose units which are covalently linked through acetal functions between the OH group of the C_4 and C_1 carbon atoms (β-1,4-glucan) [107]. Cellulose is a large, linear-chain polymer with a large number of hydroxyl groups (three per anhydroglucose (AGU) unit) and present in the preferred $^4C_1$ conformation [107]. Cellulose has a ribbon shape which allows it to twist and bend in the direction out of the plane, so that the molecule is

16
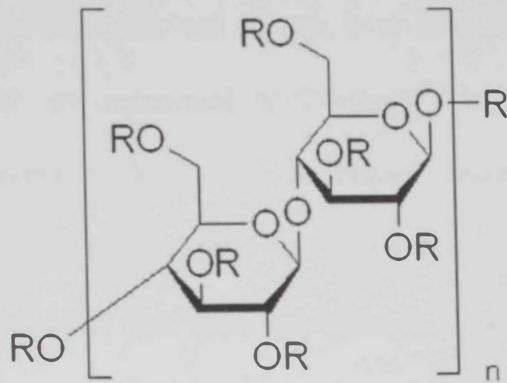
Figure 4. Chemical Structure of Cellulose (R=H) and Cellulose Acetate (R=AcO⁻)

moderately flexible. There is a relatively strong interaction between neighboring cellulose molecules in dry fibers due to the presence of the hydroxyl (–OH) groups, which stick out from the chain and form intermolecular hydrogen bonds [107]. Regenerated fibers from cellulose contain 250–500 repeating units per chain. This molecular structure gives cellulose its characteristic properties of hydrophilicity, chirality and degradability. Chemical reactivity is largely a function of the high donor reactivity of the OH groups [107]. Cellulose and its precursor; cellulose acetate, have been widely used for making nanofibrous membranes for environmental applications. The chemical structure of cellulose acetate is also shown in Figure 4. A limited number of researchers have investigated the electrospinning of cellulose due to its weak solubility in traditional solvents. Instead, cellulose acetate was used in different solvent systems to produces nanofibers, that were then converted to cellulose by de-acetylation.

Kim *et al* directly spun cellulose nanofibers from two different solvents mixtures: LiCl/DMAc and N-methyl morpholine oxide/water. The obtained nanofibers of 250-750 nm size range [108]. Moreover, Xu *et al* investigated the direct electrospinning of cellulose in a room temperature ionic liquid (1-allyl-3-methylimidazolium chloride (AMIMCl)), with the introduction of a co-solvent dimethyl sulfoxide (DMSO), found that it enhanced the spinnability of cellulose [109]. On the other hand, Ma *et al* [75], Lu *et al* [110], Zhang *et al* [111], and Ritcharoen *et al* [112] investigated the electrospinning of CA in a 2:1 acetone: DMAc solvent mixture at a maximum CA concentration of 15% by weight. Son *et al* obtained microfibrous CA membranes after electrospinning solutions containing a max of 12 wt% of CA in acetone and acetone/water solvent mixtures [113]. The obtained fibers had a size range of 2.25-3.23 mm. Liu *et al*, on the other hand, electrospun CA after dissolving it in a acetone, dimethylacetamide (DMAc), as well as

their miXture [107]. Using DMAc alone, only beads were formed. Using acetone as the sole solvent helped in the formation of a mixture of fiber and bead morphologies. Using a solvent mixture of acetone and DMAc (2:1 by weight) produced beads-free nanofibers, while nanofibers with smoother surfaces were produced when an acetone-DMAc mixture of 10:1 by volume was used [107]. Yoon *et al* produced CA nanofibers after electrospinning its solutions in methylene chloride/ethanol solvent (in different proportions) mixtures at a maximum concentration of CA of 5 wt % [114]. Han *et al* electrospun a 17 wt % CA in a mixed solvent of acetic acid and water (3:1), noticed an increase in the average diameter of the spun fibers with increasing the acetic acid content in the mixed solvent [106]. Tang *et al* made membranes with high visible light transmittance from a poly vinyl alcohol reinforced by CA nanofibers [115]. The later were made by electrospinning 20 wt % solutions of CA in a 2:1 acetone/DMAc solvent mixture. Taepaiboon *et al* made a vitamin-loaded electrospun CA mats to be used as transdermal and dermal therapeutic agents of vitamins A acid and vitamin E. He started with a 17 wt % CA solution in the same solvent mixture [83]. Ma *et al* made electrospun regenerated cellulose nanofibrous affinity membrane, then functionalized it with protein A/G for immunoglobulin (IgG) purification. The regenerated cellulose fibers were originally produced from the spinning of CA solutions in acetone/DMF/trifluoroethanol (3:1:1) solvent mixtures, followed by deacetylation in 0.1 M NaOH solution for 24 hours [116].

Nanofibrous composites containing CA and other polymers have been also investigated. Shukla *et al* electrospun hydroxypropyl cellulose fibers in two different solvents: anhydrous ethanol and 2-propanol. They used as a template to make SnO_2 fibers on microelectromechanical systems (MEMS) [117]. Zhang *et al* electrospun a mixture of

hydroxyethyl cellulose and polyacrylonitrile then cross-linked them using gluteraldehyde obtaining a highly hydrophilic nanofibrous network [118]. Zhang *et al* electrospun a 20 wt % binary mixture of CA and poly(ethylene oxide) in DMF or 1:1 DMF/dioxane mixture. They concluded that using dioxane improved the spinnability of the mixture compared to DMF as a sole solvent [119]. Chen *et al* electrospun a mixture of CA and polyethylene glycol and used the produced nanofibrous as a thermo-regulating composite. They first dissolved CA in a 2:1 acetone/DMAc solvent mixture then added the polyethylene glycol followed by spinning the produced mixture [120].

Based on the above citations, it is apparent that in absence of a proper solvent for cellulose, spinning of cellulose acetate is considered an acceptable pathway towards the formation of cellulose nanofibers. It is also apparent that the choice of a suitable solvent for the preparation of CA solutions to be electrospun is an important parameter that affects the characteristics of the produced nanofibers. Apart from the solvent effect, the concentration of the CA solutions as well as the other electrospinning parameters are also as important and effective towards the fabrication of nanofibrous membranes with characteristics that are superior to those of the available membranes.

Chapter II
Objectives

Chapter II. Objectives

The objectives of the current study were

1. To scan the literature for the previous research performed in the area of water purification using fibrous membranes, especially those based on nanofibers. A thorough literature review on cellulose was intended.

2. To optimize the electrospinning process parameters in order to prepare nanofibrous media with homogeneous fiber dimensions, homogeneous pore size distribution and interconnectivity of the pores.

3. To characterize the formed media in terms of its chemical composition, and morphology, in addition to their physical properties

4. To evaluate the prepared nanofibrous media by measuring their efficiencies for the filtration of simulated water samples containing different sizes of particulate materials compared to commercially available filters.

Chapter III
Materials and Methods

III. Materials and Methods

III.1 Materials:

Most of the materials utilized in the current study were purchased from Sigma-Aldrich, USA. Cellulose acetate (CA) contained 39.7 wt% as acetyl content with an average M_n ca of 50,000 (by GPC). Cellulose was obtained in the form of microcrystalline powder with an average particle size of 20 μm. Both cellulose and cellulose acetate were characterized by infrared spectroscopy (IR), differential scanning calorimetry (DSC), and scanning electron microscopy (SEM), to fully identify their structure and characteristics and ensure their phase purities. De-ionized water was made in the department of chemistry using Culligan deionizer, Bogolona, Italy. N,N-dimethyl acetamide (DMAc) was obtained as a ReagentPlus® with a min. assay of ≥ 99%. Ethyl alcohol was also obtained as an analytical reagent with a min. assay of 96%. Acetone was purchased from Merck, Darmstadt, Germany with a min. assay of ≥ 99.8%. Both sodium hydroxide and calcium phosphate (CaP) were also obtained from Sigma-Aldrich, USA in a powder form as A.C.S. reagents of 99+% min. assay. The particle size and particle size distribution of the CaP powder were measured by scanning electron microscopy (SEM).

III.2 Methods:

A solvent mixture containing acetone and DMAc with a volume ratio of 2:1 was prepared by stirring their respective volumes at room temperature for 1 hour. Solutions containing 10, 12, 15, 17 and 20 % of CA, as weight of CA per volume of the solvent mixture, were prepared by dissolving the appropriate amount of CA powder in the solvent mixture with warming at a temperature around 30-35°C. The viscosity of each of these solutions was measured. Solutions were kept in their beakers, completely sealed by a

parafilm and Aluminum foil to avoid evaporation of the solvents, until being used in electrospinning.

To carry out an electrospinning experiment, a 20 cc syringe was filled with 5 cc of a polymer solution, hocked onto the automatic syringe pump. The positive electrode of the high voltage power supply was connected to the tip of the stainless steel needle of the syringe. A 5 cm long needle with gauge 18 was used throughout the study. The high voltage power supply used in the current study produces a maximum of 40 kV, and was purchased from Gamma High Voltage Research, Florida, USA. The syringe-pump assembly was held vertically with the needle pointing downward. A flat square shape copper collector completely covered with aluminum foil was placed in front of the tip of the needle, and was grounded. The whole system was kept inside a home-made plexiglass box, with a 9 mm wall thickness, to avoid the effect of external air flow and changes in temperature around the system when it is in use. Figure 5 shows a photograph of the electrospinning assembly. The following parameters were studied:

1. Type of atmosphere within the plexiglass box in which electrospinning experiments were carried out.

2. Status of the grounded collector, whether fixed or moved in front of the fixed syringe.

3. Concentration of the cellulose acetate (CA): 10, 12, 15, 17 and 20 wt/vol in an acetone/DMAc solvent mixture (2:1 by volume)

4. Operating voltage, provided by the high voltage power supply: 12, 15, 18, 20, 22 kV

5. Flow rate, as controlled by the automatic syringe pump: 4 – 100 mL/hr

6. Distance between the tip of the needle and the grounded collector: 10-20 cm
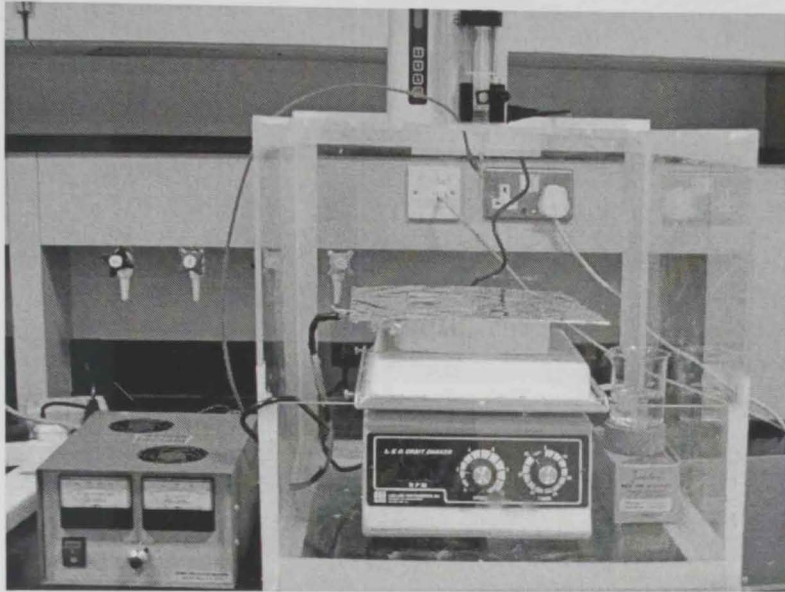
Figure 5. A photograph of the electrospinning setup used for making CA nanofibrous

membranes

At the end of every experiment, the fibrous mat collected on the Al foil was kept in the fuming hood at room temperature for 24 hours, to evaporate the remaining solvents. Each sheet was further dried at 80°C for another 24 hours to ensure the removal of all trapped solvents. The dried sheets were then characterized for their composition by infrared spectroscopy (IR), and morphology by scanning electron microscopy (SEM). Moreover, the BET surface area, porosity, pore size distribution and average pore volume characteristics were measured by nitrogen (N_2) adsorption. In addition, the average molecular weight of a selected membrane was measured by gel permeation chromatography (GPC). The apparent bulk density and % porosity of the dried electrospun membranes were determined using the following formulas [12]

$$Density(\rho) = \left(\frac{Mass(g)}{Volume(cm^3)} \right)$$

$$\%Porosity = \left(1 - \frac{\rho}{D} \right) x100$$

Where

      D: manufacturer's provided bulk density of cellulose acetate ($1.3\ g/cm^3$)
        or cellulose ($0.5\ g/cm^3$)

After optimizing the electrospinning parameters, selected membranes were used to study the effect of thermal treatment on their structure and morphology. Thermal studies were carried out by placing each CA fibrous sheet in a sandwich between square 3mm Teflon sheets, which in turn were heated in an oven for 1 hour at 150, 200 and 208°C. In a parallel experiment, selected membranes were placed in open Pyrex beakers and heated at the same temperatures for the same time periods. At the end of each thermal treatment, the heated membranes were taken to room temperature, and then analyzed for their structure and morphology using IR and SEM, respectively.

Regeneration of cellulose is known to take place in alkaline media, where the acetyl groups on the CA structure are replaced by hydroxyl groups. To study the process of cellulose regeneration, CA nanofibrous membranes made at the optimized electrospinning conditions were first weighed, on dry basis, then soaked in acetone/de-ionized water (1:1 by volume) mixtures for 24 hours. This is known to help in the swelling of the membranes, increasing the distance between the fibers, which is expected to facilitate the alkali treatment [12] A pre-calculated volume of a 0.5M solution of NaOH, in ethanol, was added to each membrane soaked in the acetone-water solutions. Membranes were removed from these alkaline solutions after 5, 10, 15, 20 and 24 hours, rinsed with fresh de-ionized water for more than 5 times, then dried until a constant weight. Each of the post-treatment alkaline solutions was titrated against 0.5M HCl solution to determine the exact volume of NaOH used in the de-acetylation of CA nanofibrous membranes. Completely dry CA membranes were then examined for their composition and morphology by IR and SEM techniques, respectively. BET surface area, porosity, pore size distribution and pore volume were also determined for those membranes alkali-treated for 24 hours.

Selected electrospun membranes were used in the filtration experiments using a simple filtration system, shown in Figure 6, that was connected to a vacuum pump operating at a maximum pressure of 4 bar. Two commercially available membranes were also evaluated for the sake of comparison with those prepared in the current study. The first commercial membrane was a microfibrous cellulose in the form of 10 cm x 10 cm square sheets with a thickness of 5 mm, and is usually used for filter press machines to remove clays and similar solid materials from water. The second commercial membranes
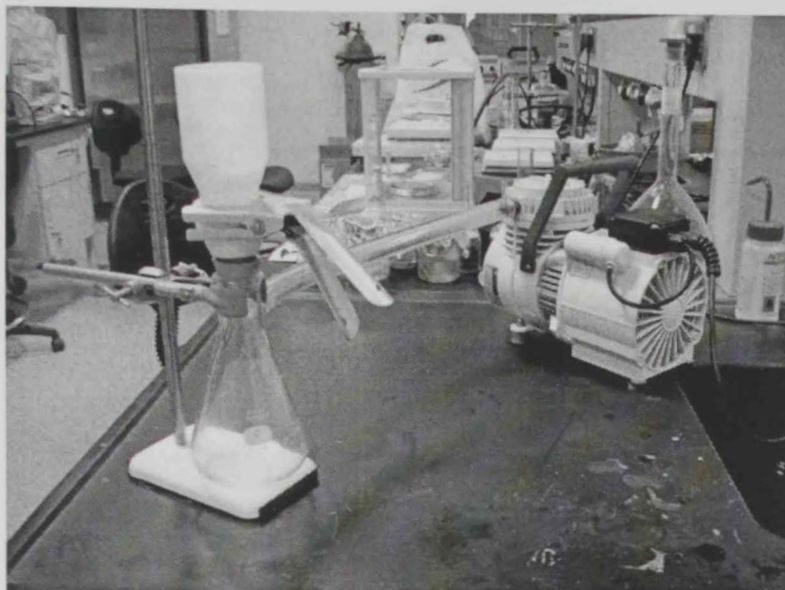
Figure 6. The filtration setup using for testing the commercial and prepared nanofibrous

membranes

was made of polypropylene microfibers, and is usually used for home filtration systems, in the form of a cylinder that is 20 cm long, with internal diameter of 7 cm and external diameter of 8.5 cm. This membrane was longitudinally sliced and flattened. Both commercial membranes were sliced to make filtration samples of 5 cm in diameter and 1-2 mm in thickness. The internal morphologies of both commercial membranes were investigated by SEM.

One type of solid particulate pollutant was used in the simulation of contaminated water solutions; calcium phosphate (CaP). This was selected because of its limited solubility in water ($K_{sp} = 6.8 \times 10^{-37}$). The morphology, particle size, and particle size distribution of CaP powder were investigated by SEM before suspending it in water. Simulated solutions containing 300 and 1000 ppm were prepared by suspending the proper amount of CaP in water and continuously stirred throughout the filtration experiments to maintain their homogeneity. Aqueous suspensions, 50 cc each, containing CaP solid particulates were carefully poured onto each of the commercial and prepared membranes until the whole amount of suspension was passed through the membranes. Around 5 cc of DI water was further used to confirm the transfer of all solid particulates from the stock suspensions through the membranes under investigation. The filtration efficiency of all membranes was investigated by measuring the change in the total calcium in the filtered suspensions relative to the unfiltered ones. In addition, completely dried membranes were investigated for their morphologies by SEM. The ability of these membranes to separate solid particulates from water was also confirmed by analyzing the trapped solid particulates by energy-dispersive X-ray analysis (EDX).

III.3 Characterization:

Different techniques were used throughout the current study to characterize the starting materials, nanofibrous membranes made at different electrospinning conditions, during the thermal and alkaline treatments and to follow up the filtration experiments.

Structural composition of the samples was followed by Fourier transform infrared spectroscopy using a Nicolet Nexus 470 spectrophotometer, USA. All samples were scanned over the normal range of 4000-400 cm^{-1} using a reflectance mode. A pre-weighed sample was mixed with a dry KBr and pressed at 10 tons forming a thin disk on which reflection of IR was recorded.

Molecular weights of the starting and as-spun CA samples were measured using gel permeation chromatography (GPC) (Agilent (Santa Clara, USA) (HP1200) apparatus connected to HPchem data acquisition system. The separation column was Agilent PLgel mixed-C 300 mm length, 7.5 internal diameter, and 5 μm packing particle size. Column temperature was 25 °C. Tetrahydrofuran (THF) was used as mobile phase at a flow rate 1.0 mL/min. isocratic elution was used over 15 minutes. Injection volume was 20 μL. Detection was obtained using refractive index detector and a UV detector at wavelength 254 nm. The GPC was pre-calibrated with 12 narrow Molecular weight distribution polystyrene standards over the molecular weight range of 162 g/mol to 5.0x 10^6 g/mol

The thermal characteristics of as received cellulose acetate and cellulose, as electrospun cellulose acetate and after the de-acetylation process, were measured using a differential scanning calorimeter (DSC 200F3–NETZSCH), Germany. Samples were heated at a rate of 20 °C/min for a maximum temperature of 270°C.

Morphologies of the nanofibrous membranes, as well as the CaP used to prepare the simulated waste water samples, were assessed using a Quanta inspect scanning electron microscope (SEM), The Netherland, operating at a maximum voltage of 20 kV. Uncoated samples morphologies were collected at both low and high vacuum modes; depending on the samples surfaces features and charging problems faced during the SEM sessions. The identification of solid particles trapped by the nanofibrous membranes, as a result of filtering them out from the simulated water solutions, was carried out using SEM together with energy dispersive X-ray spectroscopy (EDX).

Viscosities of all solutions were measured using a Rheometer, Anton Paar, Austria, while the interfacial tensions were determined using a ring tensiometer. All physical properties shown in Table 2 were measured at a room temperature ($25^{\circ}C$). Results were processed using a Rheolab plus software. For the purposes of this study, the shear-thinning behavior of CA as a non-Newtonian fluid was captured quantitatively by a power-law expression, while its elastic behavior was only characterized qualitatively by classifying the suspending fluid as weakly elastic, or highly elastic. The power law model used for the analysis is given by the following equation [121]:

$$\eta = m \, \dot{\gamma}^{\, n-1}$$

where η is viscosity in mPa.s,

$\dot{\gamma}$ is shear rate in s^{-1},

m is consistency index in mPa.s, and

n is flow behavior index.

BET surface area, porosity, pore size distribution and pore volume of the electrospun membranes, in the form of cellulose acetate and regenerated cellulose, were measured using nitrogen gas adsorption at 77 K employing a Quantochrome NOVA 1000 volumetric gas sorption instrument; Autosorb, USA. Dried membranes were cut into small pieces, around 1 cm in diameter, then filled into the glass tube attached to the instrument.

Analysis of the filtered solutions was carried out using an inductively coupled plasma-atomic emission spectroscopy (ICP-AES). Results were measured as ppm of total calcium concentration in these solutions.

Chapter IV
Results and Discussion

IV. Results and Discussion

IV.1 Characterization of cellulose acetate (CA):

Cellulose acetate obtained from Sigma-Aldrich was in the form of coarse elongated particles, with an average particle size of 300 μm, as determined from the analysis of its SEM micrograph in Figure 7. The as-received CA powder was further characterized by IR to confirm its chemical structure and purity. Figure 8 shows an infrared spectrum of as-received CA. Interpretation of the spectrum was carried out by comparing the positions at which different functional groups in the CA absorb with their corresponding data obtained from the literature [122], and is given in Table 1. All functional groups present in CA, such as C-C, C-H, and C-O-C, were observed in the IR spectrum of CA, confirming its chemical structure purity. The presence of the acetate groups in the structure of CA was confirmed by locating the acetyl carbonyl (C=O) group at 1760 cm^{-1}. Moreover, based on the information provided with the material, CA is supposed to contain 39.7 wt% as acetyl content. CA is also known as cellulose triacetate, considering substitution of the three hydroxyl (-OH) groups in cellulose by acetate. However, the uniformity of substitution, and the presence of this percentage of acetate groups in the structure of CA could not be confirmed by IR. The average number-based molecular weight (M_n) of CA provided with the material was 50,000 (by GPC). To confirm this information, GPC was used to measure the average molecular weight of the as-received CA. Figure 9 shows a GPC spectrum for the as-received CA using a UV and refractive detectors. Based on the data obtained from the spectra of both detectors, the calculated average molecular weight of the as-received CA was found to be 46,000, which is slightly lower than what was provided from the supplier.
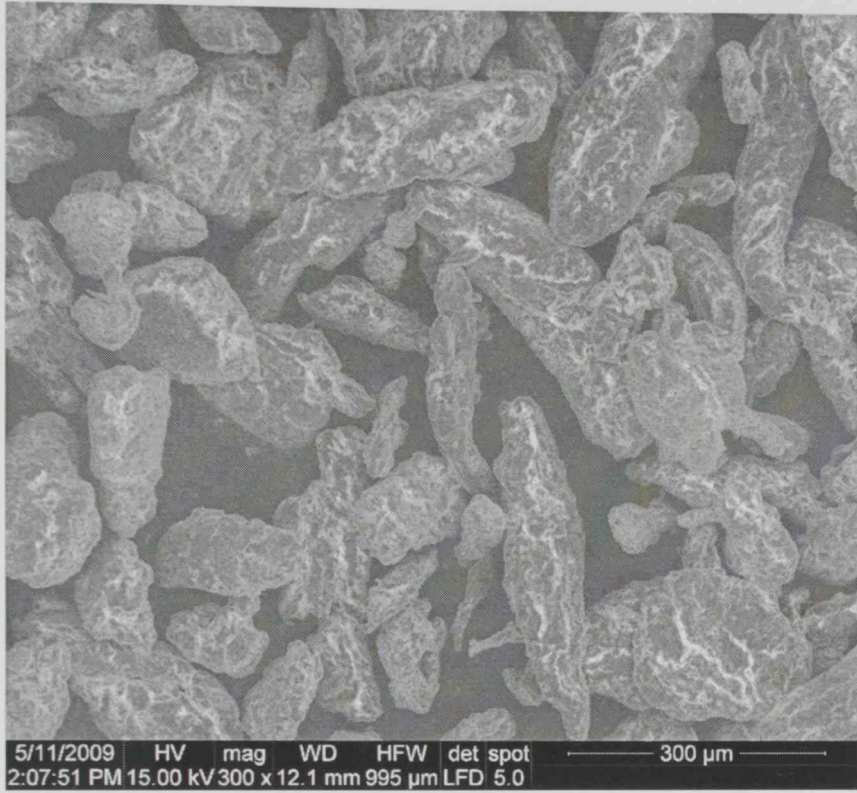
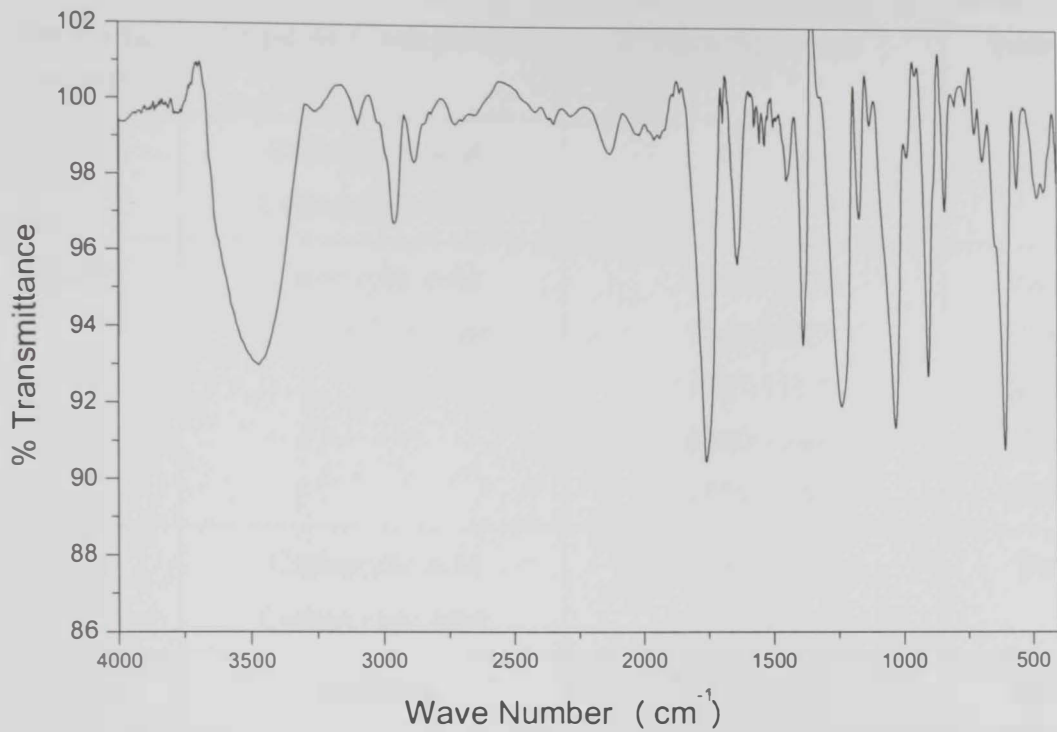Figure 7. SEM micrograph of as-received CA powder

Figure 8. Infrared spectrum of as-received CA powder

Table 1. Infrared absorption frequencies for the main functional groups in CA [122]

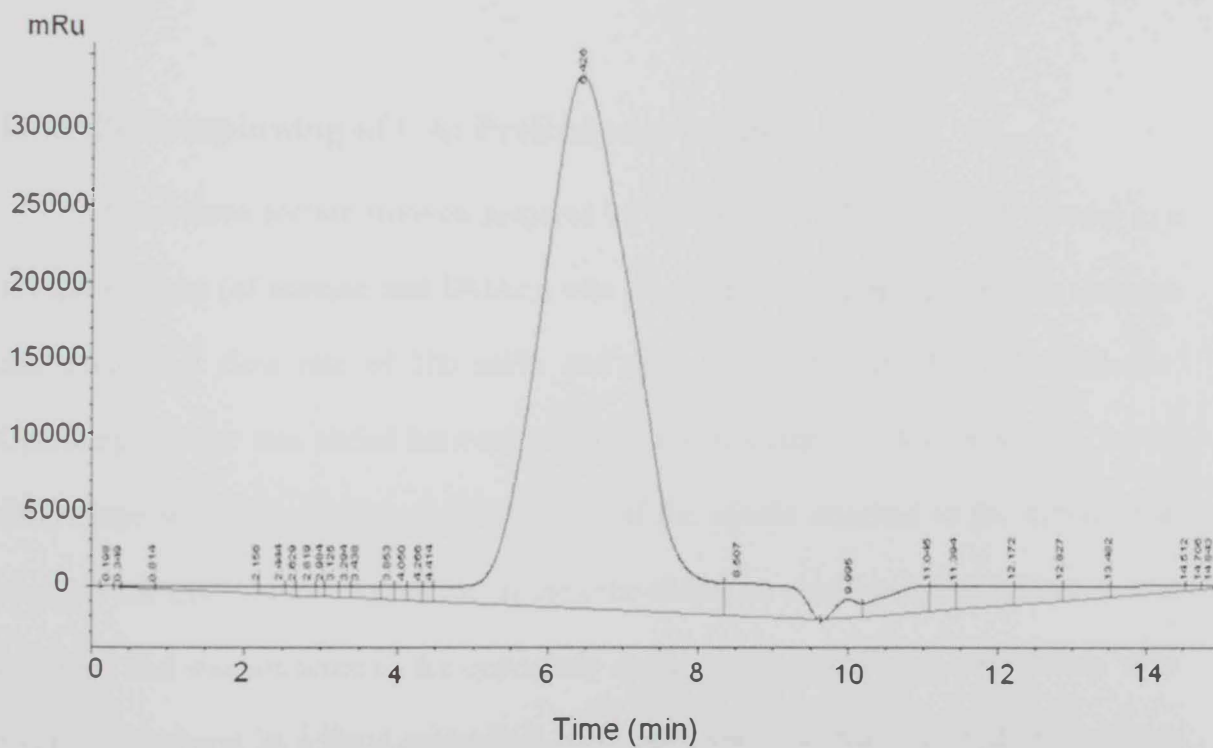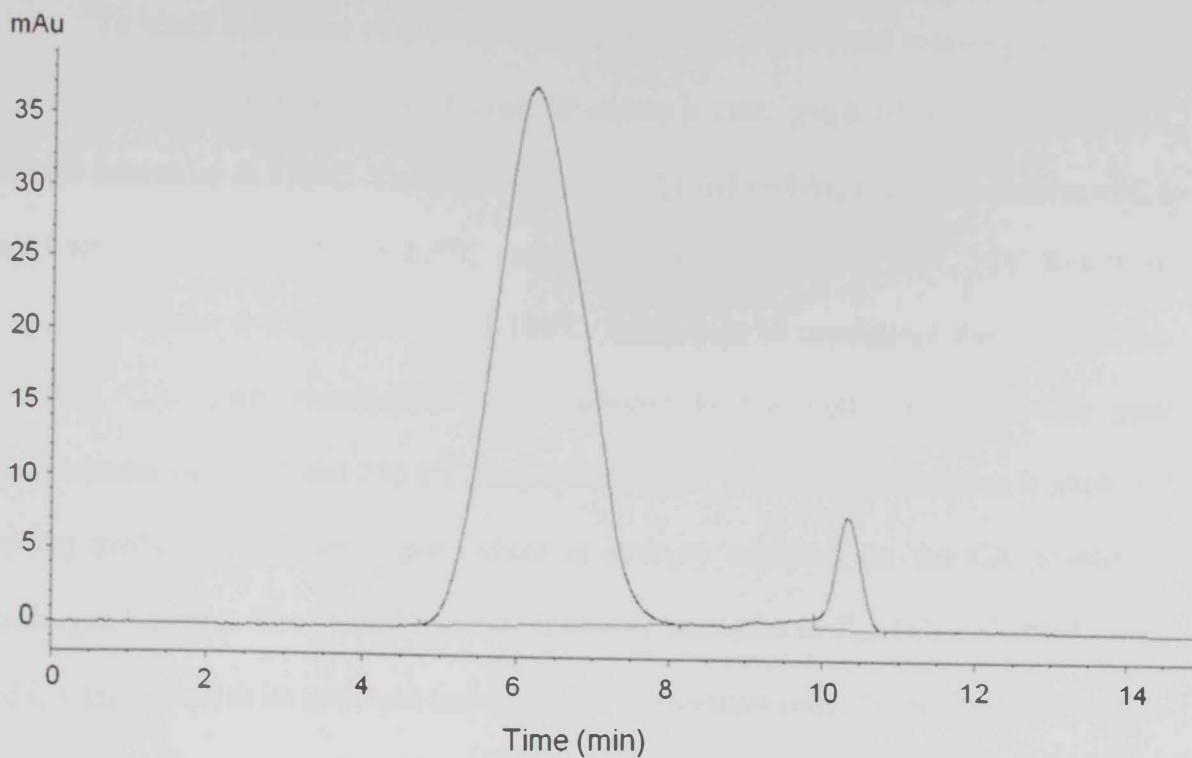| Functional Group	Type of Compound	Frequency (cm^{-1})	Intensity
C=O	Carboxylic acid Carboxylate ester	1730-1750	Strong
O-H	Carboxylic acid Carboxylate ester	3590-3650 3200-3650 1050-1150 1260-1340 1370-1440	Variable Variable Medium Medium Medium
C-O	Carboxylic acid Carboxylate ester	1050-1170 500-650	Strong
C-C	Aliphatic	1350-1400	Medium
C-H	Aliphatic	1350-1400 1360-1460 1425-1475 1000-1100 900-1000 800-900 700-800	Medium

Figure 9. GPC spectrum of as-received CA powder using A) a UV detector at
254 nm and B) a refractive index detector

To study the effect of thermal treatment of CA, differential scanning calorimetry (DSC) was used in this regard. Figure 10 shows a DSC graph of the as-received CA sample heated up to 270°C. The glass transition (T_g) and melting (T_m) temperatures of CA are known to be around 198-205°C and 224-230°C, respectively [107, 123] Results in Figure 10b show a transition around 180°C, which can be considered the T_g of the as-received CA. Two endotherms were observed in the DSC spectrum with peak temperatures of 107.2 and 236.1°C, respectively. The first broad endotherm is attributed to the evolution of water vapor, which is strongly adsorbed on the CA powder by hydrogen-bonding. The second endotherm may be attributed to T_m of CA. Thermal results of CA thus confirm its structure and suggest a temperature range for thermal treatment of CA to be within a range of >180 to < 236°C to avoid degradation of CA.

IV.2 Electrospinning of CA: Preliminary results:

A cellulose acetate solution prepared by dissolving a 17 wt% of CA powder in a solvent mixture (of acetone and DMAc), was electrospun at different operating voltages and a constant flow rate of 100 ml/hr and at a 15 cm distance from the collector. Operating voltage was varied between 10 to 20 kV at a step of 2 kV. A normal Taylor cone-shape was visually observed at the tip of the needle attached to the syringe that contains the CA solution. At the end of the cone-shape, an elastic polymeric filament was observed and was attracted to the oppositely charged collector. These observations were found normal and in a good agreement with the known mechanism of electrospinning [31]. The direction of the polymer stream was perpendicular to the grounded collector at low operating voltages. Despite the formation of non-woven fibrous deposits on the grounded collector at all operating voltages, a deflection in the direction of the stream was observed when the operating voltage was increased up to 20 kV. Figure 11 shows the

extent of this deflection with voltage. It was observed that this deflection was in the direction of approaching the edges of the grounded collector, which is known to have the highest opposite charge to that on the polymer stream. A maximum attraction is thus expected as the charge on the polymer stream was increased by increasing the operating voltage. The increase in the operating voltage is known to draw more fluid from the polymer solution reservoir, and to decrease the velocity of the deposition, causing a deflection in the pathway to occur [124]. Moreover, increasing the applied voltage causes the transiently charged fibers to carry a larger charge density, increasing the width of the deposition path, and an overall deflection from a normal perpendicular deposition of the polymer steam [124]. Based on these results, an optimum operating voltage of 12 kV was chosen to be applied throughout the electrospinning experiments of CA.

Using this voltage, a solution containing 17 wt% of CA was electrospun at a flow rate of 100 ml/hr at a tip-collector distance of 15cm. Figure 12 shows scanning electron micrographs of the collected non-woven fibers at different magnifications. The randomness of the fibers distribution is a main characteristic of fibers made by electrospinning [31]. This results in an interlocking between the fibers, creating interconnected porosities with different dimensions. Despite its random depositions, the overall distribution of the fibers is still homogeneous, and is thus expected to result in a homogeneous pore size distribution as well, as shown in Figure 12A. In addition to the high surface area of these electrospun fibers, another advantage is the possibility of forming interconnected pores similar to those observed in Figure 12A. The fiber size distribution, as calculated from the micrograph in Figure 12 C, is shown in Figure 13. It is evident that most of the formed fibers were sub-micron in diameter, while around 25% of the fibers were slightly above one micron in diameter.
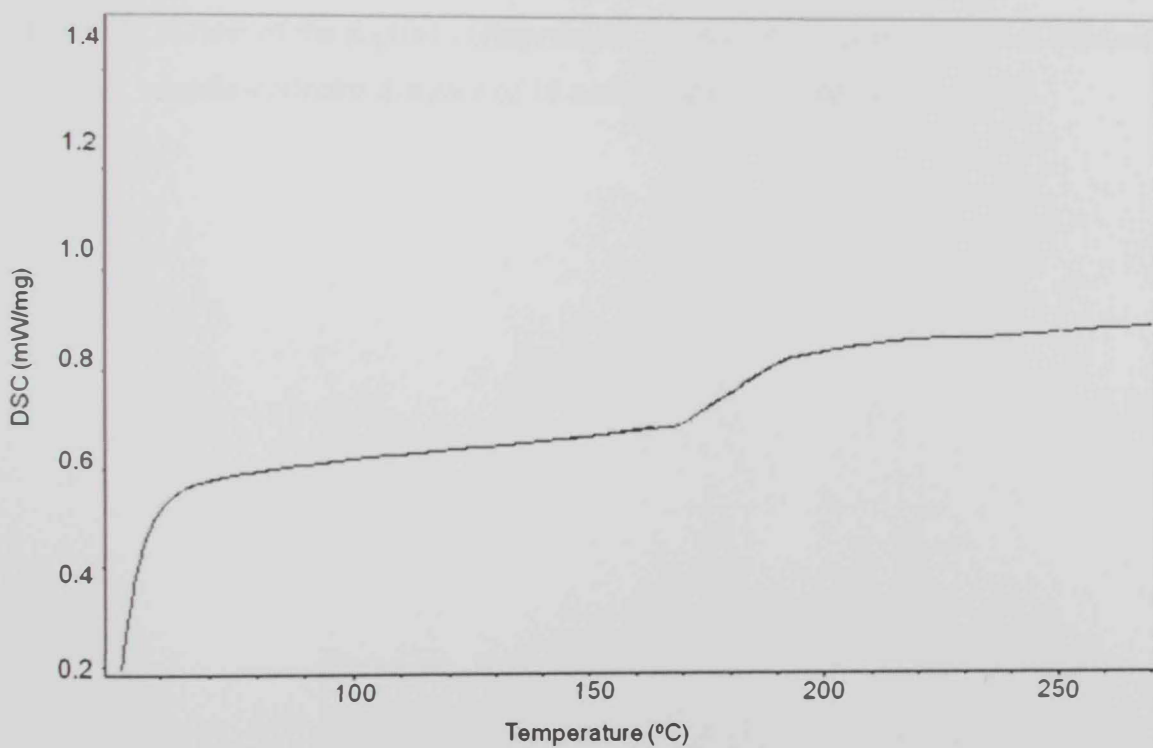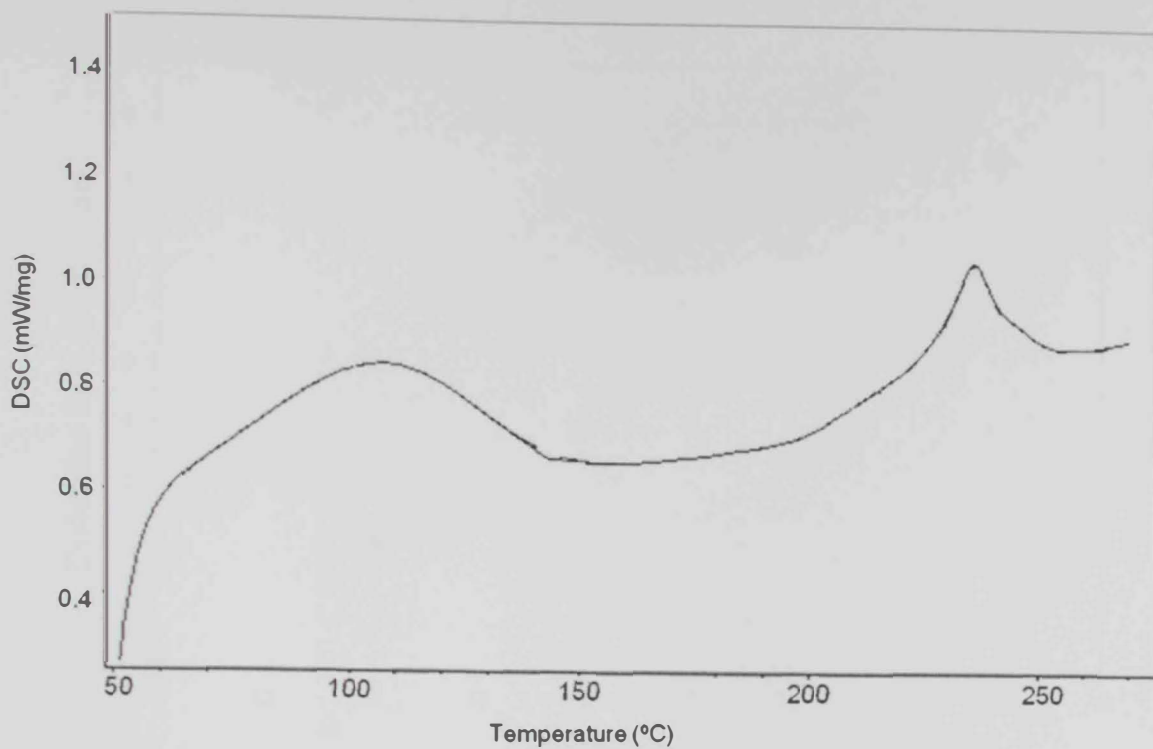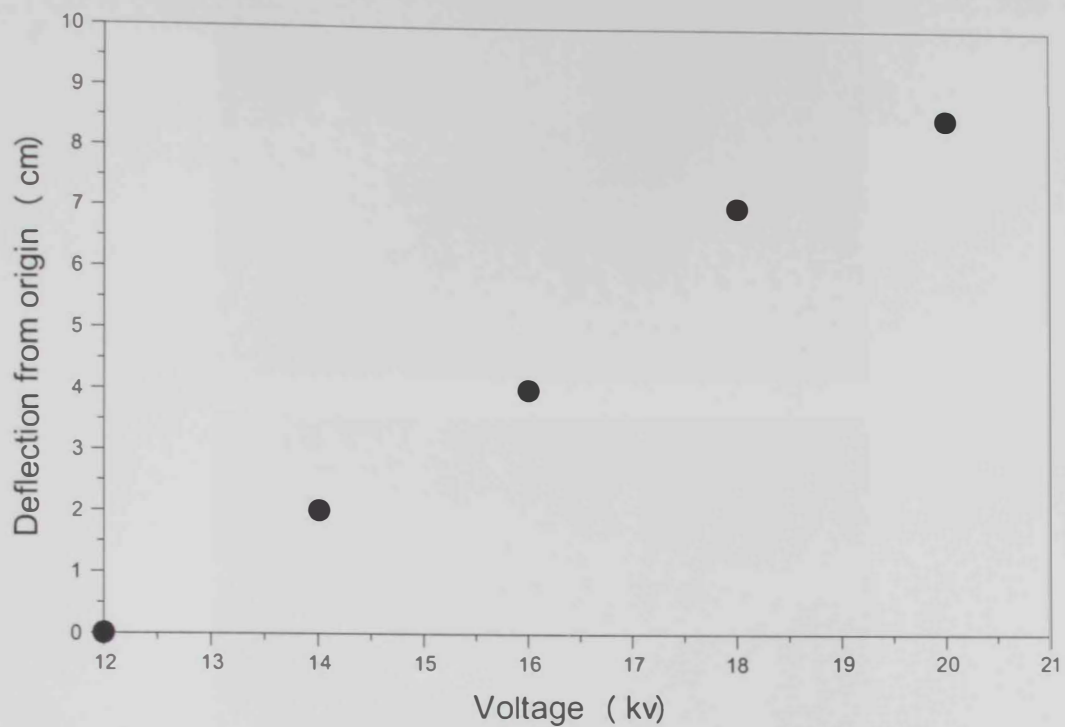
Figure 10 : DSC spectrum of as-received CA powder

Figure 11. Effect of the applied voltage on the width of the deposition path at constant needle-collector distance of 14 cm and of a flow rate of 100 mL/hr
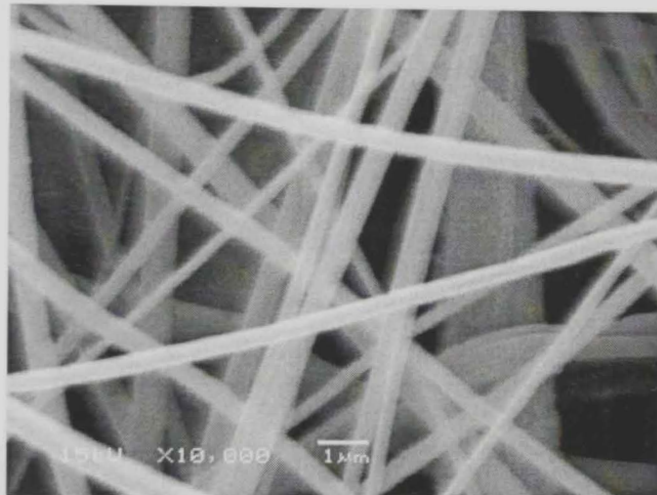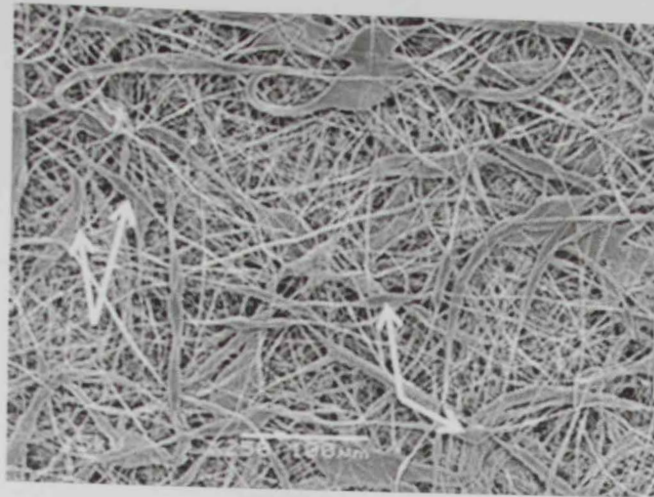
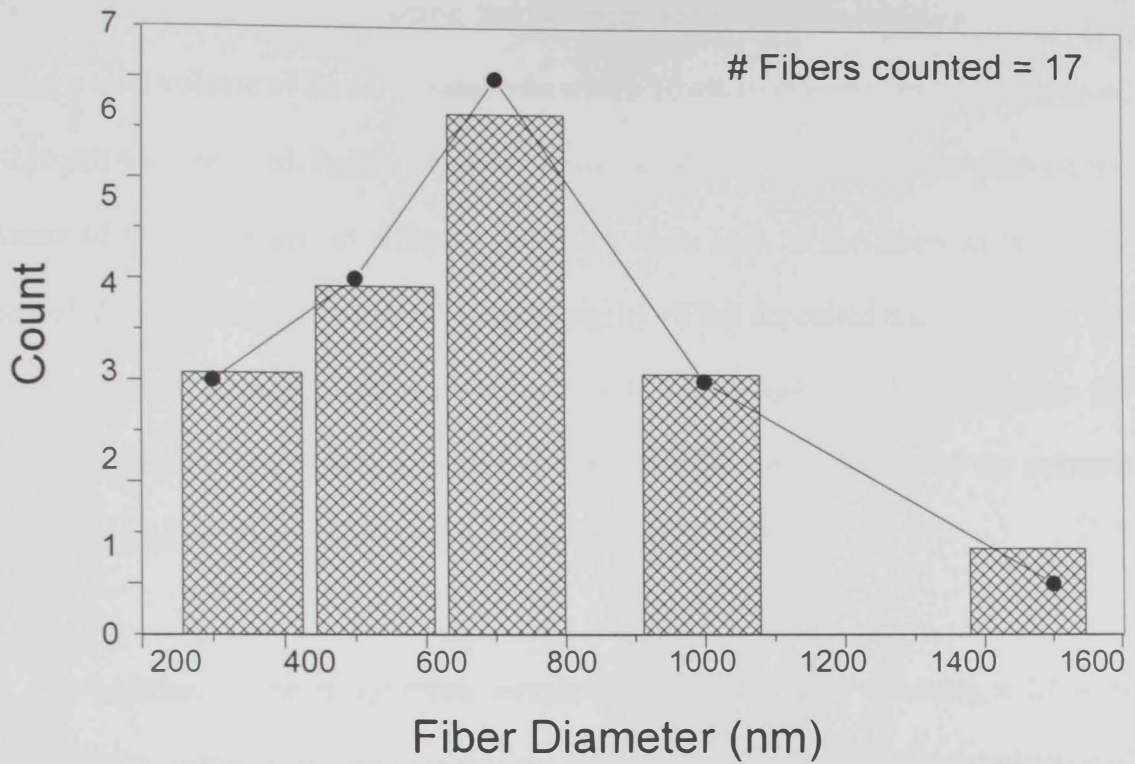Figure 12. SEM micrographs of CA nanofibers at different magnifications

Figure 13. Fiber-size distribution obtained by an image analysis of the SEM micrograph shown in Figure 12c

Despite these findings, few beads with an average thickness of 15 μm, were observed within these fibers. This is shown in Figure 12A, referred to by arrows. Bead formation is one of the possible outcomes of electrospinning is thought to depend on the electrospinning parameters, including the polymer solution characteristics [36]. After spinning a total volume of 20 cc, a membrane with a 10 cm in diameter and a thickness of 150-250 μm was prepared. Figure 14 shows a cross section of this membrane showing the thickness of the membrane at different points. A close look at the fibers in the cross-section of this membrane confirms the homogeneity of the deposited nanofibers and the absence of solvent accumulation at the bottom of the membrane. This is attributed to the complete dryness of the deposited fibers as a result of the evaporation of the solvents during the trip of the fibers towards the grounded collector [36].

In addition to the nanofibrous morphology obtained after spinning a 17 wt% solution of CA, different morphologies were also obtained during the electrospinning of CA solutions with different contents of CA at variable spinning conditions. These were obtained during the process of optimization of the process, and are worth noting here to clarify all possible morphologies that may result from electrospinning of polymers in general, and CA in particular. Figure 15 shows micrographs of fibrous membranes with different morphologies. Formation of drops as a sole event, as shown in Figure 15B, results from spinning low operating voltages. The electrospinning phenomena is based on a competition between the surface tension and applied voltage. At low operating voltages, the surface tension of the polymer droplets emerging from the spinneret is higher than the electrostatic charge developed on the droplets as a result of the applied voltage [28]. In such a case, a Taylor cone is not formed, and the emerged polymer droplets keep their spherical morphology until they deposit as such on the
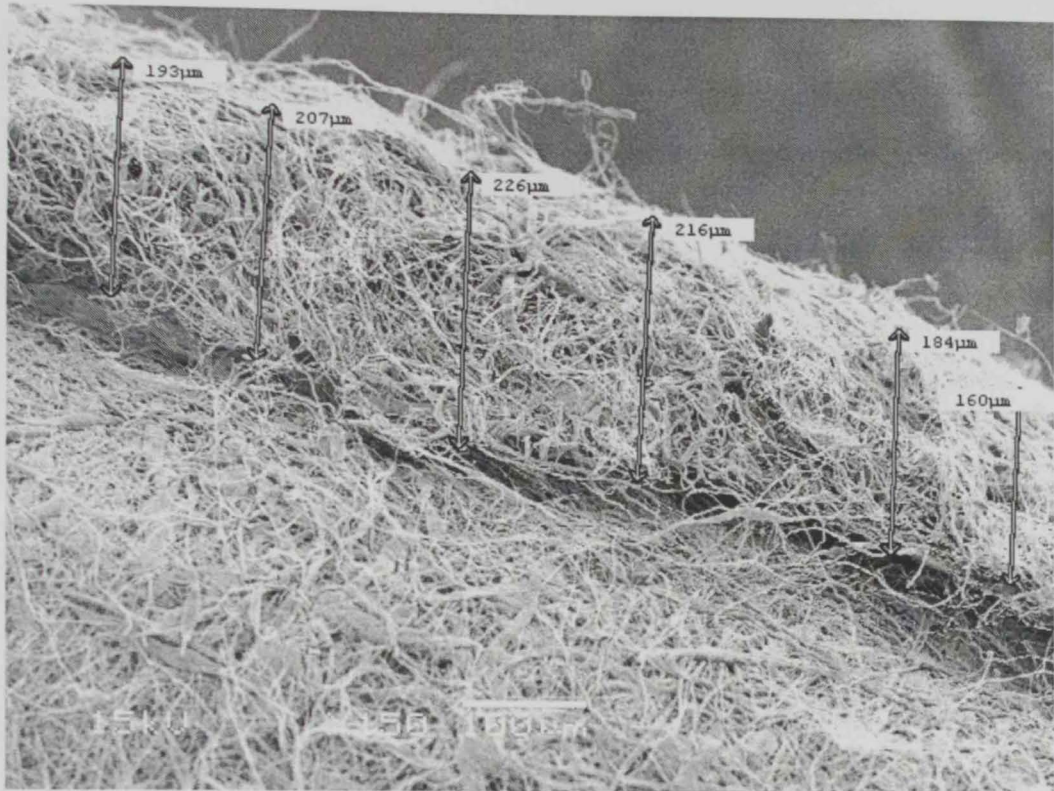
46

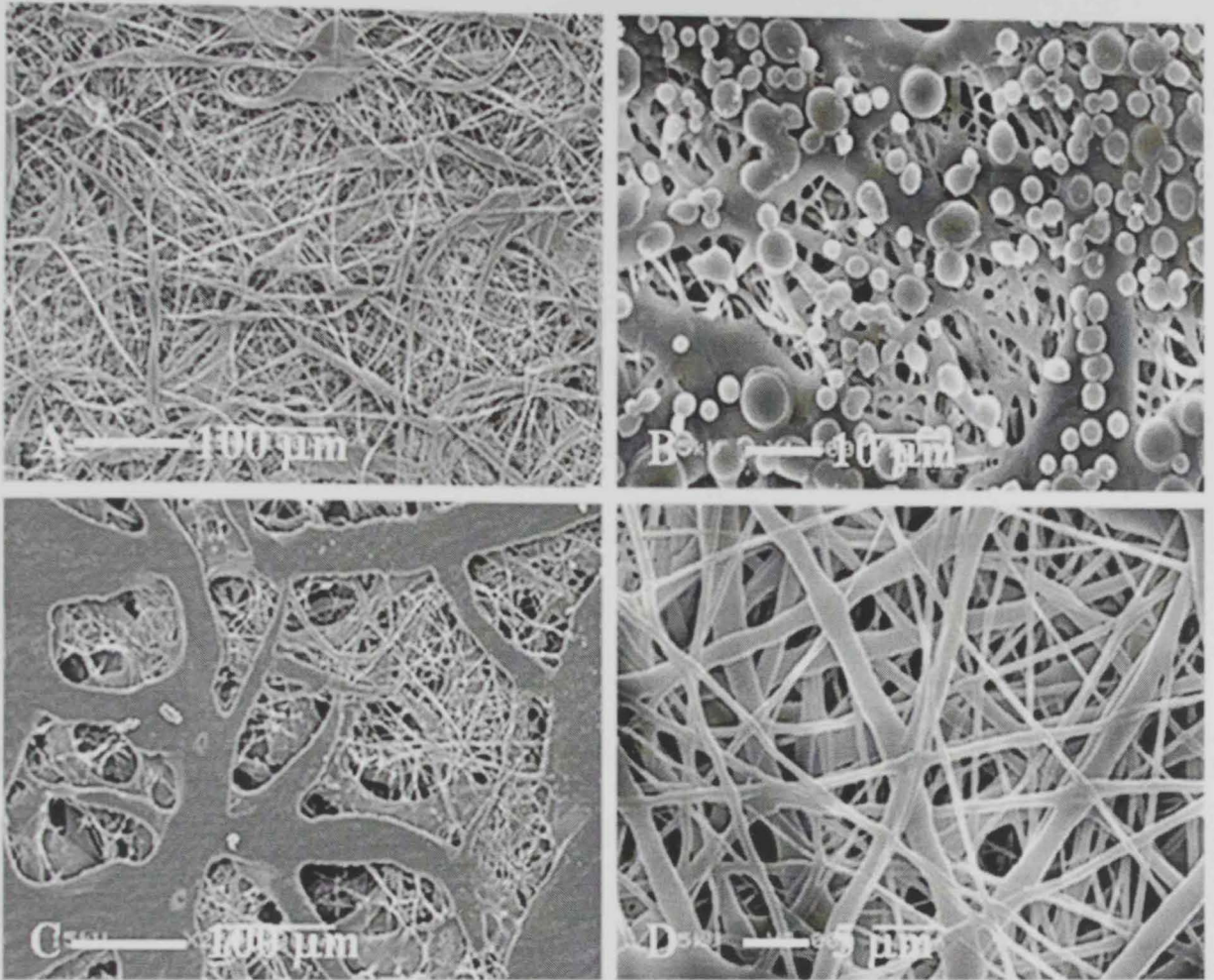Figure 14. SEM micrograph showing a side view of the electrospun CA fibrous

membrane

Figure 15. SEM micrographs showing different morphologies obtained during
preliminary electrospinning of CA

grounded collector [28]. Figure 15C shows a situation in which solvent is covering the fibrous assembly. This results from the use of relatively dilute polymer solutions together with an improper drying of the electrospun fibers. As stated before, a solvent mixture containing acetone and DMAc was used in the dissolution of CA. These solvents are supposed to evaporate during the passage of the fibers towards the collector. Using dilute polymeric solutions together with high flow rate conditions lead to lower chances for solvent evaporation, hence their existence with the deposited fibers. In some cases, extra solvent deposited with the fibers may lead to fusion between the fibers, and the eventual formation of continuous films instead of fibers. In contrast to the fibers shown in Figure 15A, ribbon-like morphology was also observed in the micrograph shown in Figure 15D. Ribbon morphology indicates stretching of the nanofibers in the side direction, in addition to its normal stretching while being attracted to the grounded collector. This is attributed to possible blocking of the needle orifice by sudden drying of polymer droplets while exiting it. This results in the emerge of a ribbon stream of the polymer solution, which keep its ribbon morphology after deposition on the collector. As shown in Figure 15D, the presence of ribbon morphology results in an increase in the overall fiber size distribution, a subsequent decrease in the pore size distribution, and an increase in the compactness of the fibrous membranes. In order to avoid these circumstances, the effect of saturating the electrospinning chamber with acetone was studied. A beaker containing around 50 cc of acetone was placed inside the chamber around 30 minutes before starting the electrospinning experiment. Figure 16 shows two SEM micrographs of fibrous mats collected with and without pre-saturation of the chamber with acetone. Both non-woven mats were collected for the same polymer solution at constant applied voltage, flow rate and distance from the collector. It is evident that pre-saturating the electrospinning chamber with acetone highly affected the morphology of the produced fibers. This was
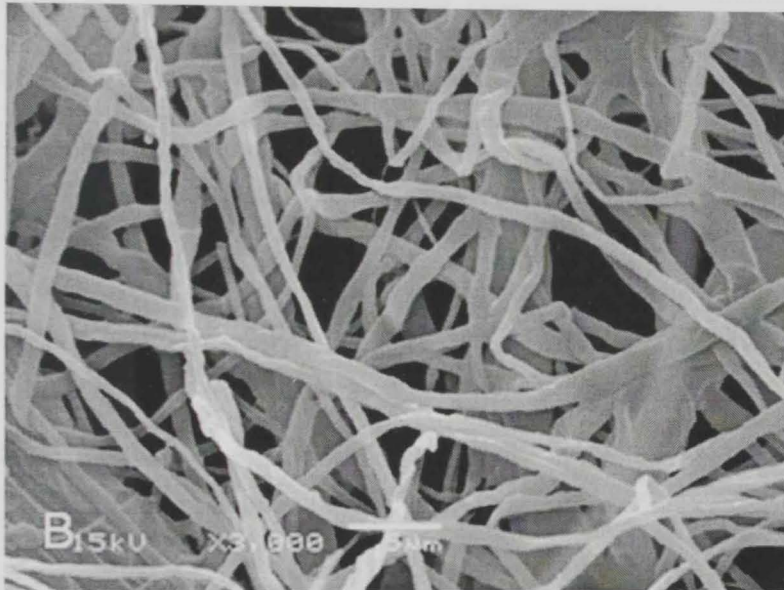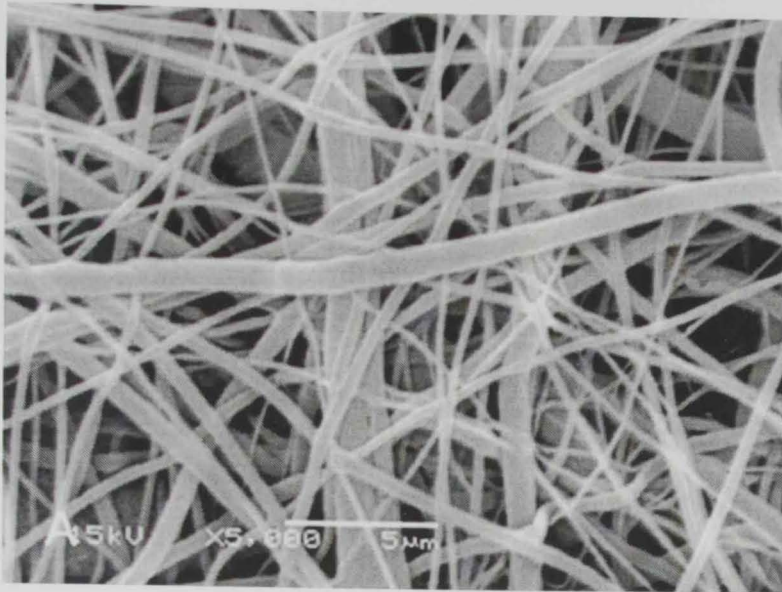
Figure 16. SEM micrographs of electrospun CA fibers in A) presence and B) absence of acetone inside the spinning chamber with and without acetone

previously found to improve the quality of the collected fibers, especially in situations where highly volatile solvents were used [125]. More fibers with ribbon-like morphology were observed in the absence of acetone, while the presence of acetone was found to slow down the evaporation of the solvent from the fibers during their trip towards the collector and afterwards. This incomplete dryness of the fibers, in presence of acetone, gave fibers with almost complete cylindrical geometry. Optimization of the electrospinning atmosphere is thus considered an important parameter that was strongly considered for the formation of fibers with normal cylindrical morphology. Collection of nanofibers, produced by electrospinning, was previously studied on fixed collectors or collectors that are mounted on motors [126,127]. When a grounded collector is fixed, non-woven fibers are produced, while woven fibers are normally produced when moving collectors are used. Using rotating collectors, single fibers were formed for specific studies [128]. Using fixed collectors is known to produce non-woven fibrous mats due to the random collection of the fibers on these collectors. Although these non-woven fibrous mats are useful for many applications, the disadvantage of using fixed collectors is the inability to control the homogeneity of fibers distribution and the thickness of the produced sheets. Due to these findings, the effect of using a collector mounted on a shaker, on the morphology of the produced fibrous membranes, was investigated. Figure 17 shows SEM micrographs of fibers collected on a fixed collector versus those collected on a collector that was mounted on a shaker adjusted at 100 rpm. It is evident that using a moving collector resulted in thinner fibers that are more homogeneously distributed on the collector. Using a fixed collector was shown to result in a non-homogeneous distribution of relatively thick fibers in which solvent was still believed to exist. Using a moving collector, on the other hand, is thus believed to accelerate the evaporation of the solvent from the deposited fibers, leading to unified fibers with smaller diameters. Using a
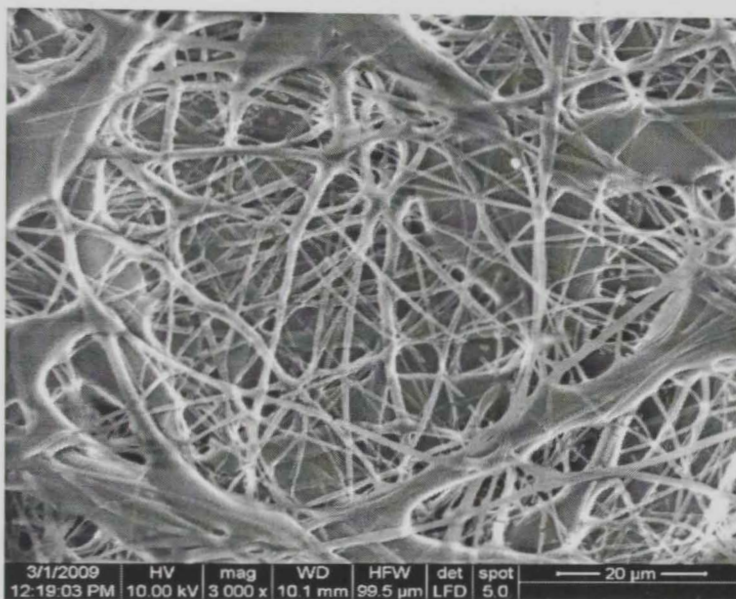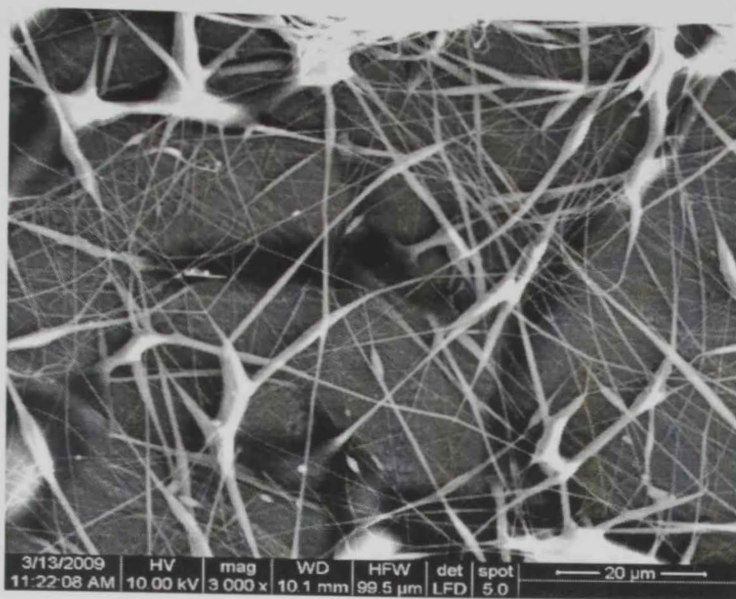
51

Figure 17. SEM micrographs of electrospun CA fibers collected in the
A) presence and B) absence of a shaker rotating at a 100 rpm

moving collector together with pre-saturating the electrospinning chamber were thus found to improve the quality of the collected nanofibers. These conditions were, therefore, considered for the rest of the electrospinning experiments carried out in the present study. A closer look at the above results indicates the importance of optimizing the electrospinning conditions and controlling the parameters that would eventually lead to the formation of homogeneous fibrous membranes.

In order to confirm the chemical structure stability of CA after electrospinning, a sample of the electrospun membrane was analyzed by IR and GPC techniques. Figure 18 shows an infrared spectrum of as-spun CA compared to that of as-received CA. A close match can be seen between the spectra of both samples; before and after spinning. This indicates the structural stability of CA. Figure 19 shows GPC spectra of as electrospun CA fibrous sample from a solution containing 17 wt% of CA. Molecular weight analysis obtained using the UV and refractive index detectors revealed the same M_n value of 46,000 for the as spun sample, which is the same as what was previously measured for the as-received sample. Both IR and GPC results indicated that electrospinning did not affect the structural characteristics of the polymer nor did reflect signs of degradation as a result of the high voltage imposed on the polymer.

IV.3 Electrospinning of CA: Effect of polymer concentration and viscosity:

Solutions containing 10, 12, 15, 17 and 20 wt% of CA in a solvent mixture of acetone and DMAc (2:1 by volume) were used in these experiments. After saturating the electrospinning chamber with acetone for 30 minutes, around 5 mL of each of these
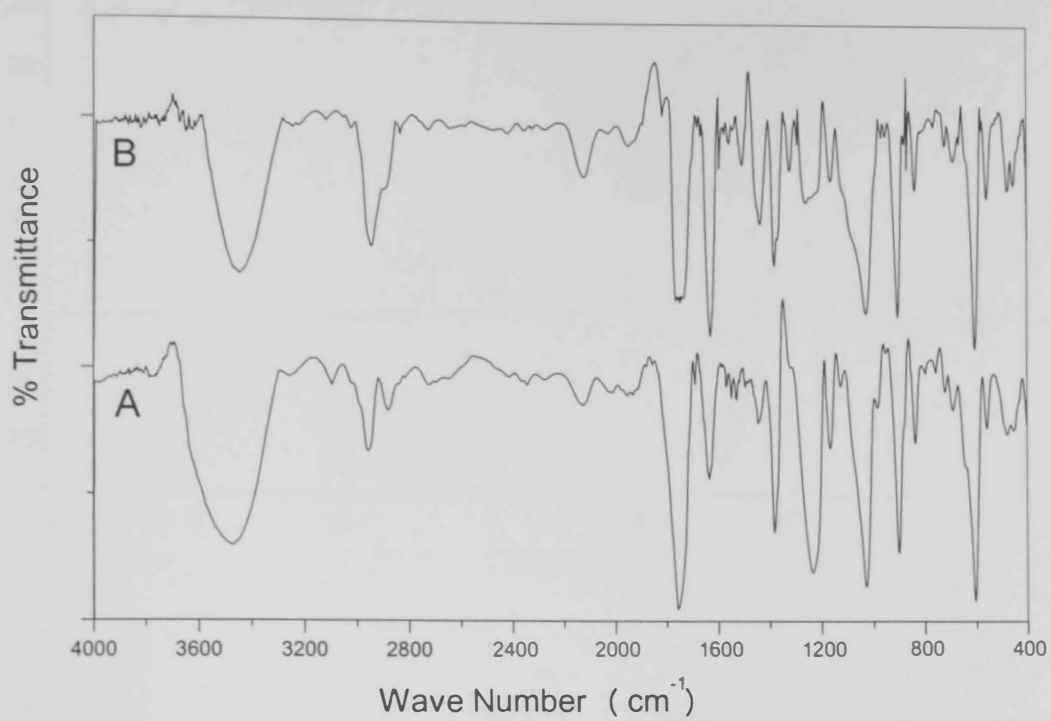
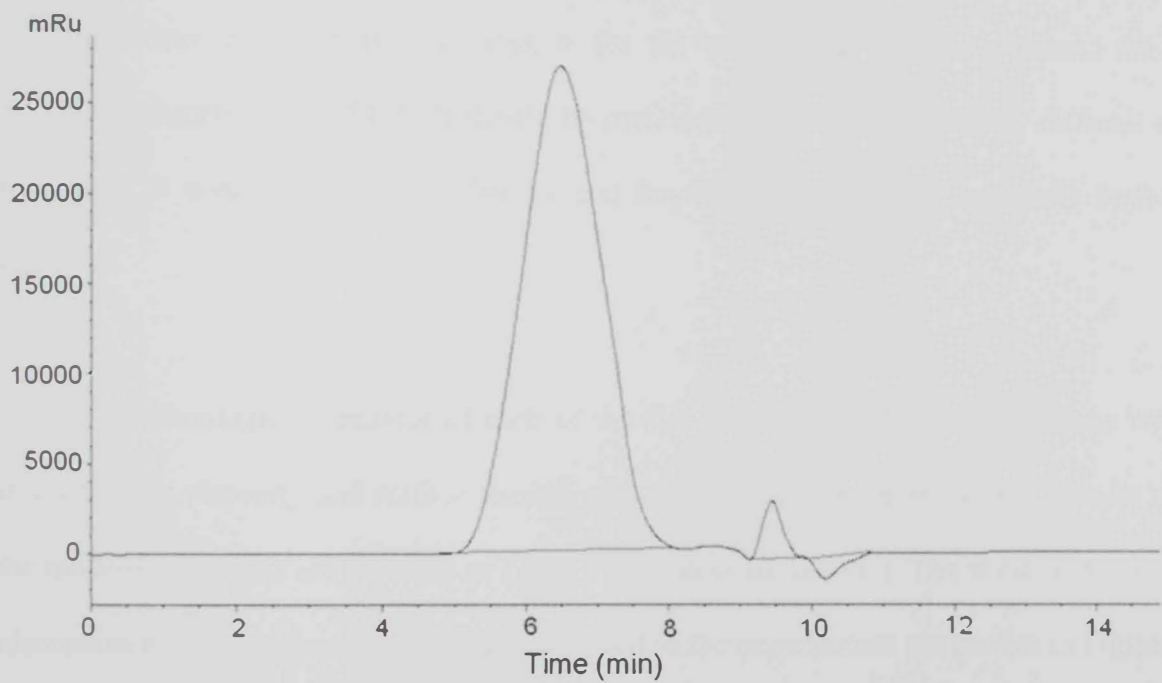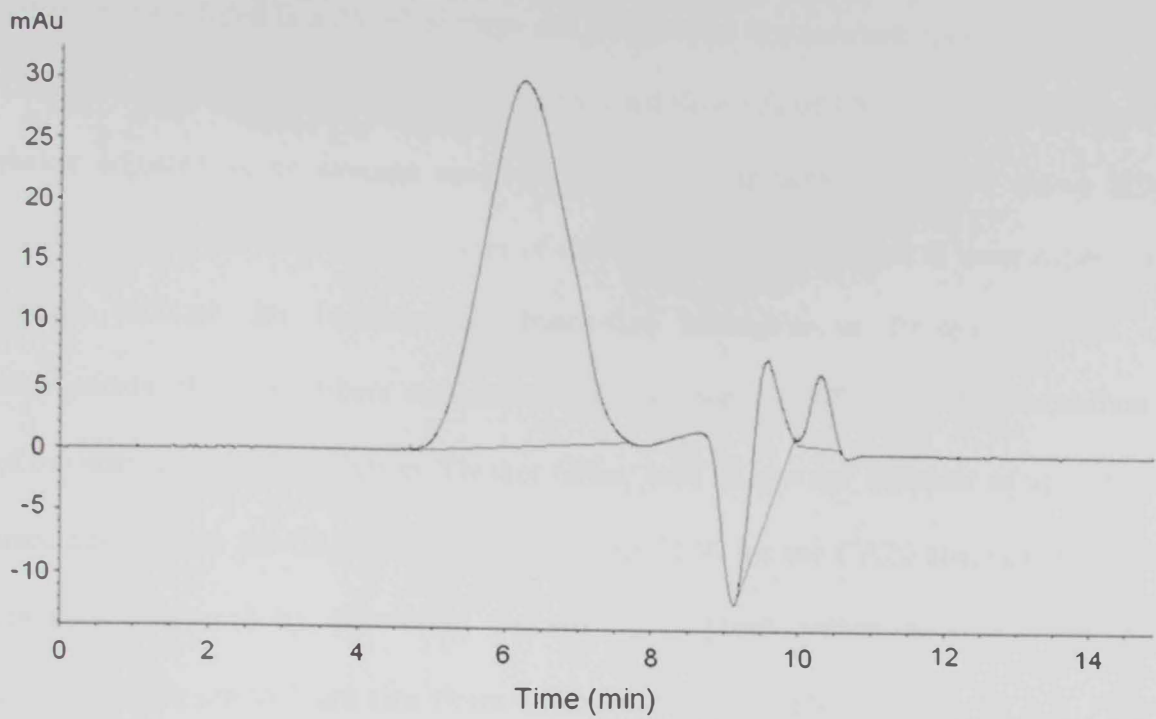Figure 18. IR spectrum of A) as-received versus B) as electrospun CA nanofibers

Figure 19. GPC spectrum of CA 17 nanofibrous membrane using A) a UV detector at 254 nm and B) a refractive index detector

solutions were filled in a 25 mL syringe and electrospun at a constant operating voltage of 12 kV, a constant distance of 14 cm and a constant flow rate of 100 mL/hr. In addition, a shaker adjusted at an average speed of 100 rpm was used. Figure 20 shows SEM micrographs of the fibrous membranes of all concentrations collected at these conditions. Results indicate the formation of beads-free homogeneous fibrous mats in all experiments. However, fibers morphologies can be seen to differ with the concentration of the starting polymer solution. Thicker fibers, with an average diameter of up to 5 μm were observed in the SEM micrograph in Figure 20E for the CA20 samples. The fiber diameter decreased by decreasing the starting polymer concentration solution to an average of sub μm to 1 μm size fibers in the SEM micrographs in Figure 20 A,B. Figure 21 summarizes the fiber size distribution for the nanofibrous meshes obtained from different concentrations of CA. It should be mentioned that it was relatively difficult to spin the CA solution containing 20wt% and beyond because of its relatively higher viscosity.

The rheological behavior of each of the CA 10, 12, 15, 17 and 20 solutions was studied. Both viscosity and surface tension of these solutions were measured. Results of the modeling analysis are reported in Table 2 for values of m and n. The shear-dependent viscosities and shear stress of the CA fluids used in the experiments are shown in Figures 22–23. Higher concentration of CA fluids exhibited qualitatively similar (shear-thinning) viscous behavior as shown in Figure 22. The CA20 solution is highly elastic while the CA10 solution is weakly elastic. This difference in behavior, that is related to their concentrations variation, was previously found to affect the morphology of the produced nanofibers. The elastic nature of the CA solutions is demonstrated by the strain dependence of the shear shown in Figures 23. The reduction in shear stress (at constant
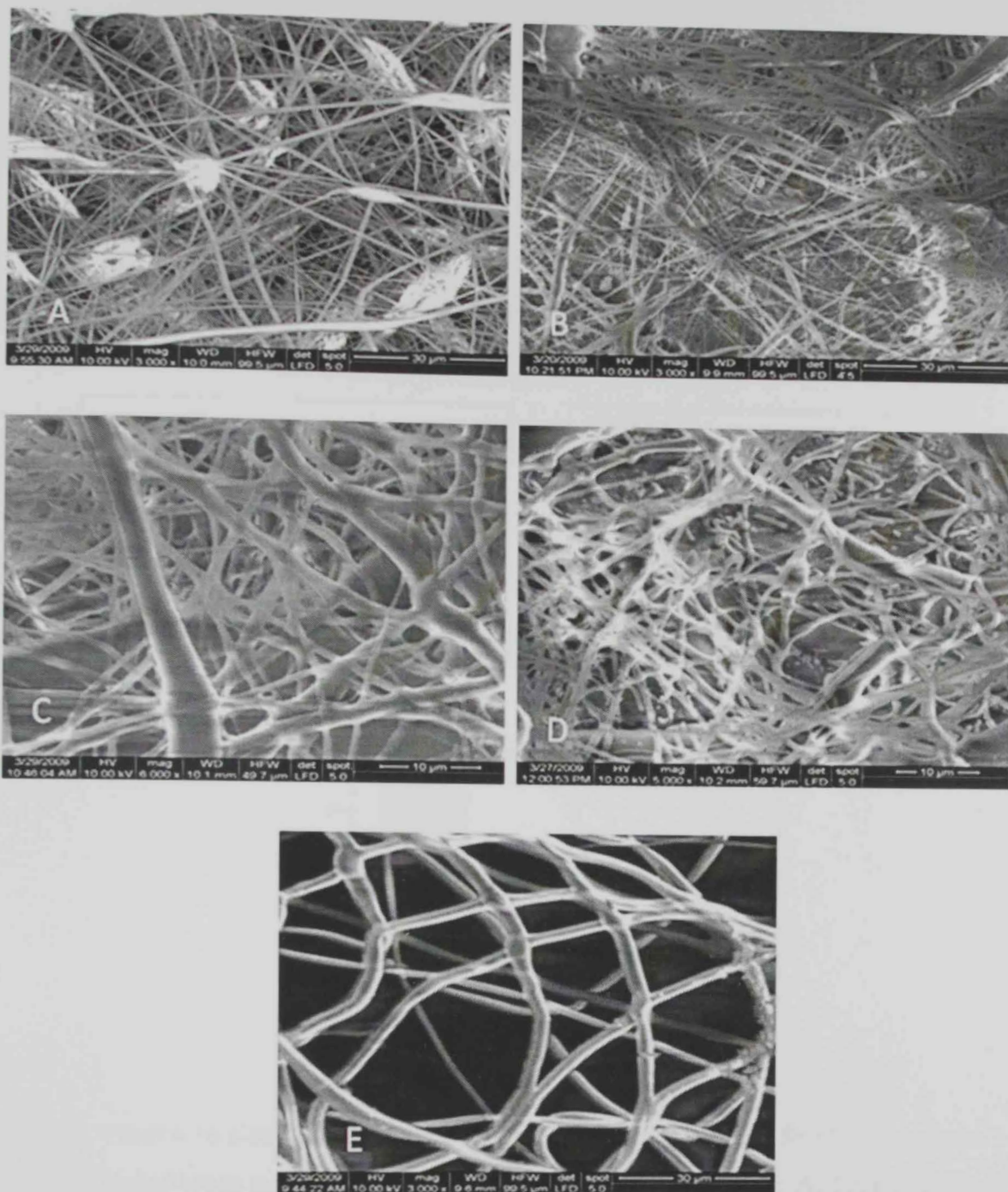
Figure 20. SEM micrographs of CA nanofibrous membranes prepared from solutions containing A) 10, B) 12, C) 15, D) 17 and E) 20 wt % of CA in a solvent mixture of acetone and DMAc (2:1)
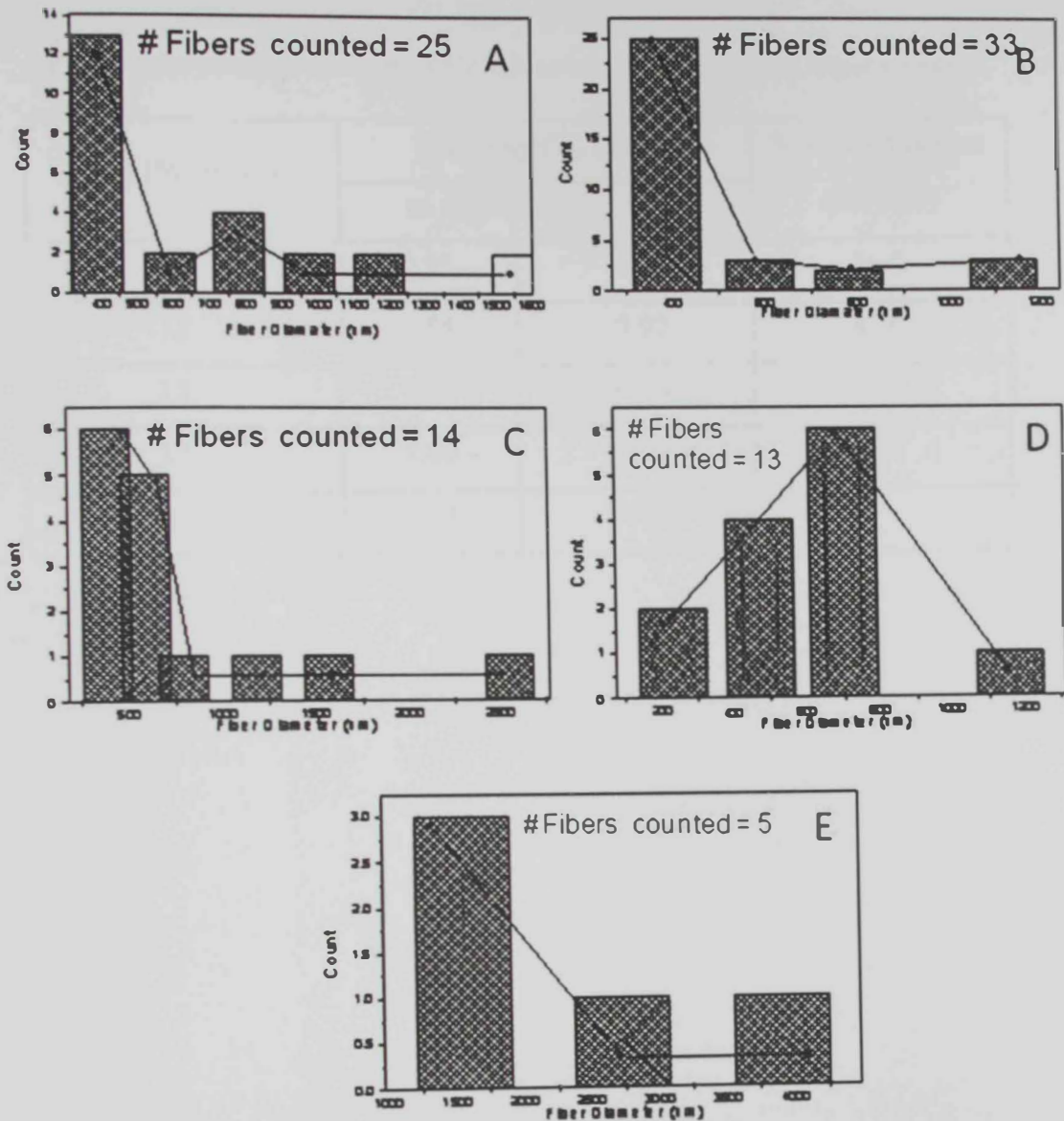
Figure 21. Fiber-size distribution obtained by an image analysis of the SEM micrographs of the CA nanofibrous membranes prepared from solutions containing A) 10, B) 12, C) 15, D) 17 and E) 20 wt % of CA in a solvent mixture of acetone and DMAc (2:1)

Table 2. Physical properties of Cellulose acetate used in the experiments

[CA] (% by wt)	Viscosity (η, mPa.s)		Surface Tension (mN/m)
	m	n	
10	0.95	0.99	36.0
12	1.65	0.97	41.0
15	4.21	0.93	52.0
17	7.09	0.90	93.5
20	9.63	0.99	-
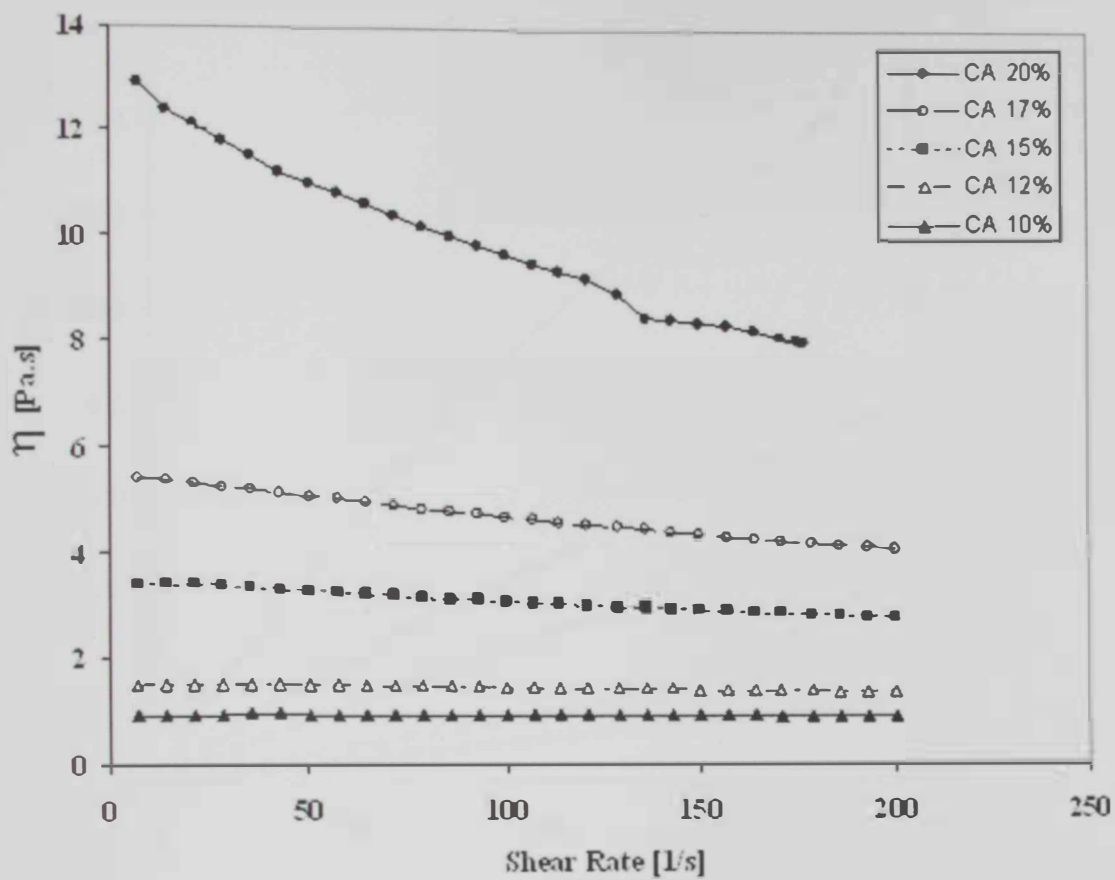
Figure 22. Viscosity curves of CA solutions as a function of shear rate.
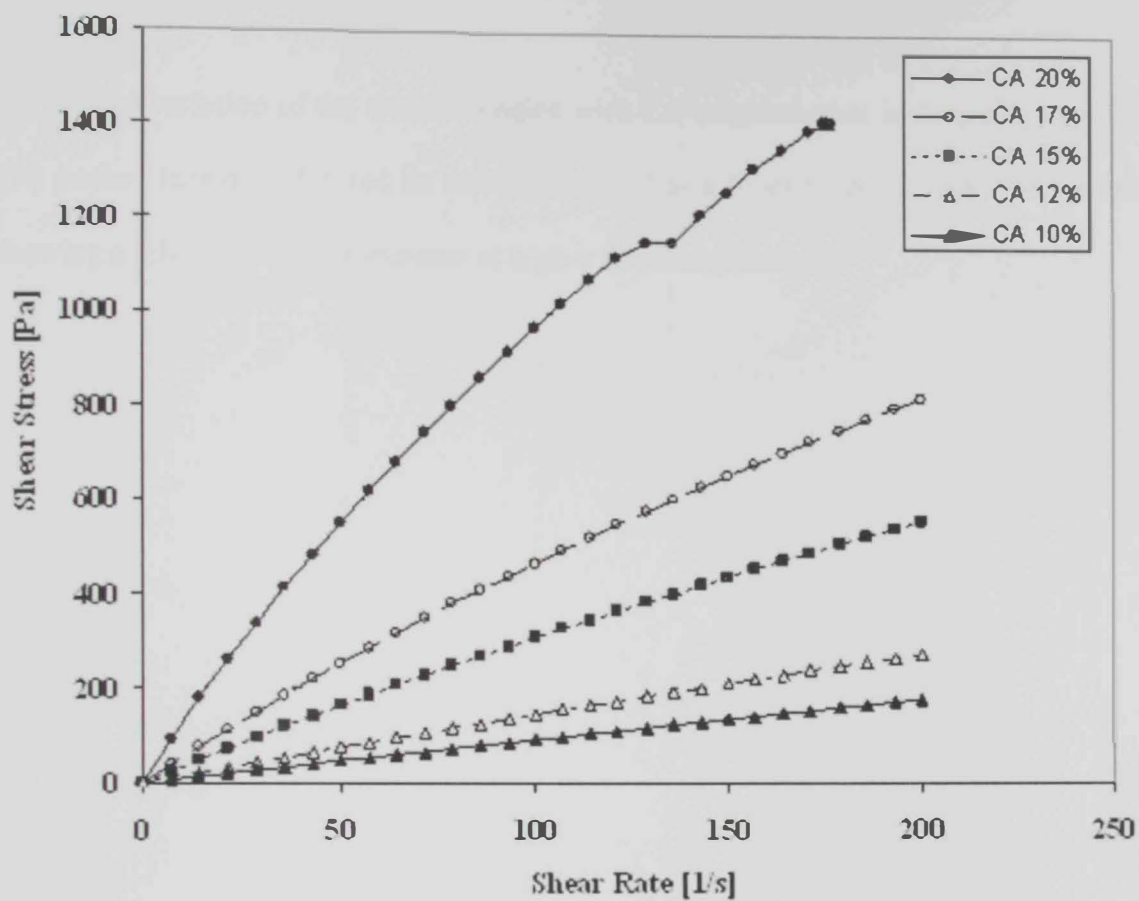
Figure 23. Shear stress curves of CA solutions as a function of shear rate

shear rate) increased with the increase in the CA concentration. Lower concentrations of CA (CA10, CA12) exhibited a constant slope, suggesting that these CA solutions behave as Newtonian fluids.

The variation of the surface tension with CA concentration is shown in Figure 24. The surface tension exhibited an increasing trend as a function of the CA concentration, showing a relatively higher increase at higher CA concentration.
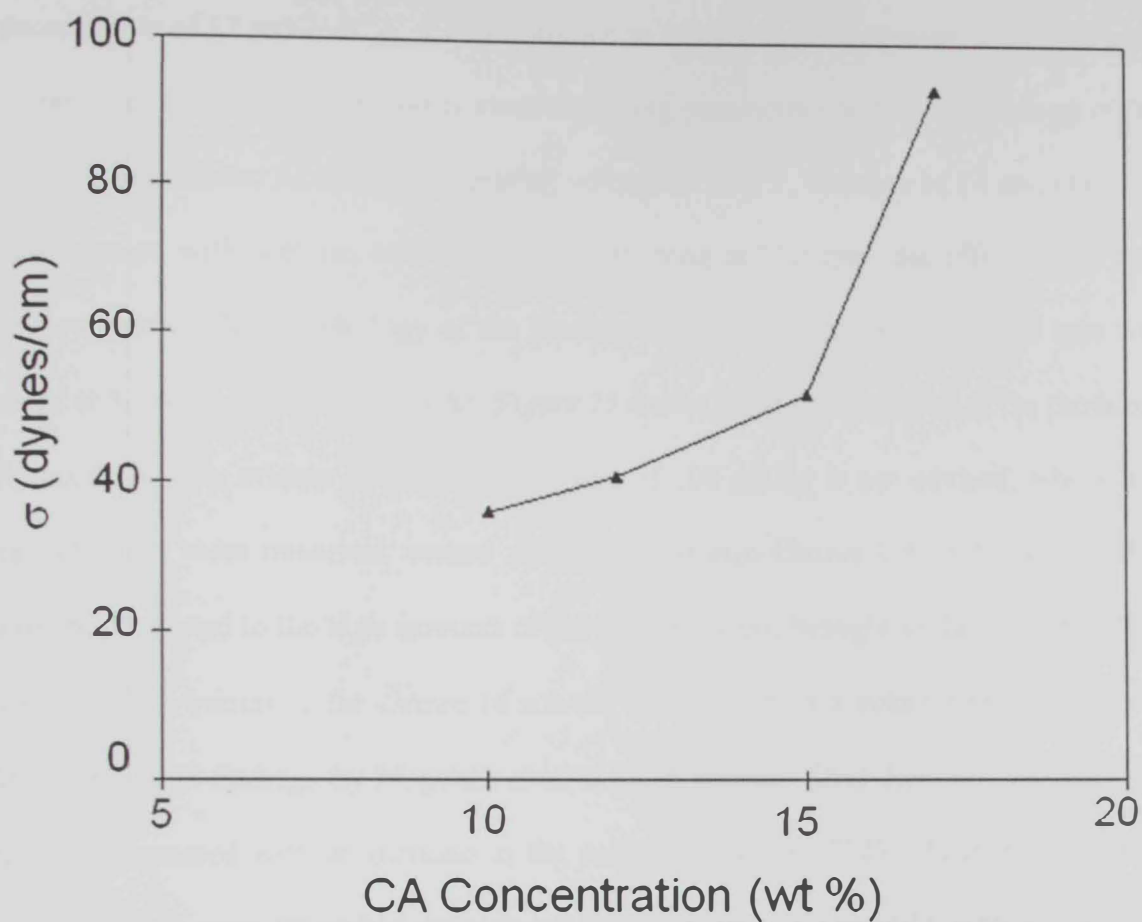
Figure 24. Effect of CA concentration on the surface tension of the prepared solutions.

IV.4 Electrospinning of CA: Effect of flow rate:

Based on the above results, a representative CA solution containing a concentration of 12 wt% of CA, that was shown to behave as a Newtonian fluid, was used to study the effect of changing other electrospinning parameters on the morphology of the produced nanofibers. At constant operating voltage of 12 kV, distance of 14 cm, chamber pre-saturation with acetone, and using shaker running at 100 rpm, the effect of varying the flow rate on the morphology of the produced fibers was studied. The flow rate was varied at 5, 10, 25, 50 and 100 mL/hr. Figure 25 shows SEM micrographs of the produced fibrous mats. It is evident that a high flow rate of 100 mL/hr is not advised, where few distinct fibers were observed, coated with layers of non-fibrous CA and solvent. This could be attributed to the high amounts of polymer solutions brought to the collector. This is expected to minimize the chance of solvent evaporation in a suitable rate to produce fibers. Previous findings by Megelski *et al* showed that the fiber diameter and the pore diameter increased with an increase in the polymer flow rate [129]. They found that at very high flow rates, fibers had pronounced beaded morphologies and the mean pore size increased from 90 to 150 nm [129]. Based on these findings, a high flow rate of 100 mL/hr was avoided. It is also evident from Figure 25 that the diameter of the produced fibers increased by increasing the flow rate, producing more fibers with ribbon-like morphology at a flow rate of 50 mL/hr. Based on these observations and based on the fiber size distribution analyses of these meshes shown in Figure 26, a maximum flow rate of 25 mL/hr was recommended. Further experiments were carried out to investigate the morphology of fibrous mats produced at a flow rate range of 5-25 mL/hr. Figure 27 shows SEM micrographs of these fibrous mats, while the fiber size distribution in these micrographs is given in Figure 28. These results collectively recommended the use of a
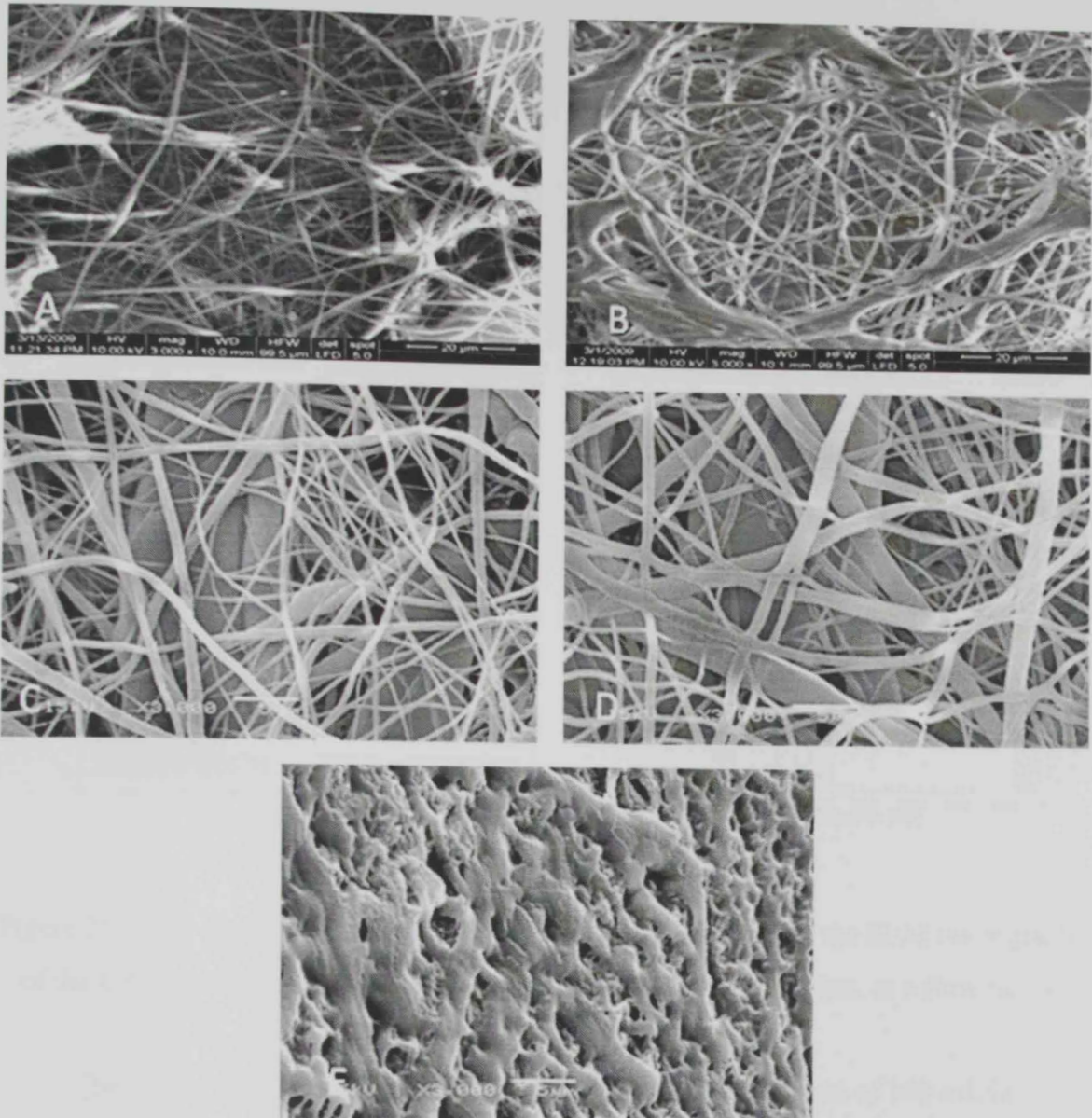
64

Figure 25. SEM micrographs of CA nanofibrous membranes prepared from a 12 wt%
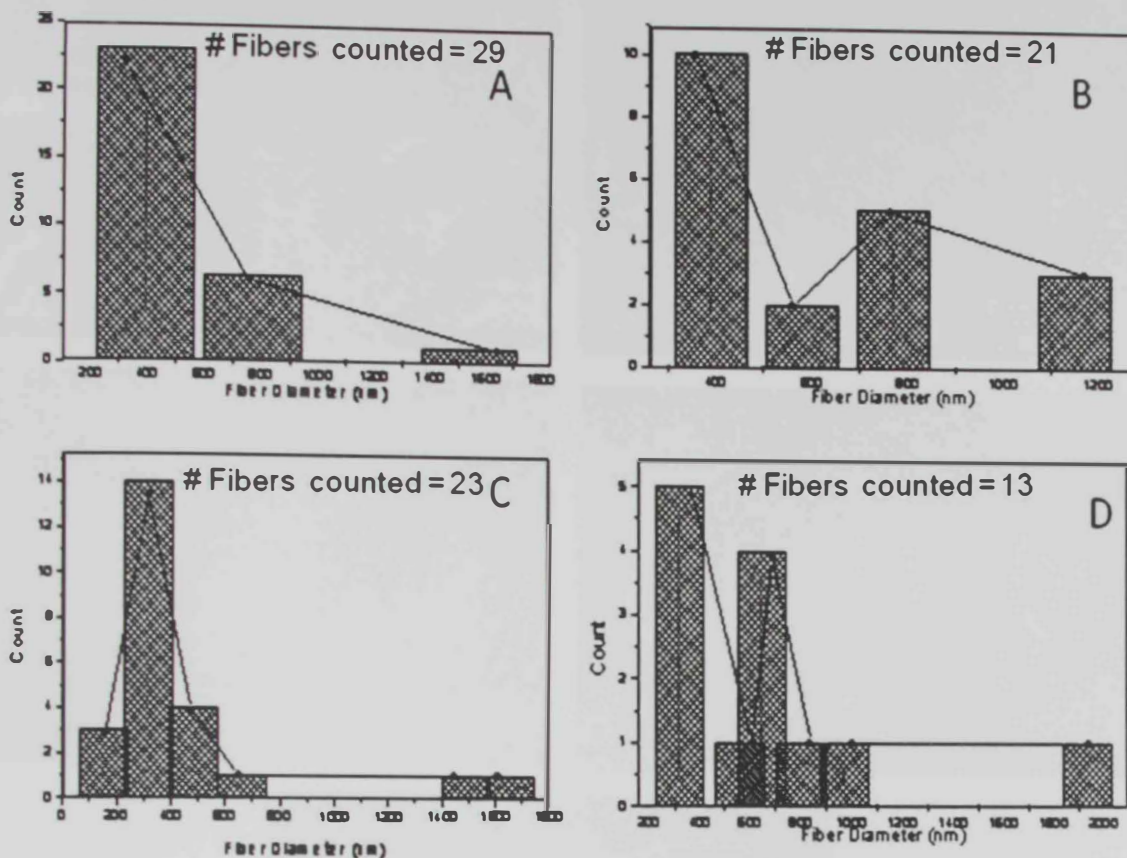solution, at a flow rate of A)5, B)10, C)25, D)50 and E)100 mL/hr

Figure 26. Fiber-size distribution obtained by an image analysis of the SEM micrographs of the CA nanofibrous membranes prepared from a 12 wt% solution, at a flow rate of A)5, B)10, C)25, and D)50 mL/hr.

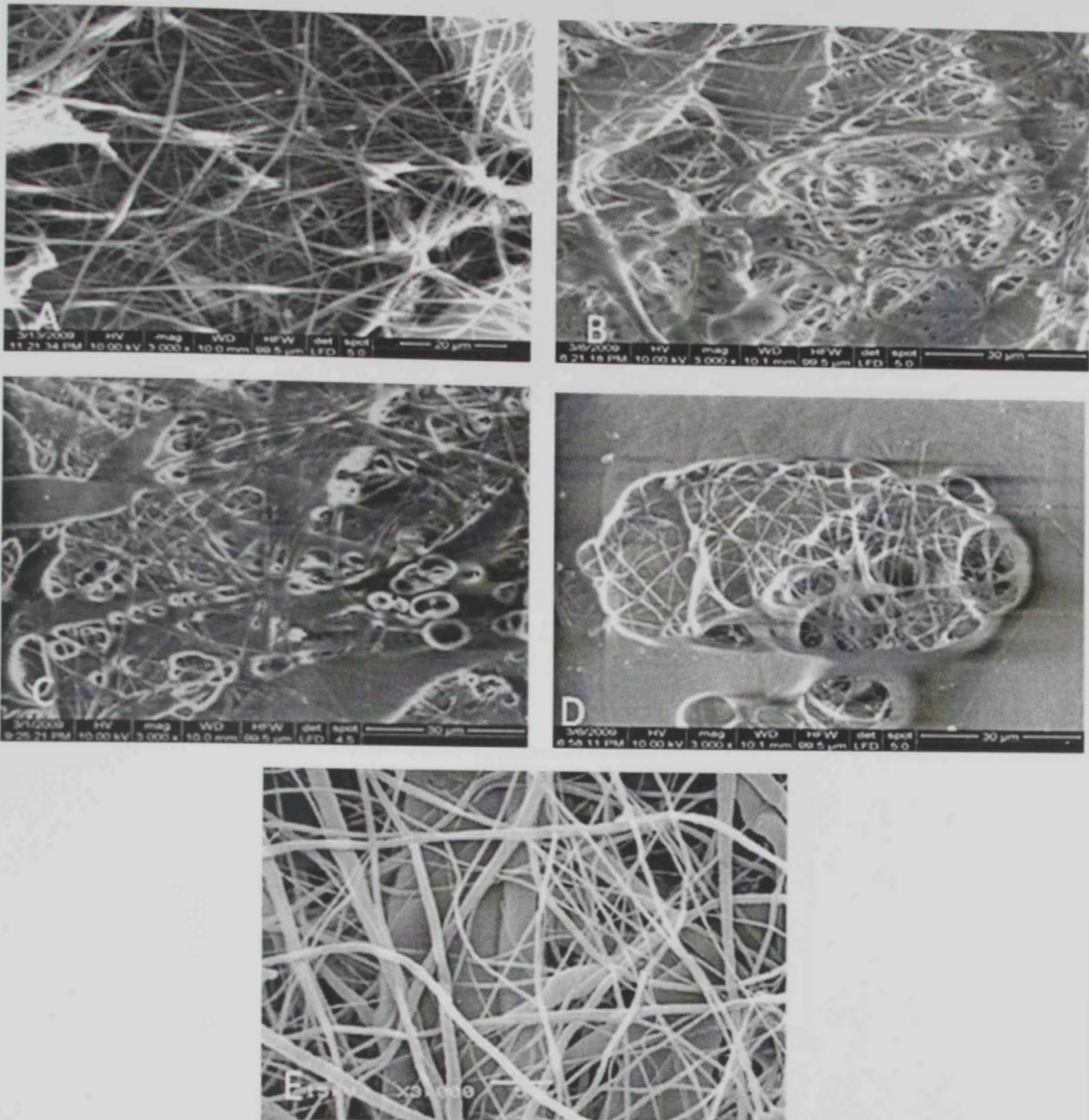[No fibers were observed in the sample prepared at a flow rate of 100 mL/hr]

Figure 27. SEM micrographs of CA nanofibrous membranes prepared from a 12 wt% solution, at a flow rate of A)5, B)10, C)15, D)20 and E)25 mL/hr
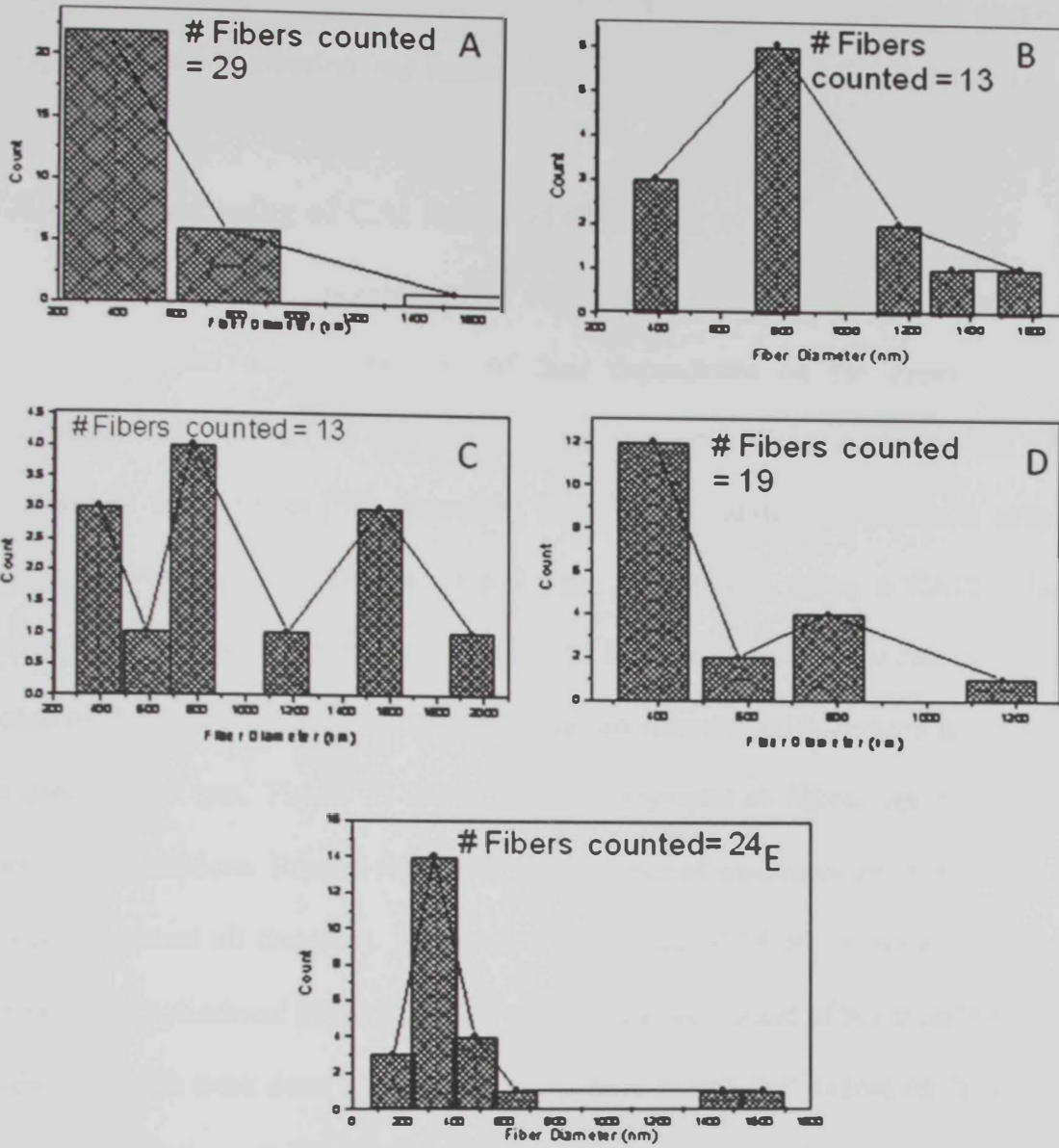
Figure 28. Fiber-size distribution obtained by an image analysis of the SEM micrographs of the CA nanofibrous membranes prepared from a 12 wt% solution, at a flow rate of A)5, B)10, C)15, D)20 and E)25 mL/hr

low flow rate of 5 mL/hr as an optimum value for obtaining fibers with small diameters, homogeneous size distribution, and consequently homogeneous pore size distribution.

IV.5 Electrospinning of CA: Effect of distance:

The structure and morphology of electrospun fibers is easily affected by the nozzle to collector distance because of their dependence on the deposition time, evaporation rate, as well as the whipping or instability interval during the fibers deposition on the collector [39]. Therefore, the effect of varying the nozzle to collector distance between 12 and 20 cm (step 2 cm) was studied using a CA12 solution electrospun at a constant operating voltage of 12 kV, and constant flow rate of 5 mL/hr. In each of these experiments, the chamber was pre-saturated with acetone and a shaker was used at 100 rpm. Figure 29 shows SEM micrographs of fibrous meshes prepared under these conditions. Results illustrated the presence of un-evaporated solvent as well as beads at almost all distances. However, at a distance of 14 cm, a more homogenous distribution of cylindrical fibers was observed with a lower extent of beads and remaining solvent. Previous work done by many scientists have shown that increasing the spinning distance resulted in more chances for thinning of the polymeric stream on its way to the collector, and eventually deposit as fibers with smaller diameter [114-116]. A closer look at the micrographs in Figure 29 shows an agreement with these previous observations. This is also evident from the graphs given in Figure 30 for the fiber size distribution obtained by image analysis of the micrographs in Figure 29. The presence of beads and un-evaporated solvent in these samples could, therefore, be related to other polymer-specific parameters. Beaded structure is known to reduce the surface area, which ultimately influences the filtration abilities of nanofibrous membranes [39]. The absence of beads and the better fiber size distribution and homogeneity of the fibers morphology
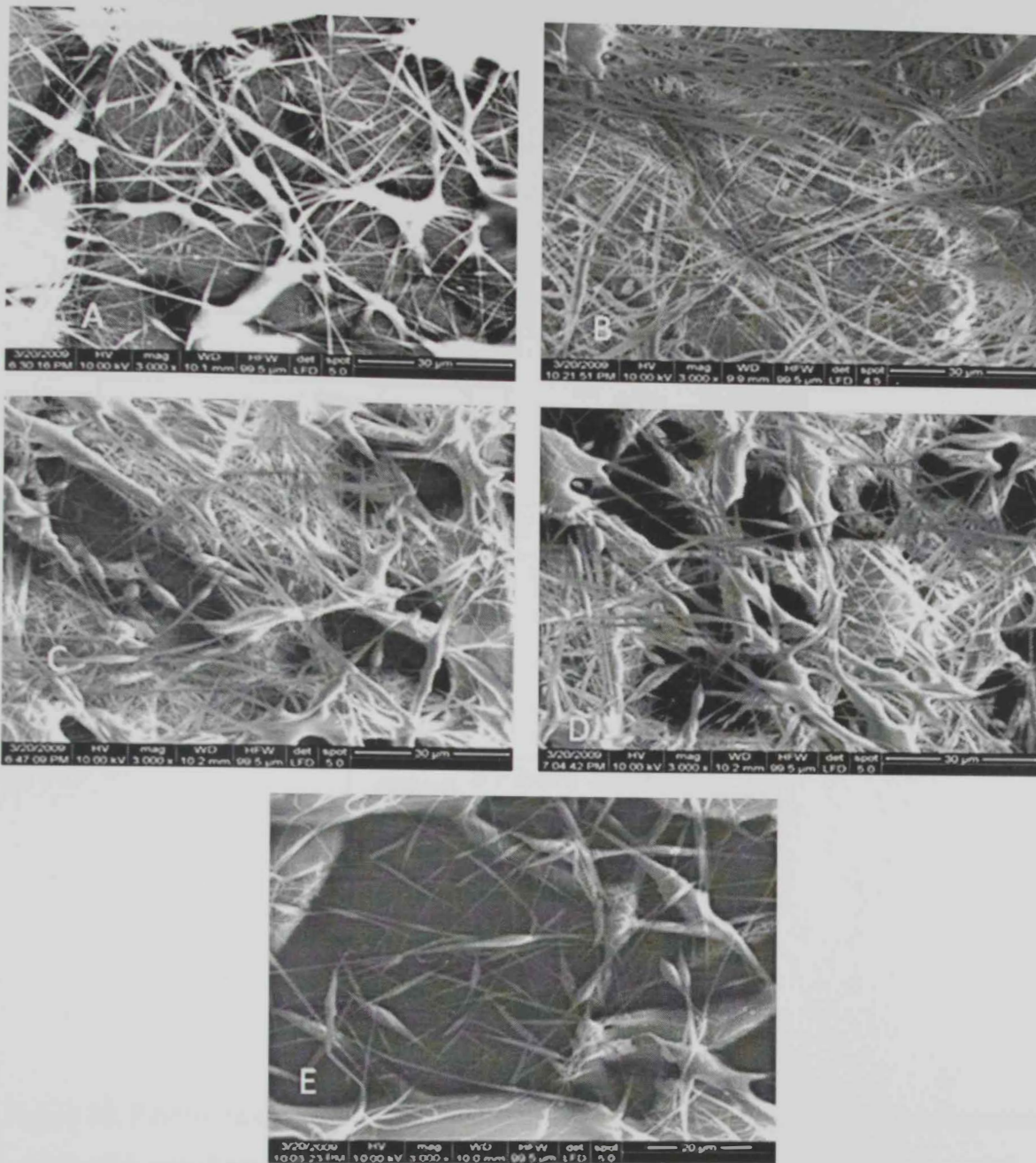
69

Figure 29. SEM micrographs of CA nanofibrous membranes prepared from a 12 wt% solution, at a flow rate of 5 mL/hr and a distance of A)12, B)14, C)16, D)18 and E)20 cm from the collector
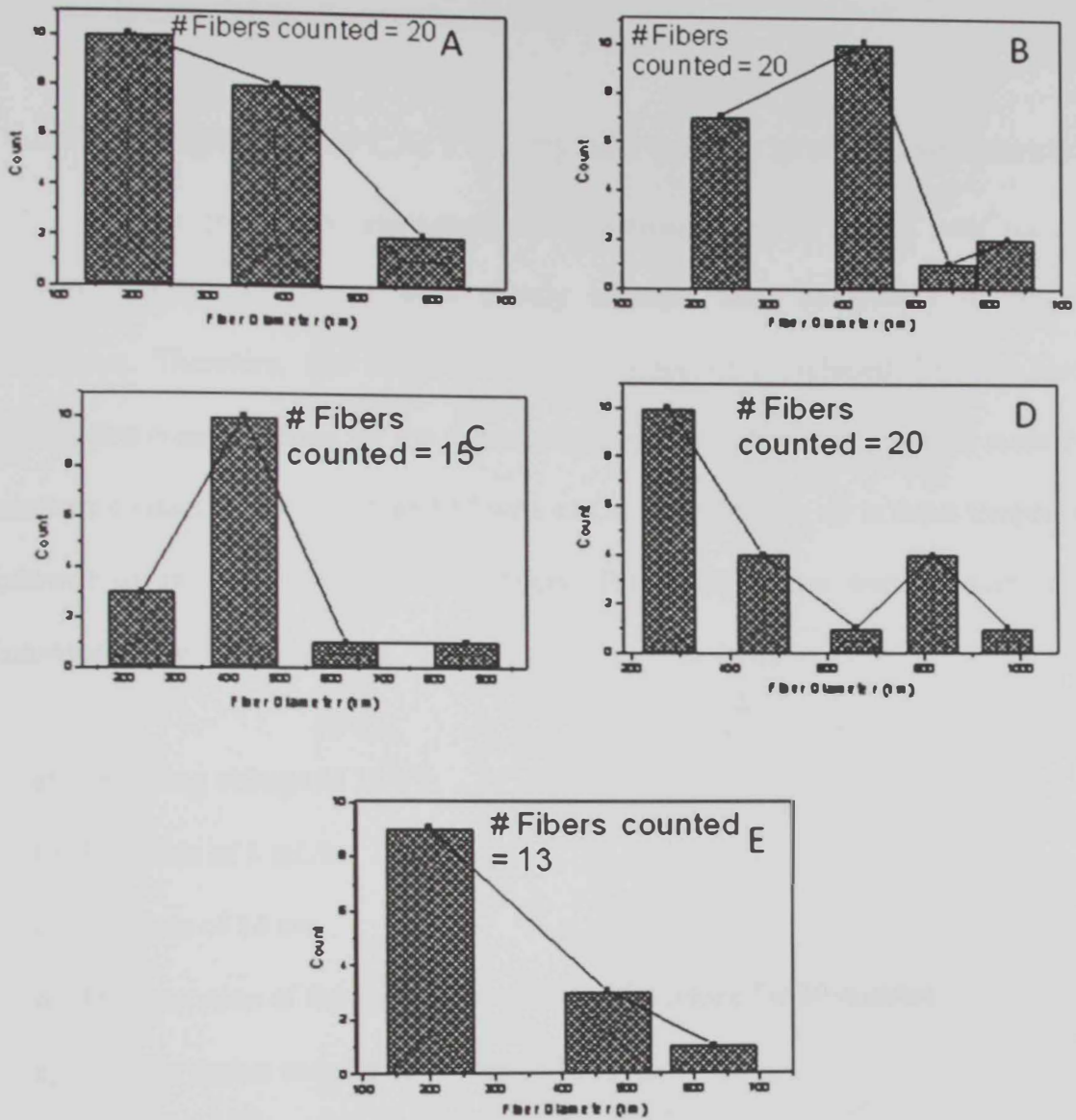
Figure 30. Fiber-size distribution obtained by an image analysis of the SEM micrographs of the CA nanofibrous membranes prepared from a 12 wt% solution, at a flow rate of 5 mL/hr and a distance of A)12, B)14, C)16, D)18 and E)20 cm from the collector

obtained at a spinning distance of 14 cm recommend this distance to be used as an optimum distance for the electrospinning of CA.

IV.6 Electrospinning of CA: Porosity and surface area measurements

As was previously mentioned, the electrospinning of CA20 was relatively difficult. Glassy membranes were mainly obtained after completely drying their membranes. Therefore, this concentration was temporarily excluded from the rest of investigated concentrations for the coming experiments. Fibrous membranes made from solutions containing 10, 12, 15 and 17 wt% of CA were dried in air at room temperature, followed by drying at 100°C for 24 hours. Those membranes were obtained at the following optimized conditions:

a) Operating voltage of 12 kV

b) Flow rate of 5 mL/hr

c) Distance of 14 cm

d) Pre-saturation of the spinning chamber with acetone for 30 minutes

e) Using a shaker running at a speed of 100 rpm

Porosity is known to play an important role in determining the physical and chemical properties of porous membranes and have a deterministic effect on the performance of these membranes [36]. Measurements of adsorption isotherms, pore size distribution, surface area, and pore volume were carried out for CA (10, 12, 15, 17) membranes made at the above mentioned optimized conditions. Results are shown in Figures 31-34, respectively. These measurements were based on the adsorption of liquid nitrogen on the fibers as well as the walls outlining pores. Due to the randomness of fiber
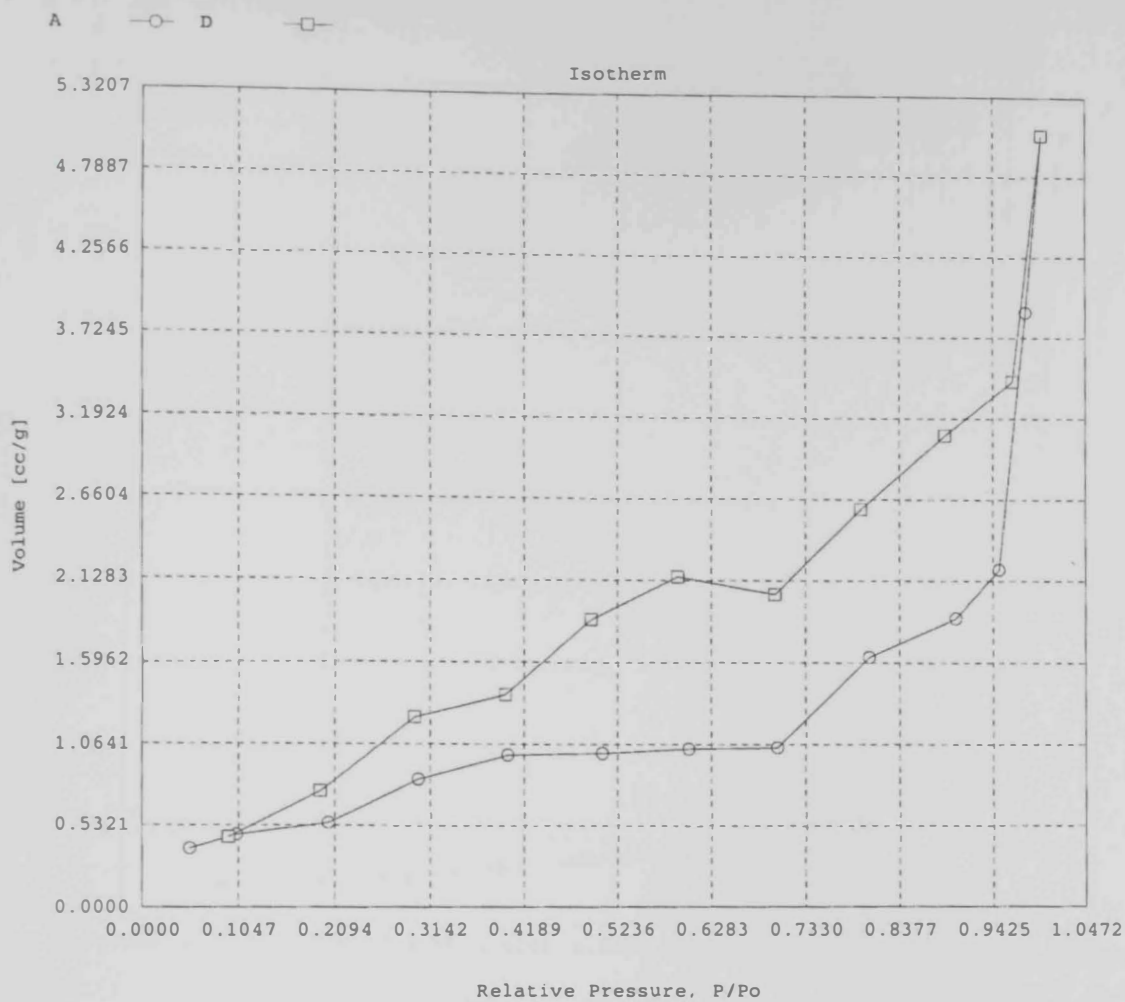
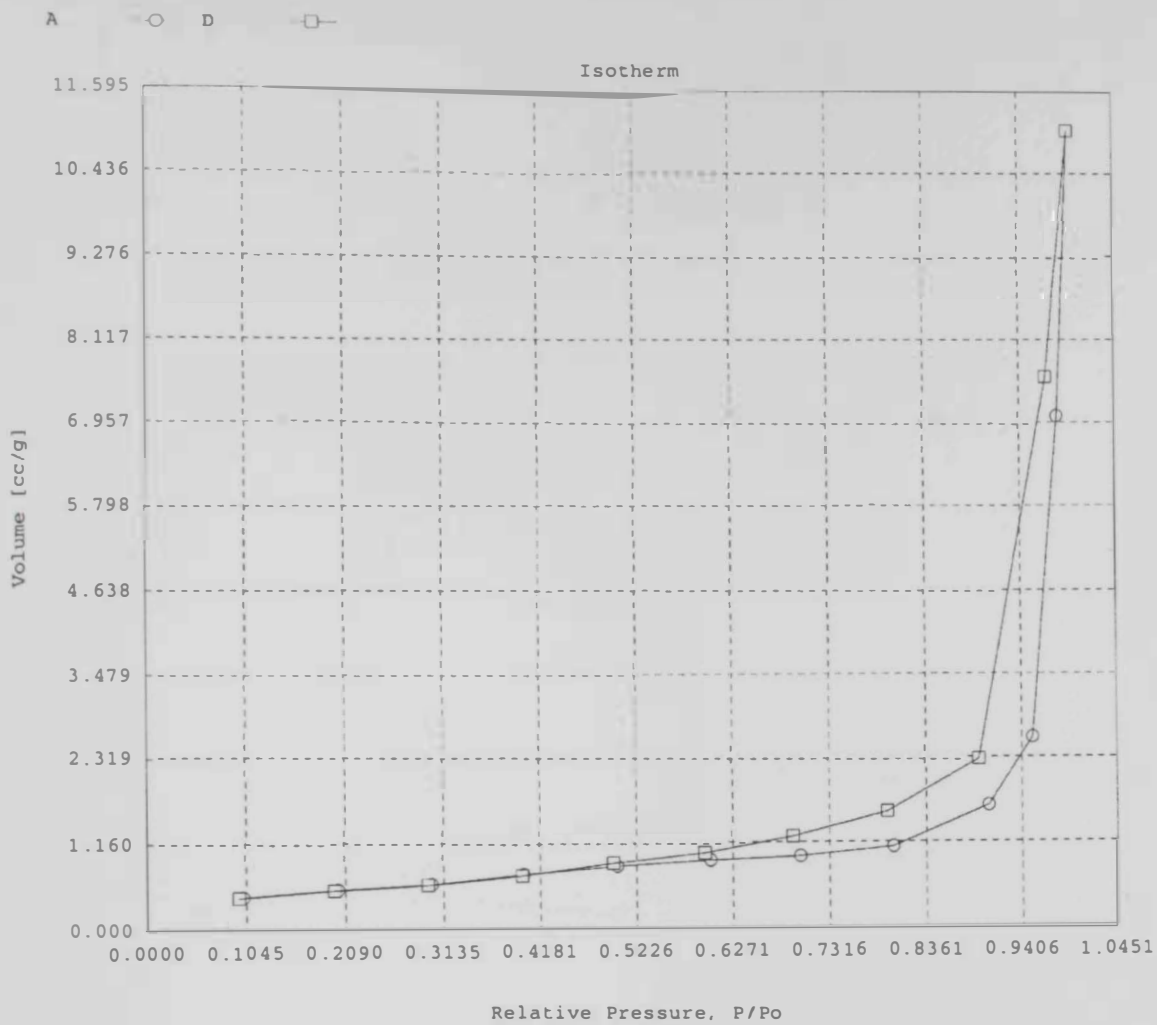Figure 31A. Adsorption-desorption isotherms of CA nanofibers made from solutions containing 10 wt %

Figure 31B. Adsorption-desorption isotherms of CA nanofibers made from solutions
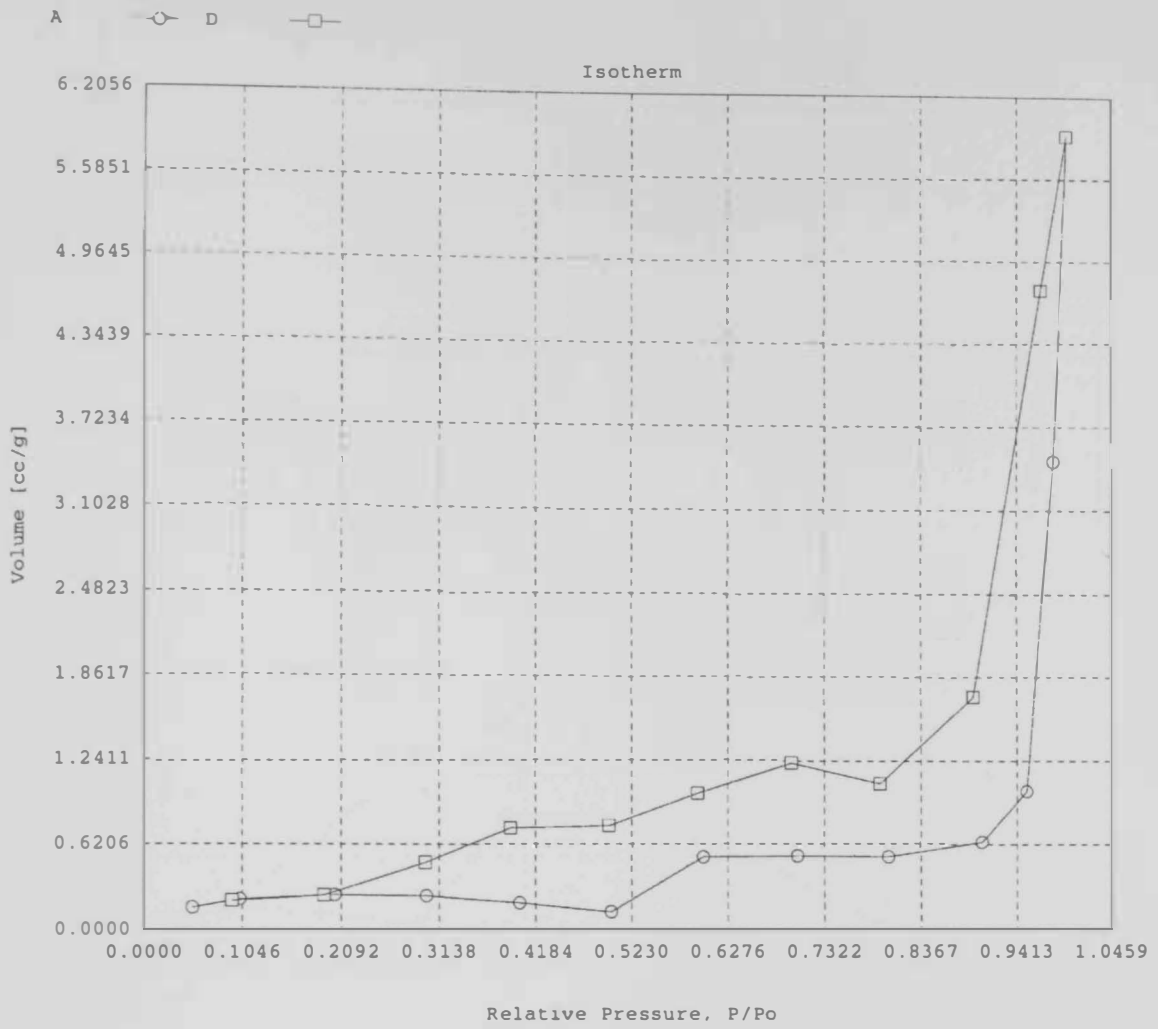containing 10 wt %

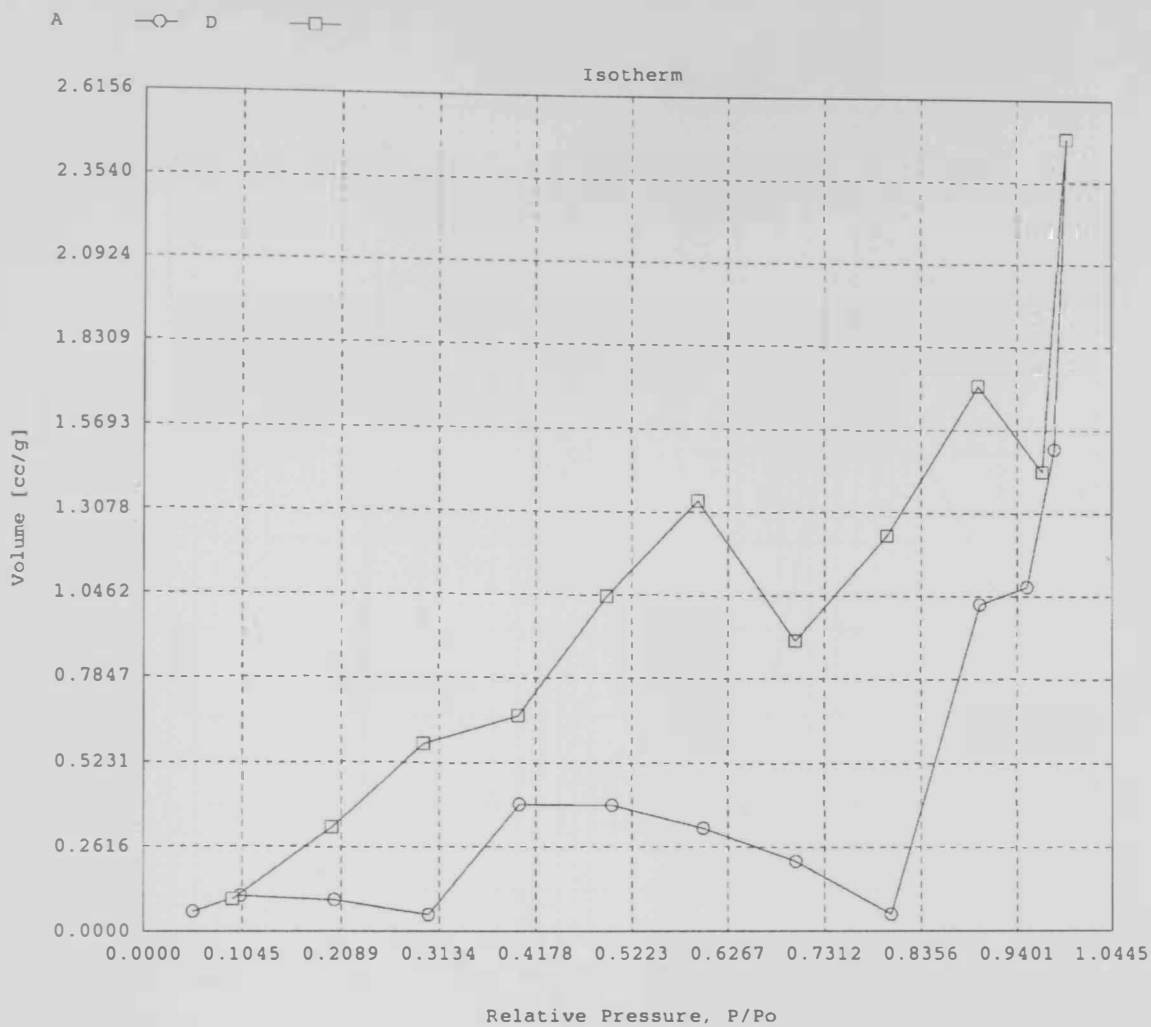Figure 31C. Adsorption-desorption isotherms of CA nanofibers made from solutions containing 10 wt %

Figure 31D. Adsorption-desorption isotherms of CA nanofibers made from solutions
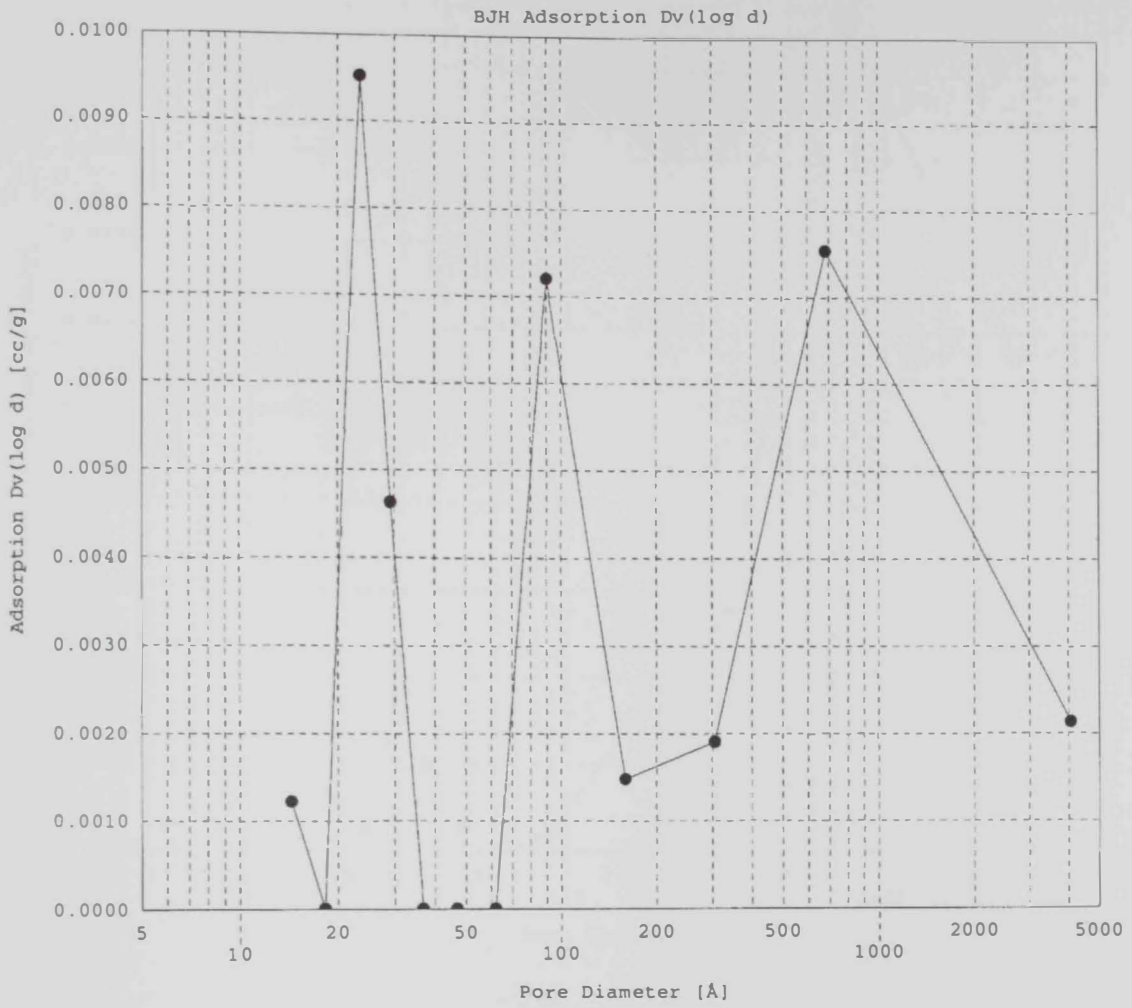containing 10 wt %

Figure 32A. Pore size distribution of CA nanofibers made from solutions containing 10 wt %
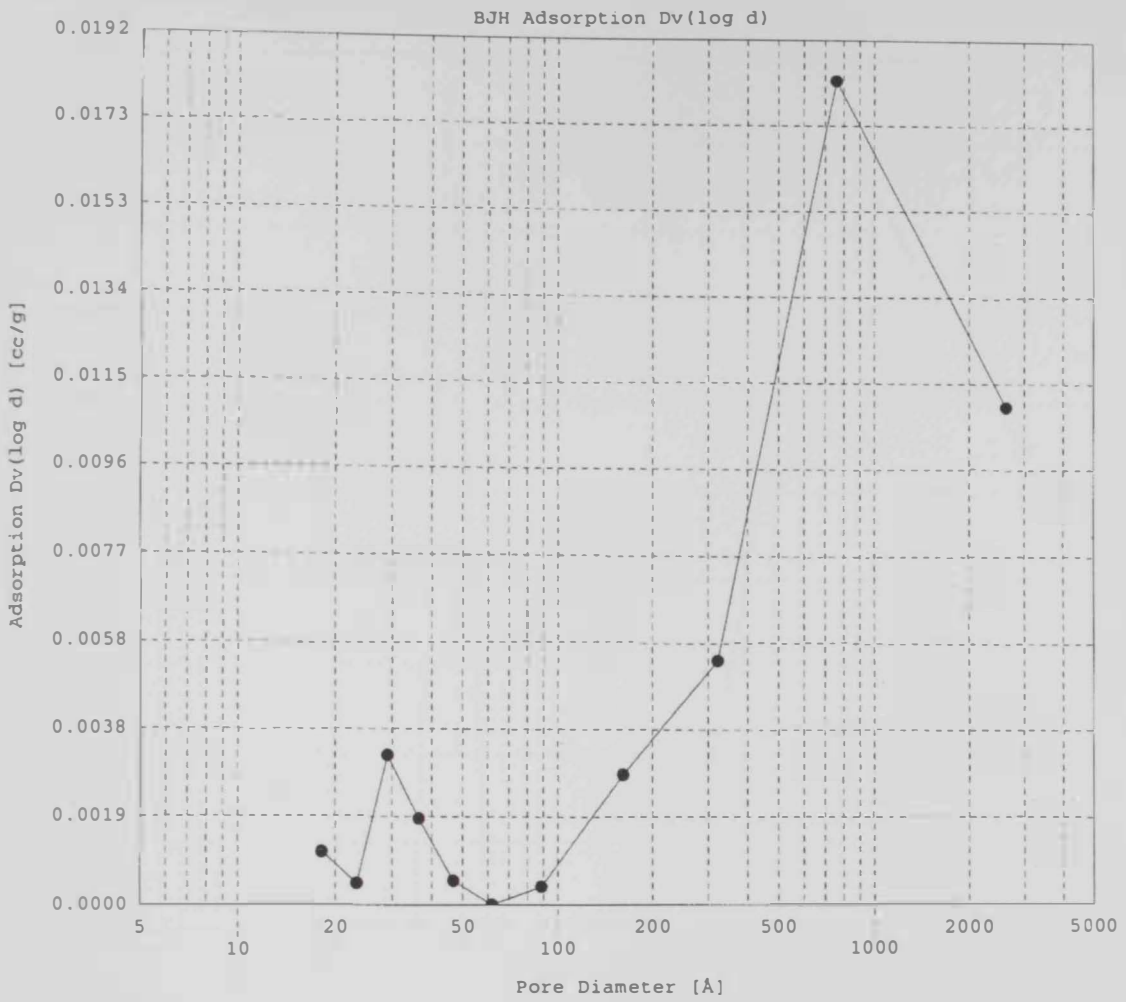
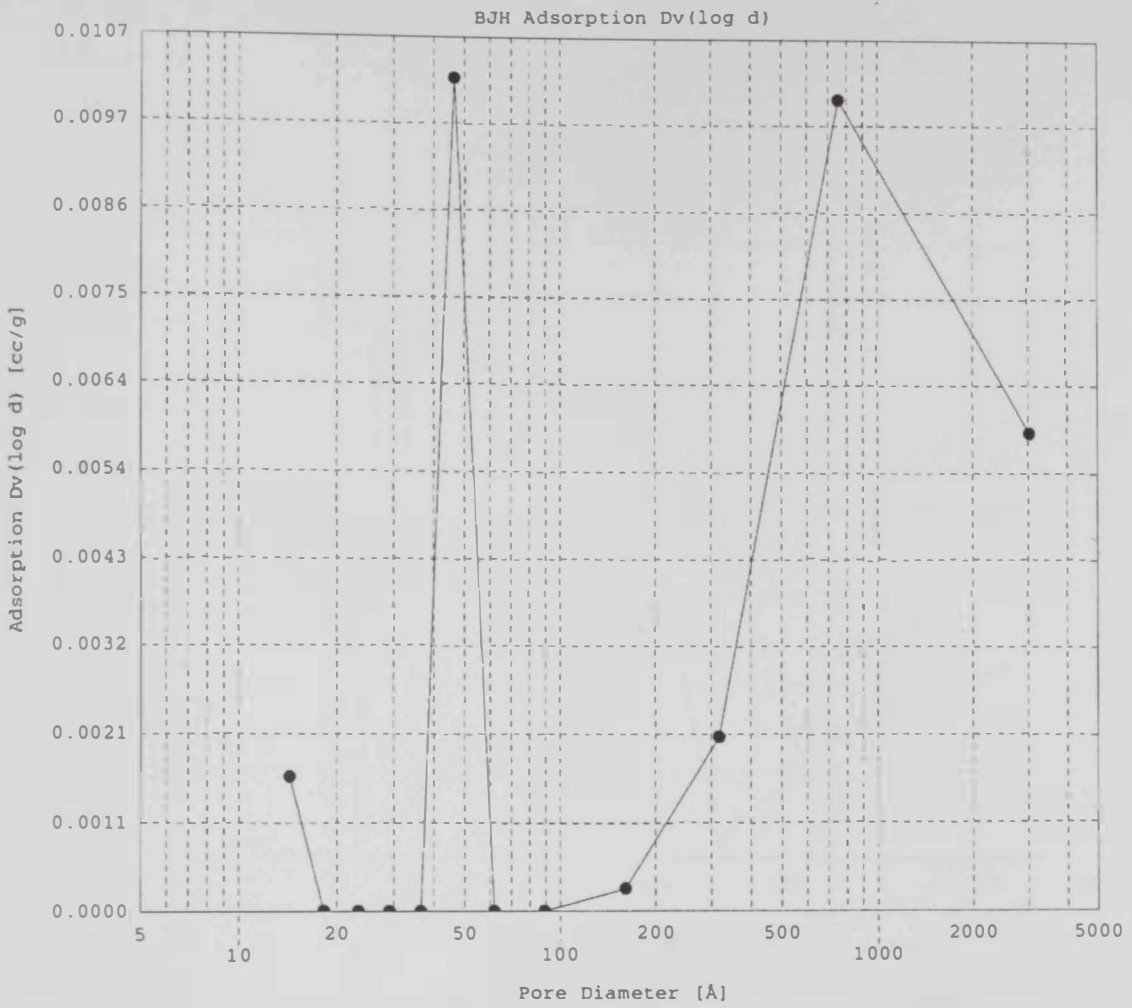Figure 32B. Pore size distribution of CA nanofibers made from solutions containing

12 wt %

Figure 32C. Pore size distribution of CA nanofibers made from solutions containing 15 wt %
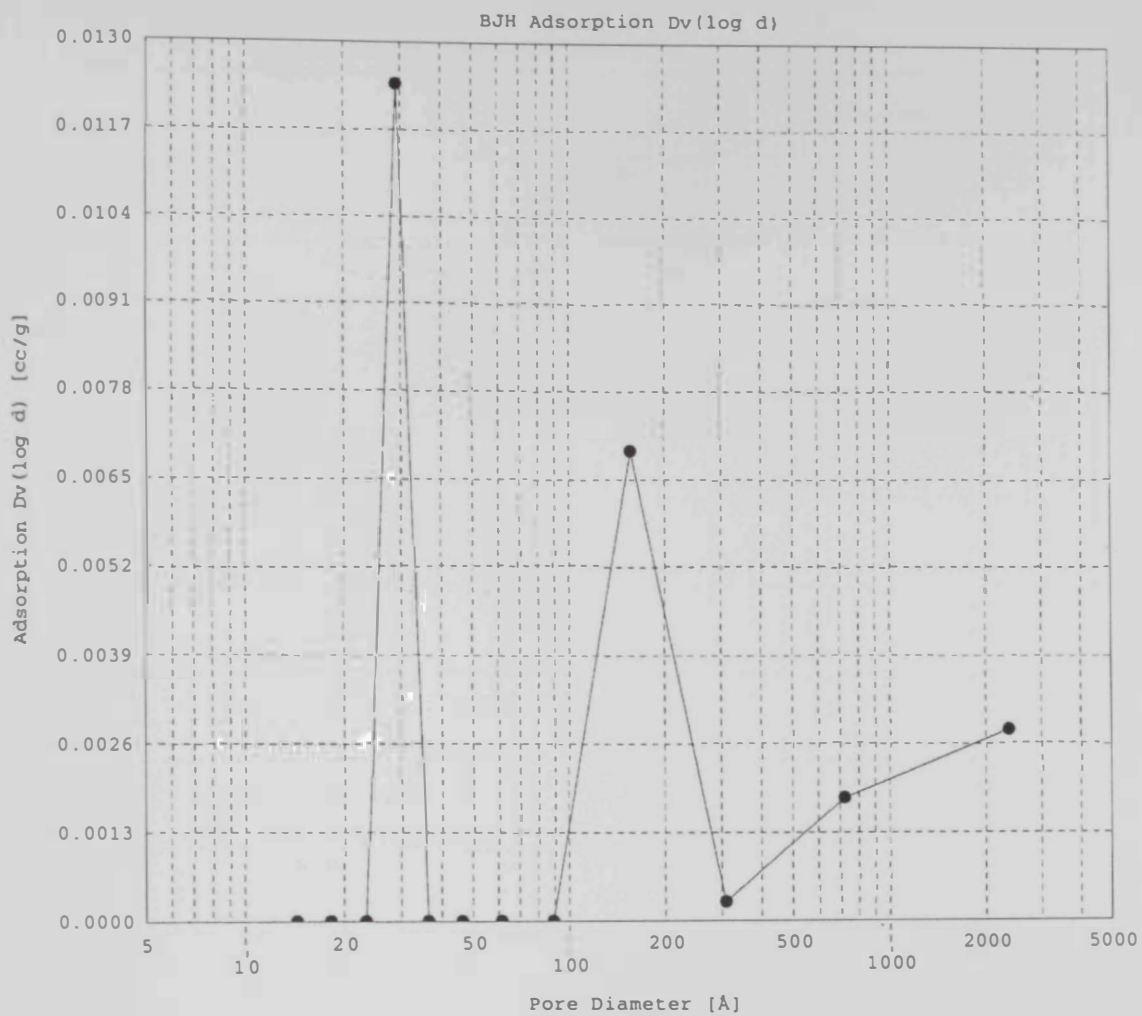
Figure 32D. Pore size distribution of CA nanofibers made from solutions containing
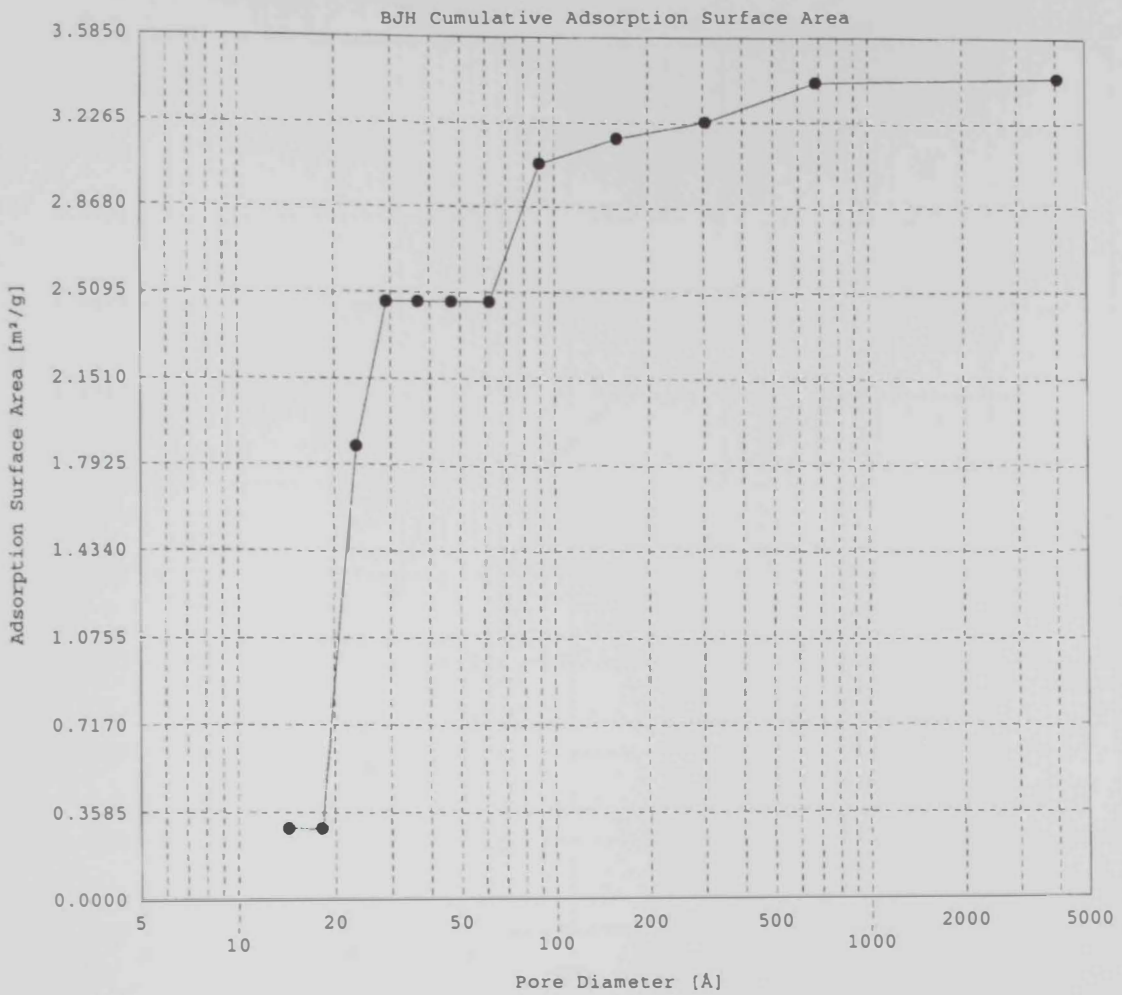
17 wt %

Figure 33A. BET surface area of CA nanofibers made from solutions containing
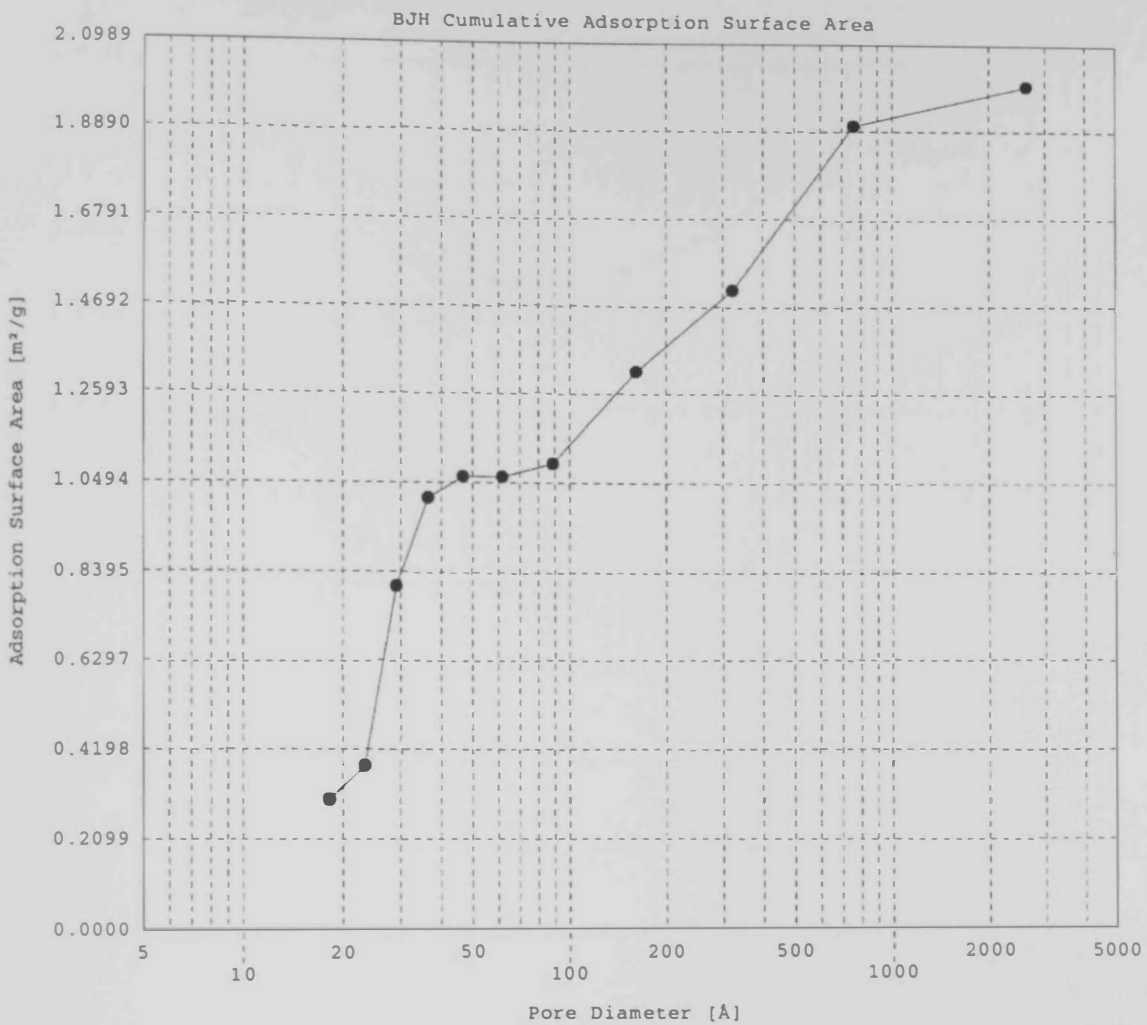10 wt %

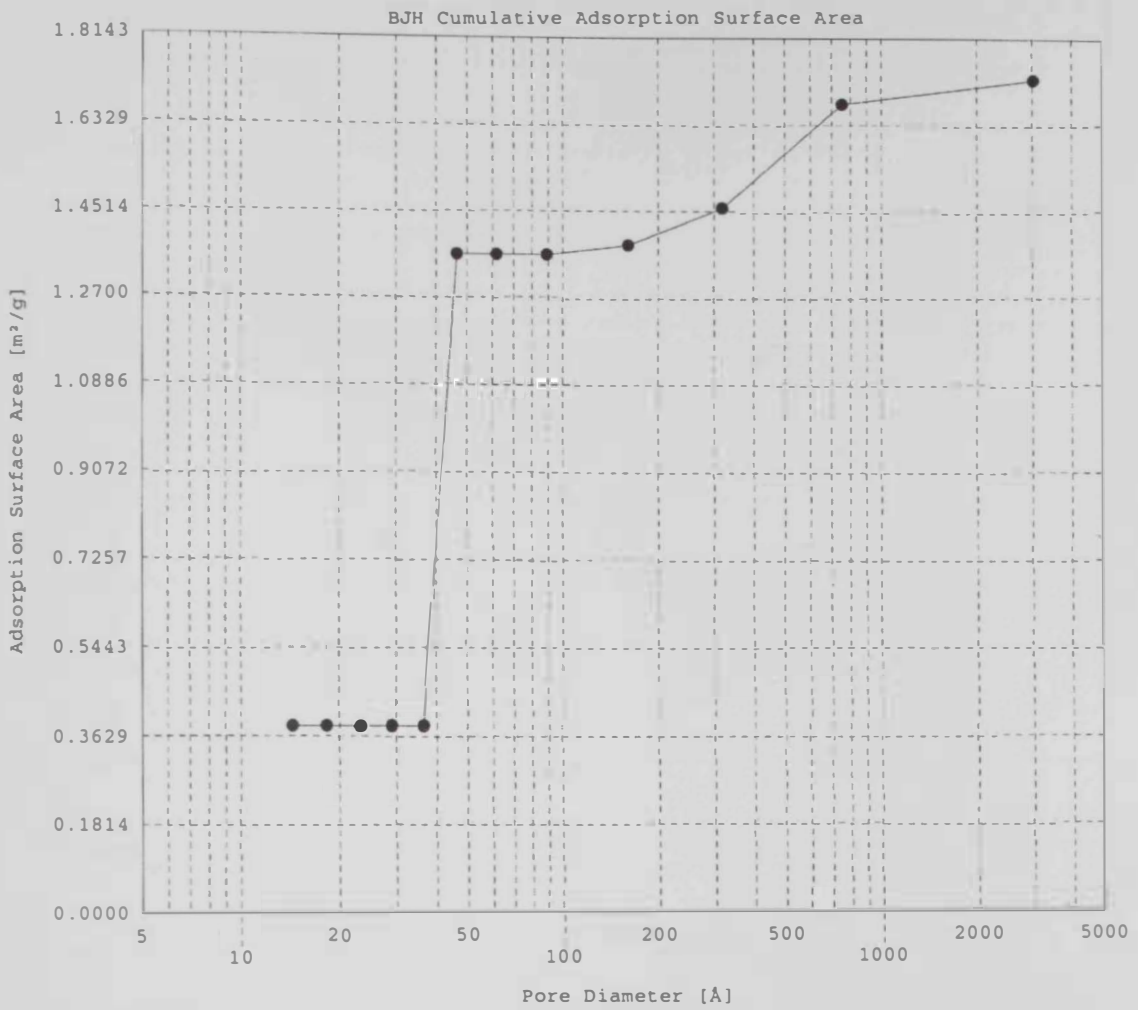Figure 33B. BET surface area of CA nanofibers made from solutions containing 12 wt %

Figure 33C. BET surface area of CA nanofibers made from solutions containing
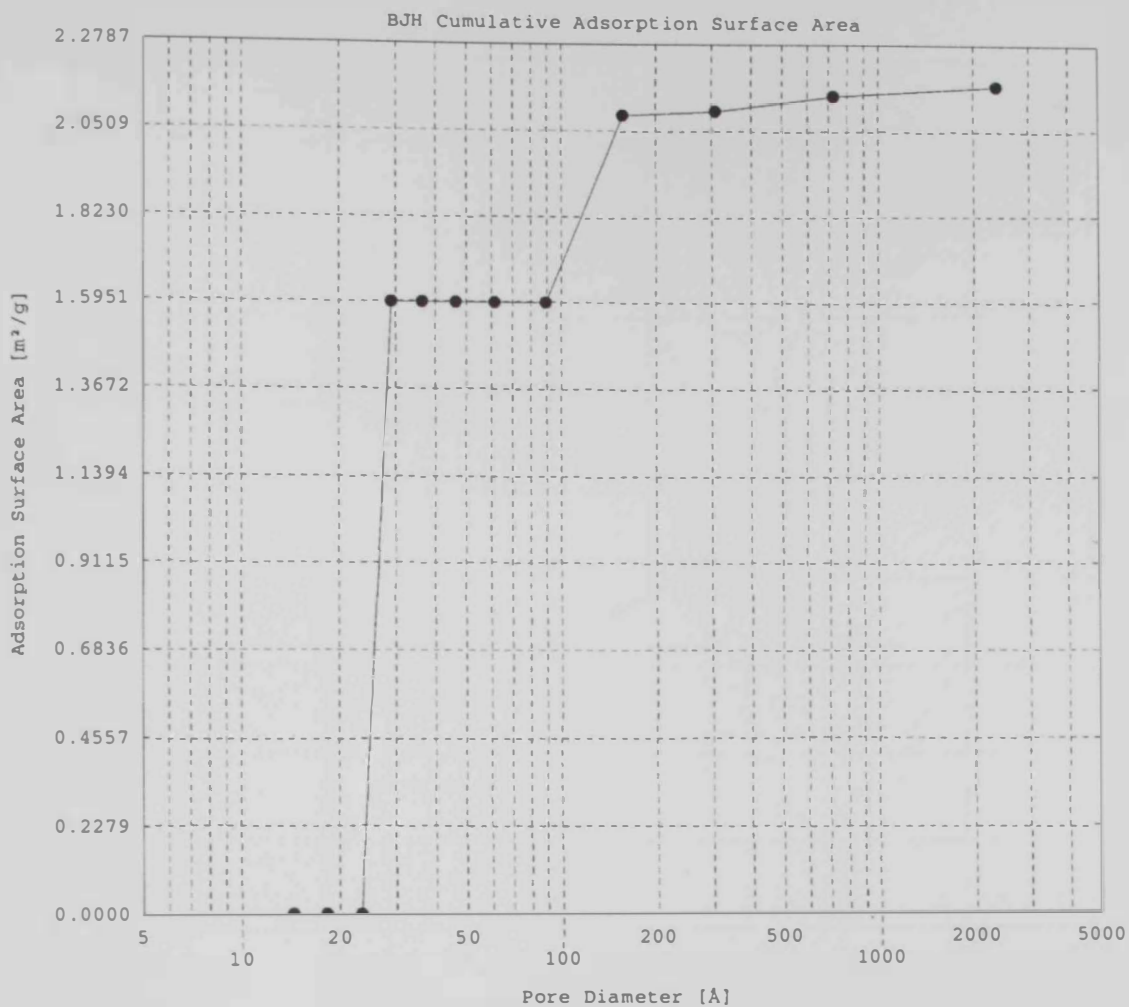
15 wt %

Figure 33D. BET surface area of CA nanofibers made from solutions containing

17 wt %

Figure 34A. Pore volume of CA nanofibers made from solutions containing

10 wt %

Figure 34B. Pore volume of CA nanofibers made from solutions containing
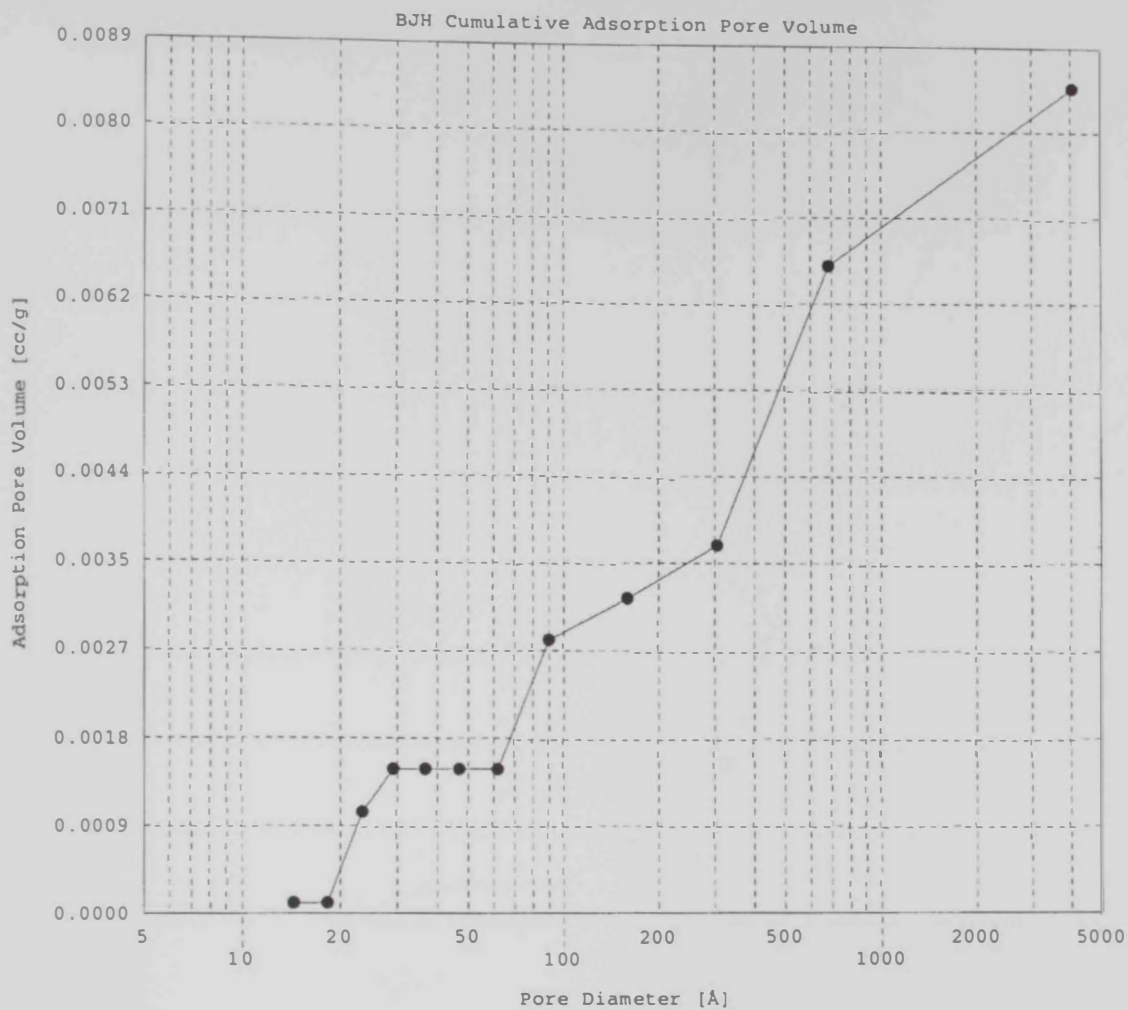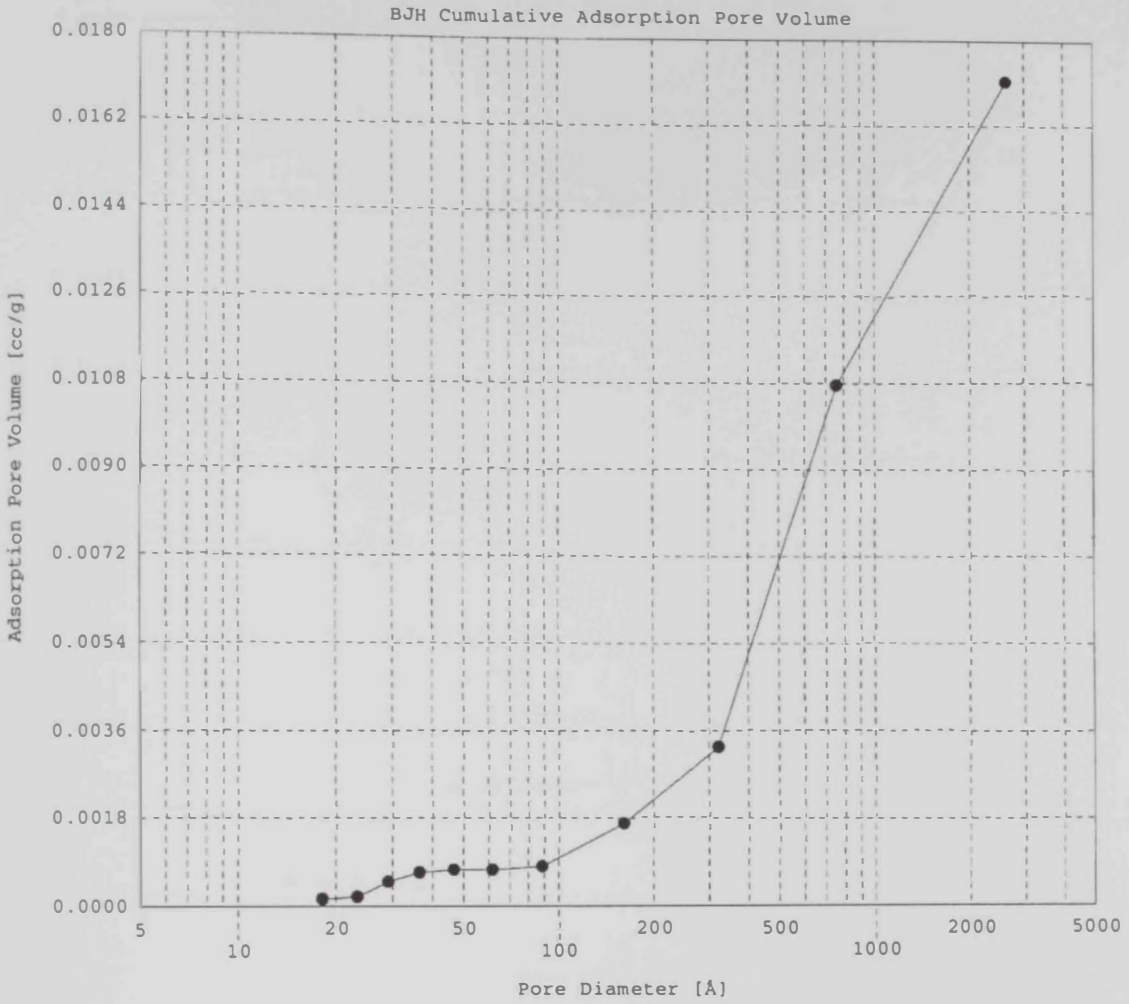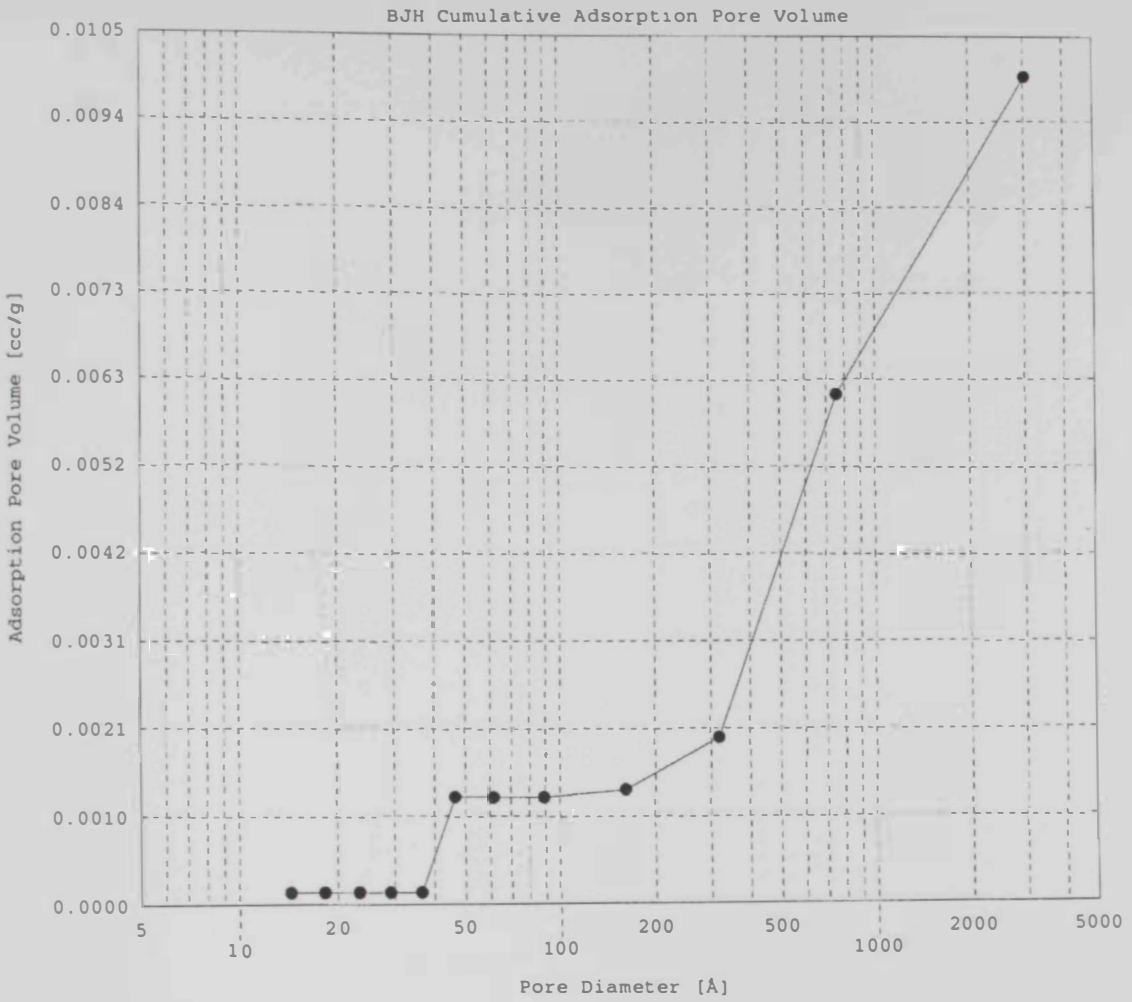12 wt %

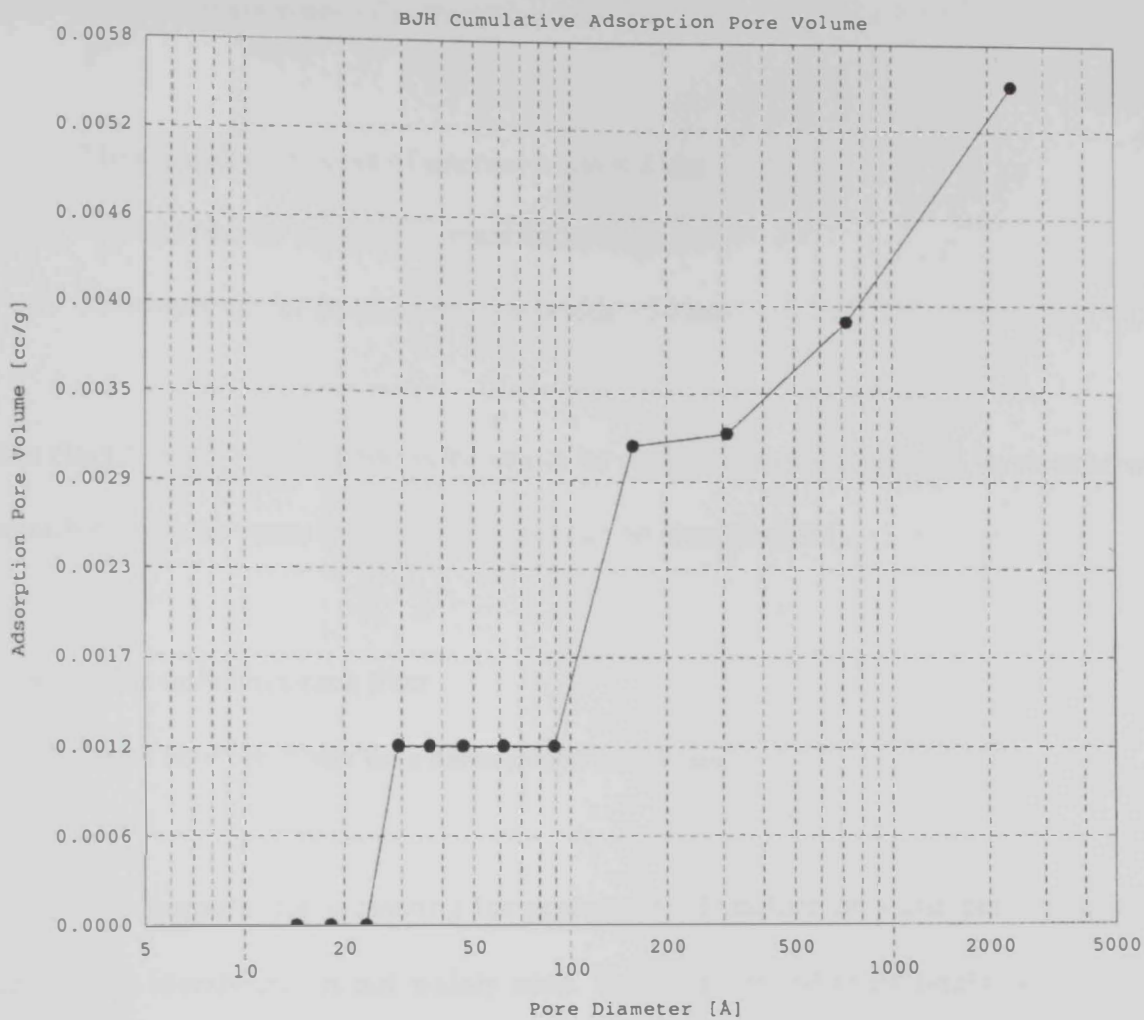Figure 34C. Pore volume of CA nanofibers made from solutions containing

15 wt %

Figure 34D. Pore volume of CA nanofibers made from solutions containing

17 wt %

size and their alignment within the membrane, different types of porosities could be observed. Three main types of porosities are known [130]:

a) **Micropores**; for pores of internal width < 2 nm
b) **Mesopores**; for pores of internal width 2-50 nm
c) **Macropores**; for pores of internal width > 50 nm

This classification of porosities is known to be applied for nano particles. In electrospun nanofibrous membranes, two types of pores can be identified [36]:

a) Pores on/within each fiber
b) Pores between fibers on a nanofibrous membrane

Using N_2 adsorption for measuring the porosity, BET surface area and pore volume of nanofibrous membranes is not widely used. This is attributed to its limitation that it is used to measure pore sizes to a maximum size of 200 nm [36]. Pores with bigger sizes are considered as open space and cannot be accurately quantified by N_2 adsorption methods. Instead Hg-porosimetry methods are used. Based on these facts, the three types of pores; micro-, meso- and macropores, were expected to be found between the nanofibers as a result of their interlocking and can just be accurately quantified. The differences between the adsorption/desorption of the different membranes in Figure 31 is contributed to the different morphologies of the fibers in these membranes and the subsequent variations in the pore types and geometries. The step-like shapes of the isotherms in Figures 31 A, C,D are attributed to the presence of different types and sizes of pores [130]. In contrast, membranes made from solutions containing 12 wt% CA showed a single type/size of

porosity, as indicated by its simple adsorption/desorption isotherm in Figure 31B, indicating its uniform pore distribution, as illustrated by the graphs in Figure 32. Membranes made of 12 wt% CA solutions showed the presence of one major type/size of porosity around 75 nm, while membranes made of other concentrations showed the presence of two or more types/sizes of porosities, mainly the micro- and meso- types. Based on the SEM results of these membranes at high magnifications, it was evident that the formed fibers had smooth surfaces without noticeable surface topographies such as surface porosity. Therefore, the current results are only attributed to porosities arising from the interlocking and overlap of the deposited fibers. Due to the limited sensitivity of the technique used in these experiments to pores with diameters beyond 200 nm, the BET surface area and pore volume data extracted from Figures 33, 34 of all samples were only limited to a maximum pore diameter of 200 nm. Both BET surface area and pore volume results are given in Table 3.

The apparent bulk density and % porosity of membranes prepared at the above optimized conditions of electrospinning are shown in Figure 35. The increase in density with the concentration of CA in these membranes represents a normal trend, where more polymer is being deposited at the same electrospinning conditions. Comparing the density values of all membranes with the theoretical density of CA (1.3 g/cm^3) shows that the prepared membranes are highly porous. This was confirmed by measuring the % porosity of these membranes. A maximum % porosity of 94.2 was obtained for CA 10 membrane. This high porosity, together with the interconnectivity of these nano-to-micro pores highly recommend these membranes for filtration applications.

Table 3. BET surface area and pore volume of as-spun nanofibrous membranes

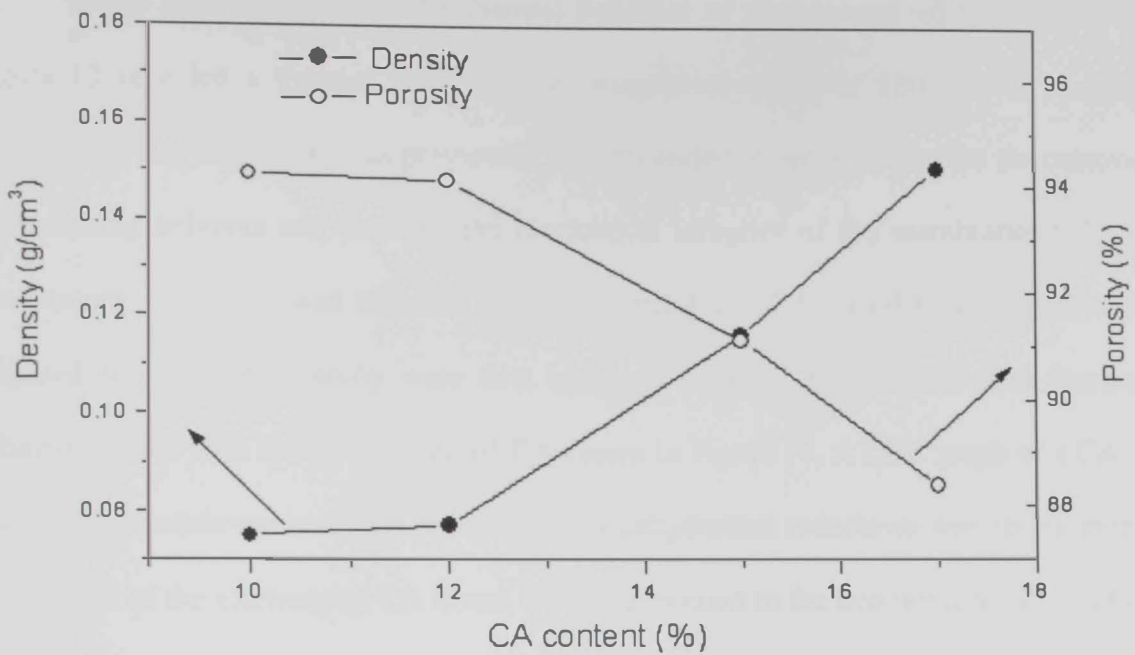| Weight % of CA	10	12	15	17
BET surface area (m^2/g)	3.4	1.95	1.75	2.15
Pore volume ($\times 10^3$ cc/g)	7.50	15.5	8.90	5.30

Figure 35. Apparent bulk density and percent porosity of CA (10-17) nanofibrous membranes

IV.7 Thermal treatment of CA nanofibrous membranes:

Initial DSC analysis for the thermal behavior of the as-received CA, shown in Figure 10 revealed a thermal stability at a temperature range of 180-236°C. Thermal treatment of CA nanofibers was previously recommended in order to confirm the removal of remaining solvents and improve the mechanical integrity of the membranes [12]. A temperature of 208°C was selected in this regard [12]. CA nanofibrous membranes prepared in the current study were first analyzed by DSC to compare their thermal behavior results with that of as-received CA shown in Figure 10. A DSC graph of a CA12 nanofibrous membrane is shown in Figure 36. A dehydration endotherm was absent in the DSC graph of the electrospun CA fibers. This is attributed to the evolution of all water of hydration as a result of drying these membranes at 100°C for 24 hours before carrying out its DSC testing. A couple of endotherms were observed between 190 and 235°C. The last endotherm, at 230°C, is attributed to the melting temperature (T_m) of CA, which is in accordance with that observed for as-received CA; Figure 10. The three endotherms at 190, 208 and 215°C are, therefore, attributed to a series of events taking place at these temperatures before melting of the fibers. These events were explained based on detailed thermal investigation of these samples, as will be shown later in this section. Figure 36B shows a glass transition temperature (T_g) of around 186°C, which is slightly higher than that of the as-received CA shown in Figure 10B. A final conclusion in this respect is the absence of any thermal events at temperatures below 186°C, indicating its expected stability up to this temperature. In fact, at temperatures below the melting temperature of CA, the chemical structure stability of CA is presumably constant.

Infrared investigation of CA 10-17 membranes that were thermally treated at 208°C, was carried out to study the structure stability of the produced membranes. Results
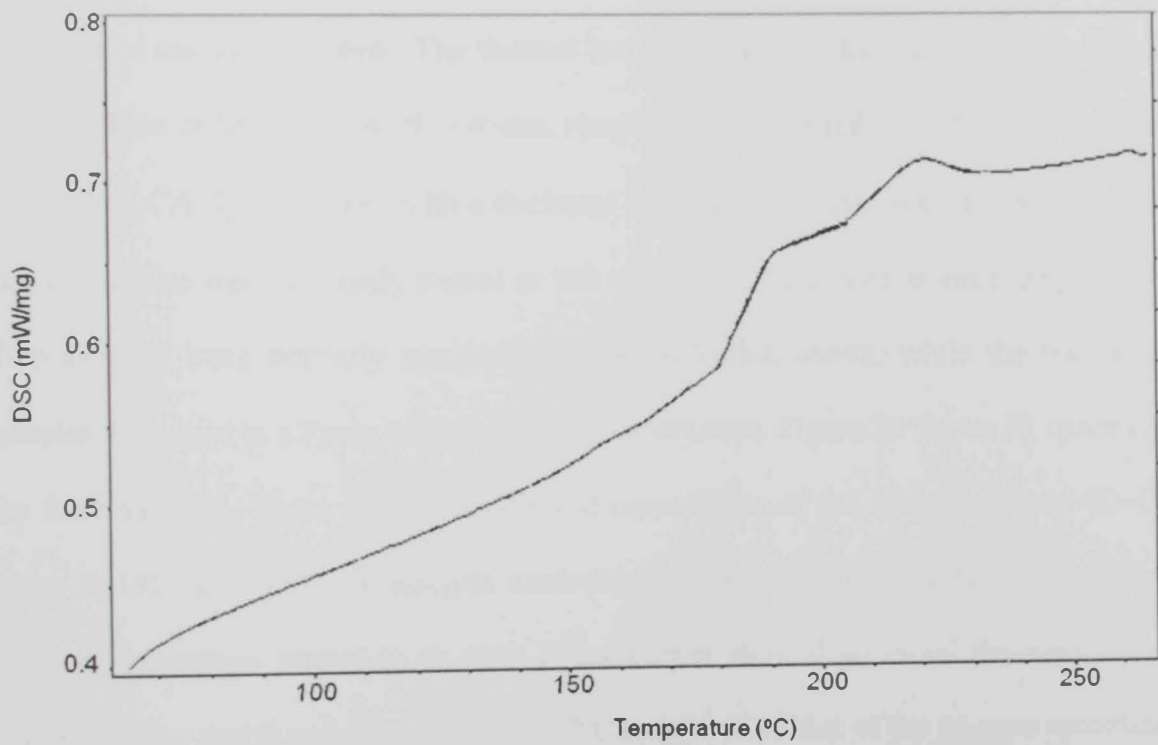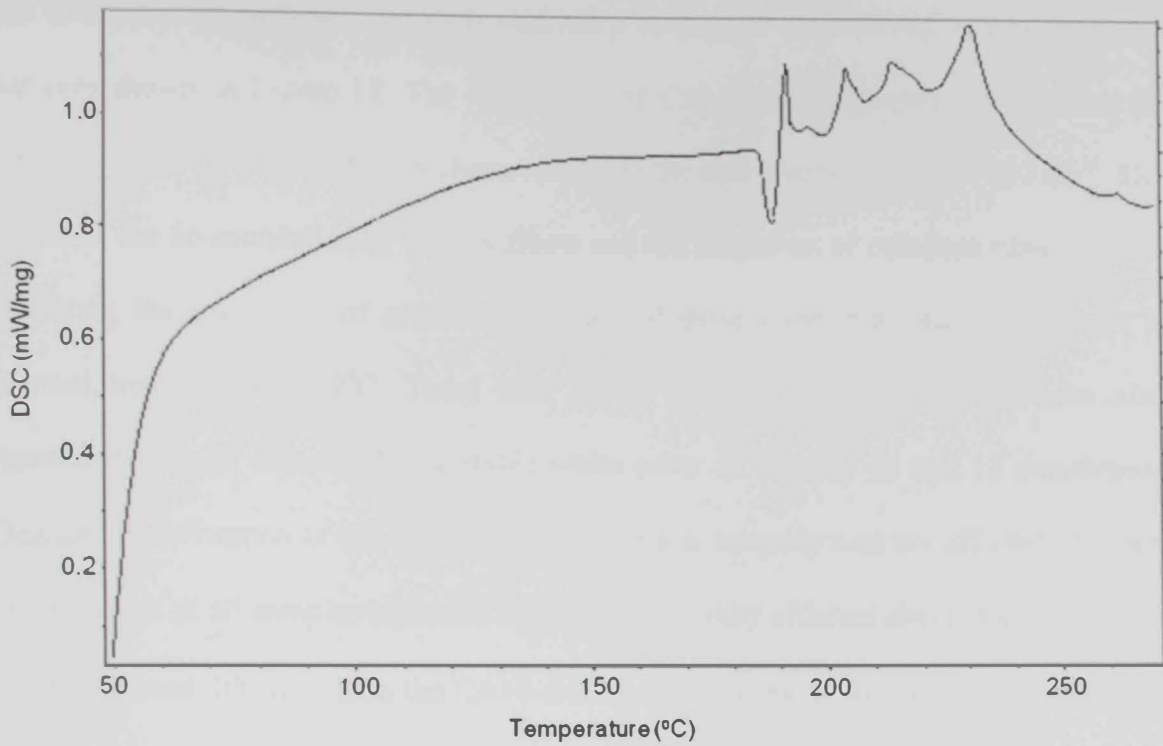
Figure 36. DSC spectrum of as-electrospun CA from a solution containing 12 wt%

are shown in Figure 37. The IR spectra of CA 10 and 12 illustrate the thermal stability of the CA fibers as indicated by their similarity to that of as received and as spun CA samples shown in Figure 18. The IR spectra of CA 15 and 17, however, reflected the absence of the C=O group that is characteristic to the acetyl group around 1750 cm^{-1}. This indicates the de-acetylation of the CA fibers and the formation of cellulose fibers instead, reflecting the instability of membranes made of these concentrations in particular to thermal treatment at 208°C. These later sheets showed brownish yellow color after thermal treatment, compared to a stable white color of the CA 10 and 12 membranes. Despite this coloration of the sheets, their mechanical integrity was not affected. A closer investigation of all samples indicated that those thermally affected sheets were originally thinner (around 100 μm) than the CA10 and 12 membranes. It should be mentioned that each membrane was originally sandwiched between 3 mm Teflon sheets to avoid direct exposure of the sheets to heat. The thermal instability is, therefore, attributed to a local concentration of heat on these thin sheets, resulting in their instability. To confirm these findings, A CA12 membrane, with a thickness of around 100 μm, was cut to four equal sections. These were thermally treated at 150 and 200°C for 1 hour at each temperature. Two samples were similarly sandwiched between Teflon sheets, while the two other samples were kept in a Pyrex beaker at these temperatures. Figure 38 shows IR spectra of the fours samples. These spectra show the disappearance of the acetyl carbonyl (C=O) group at 150° and 200°C in samples sandwiched between Teflon sheets. On the other hand, those samples treated in an open Pyrex beaker showed an initial decrease in the intensity of the acetyl carbonyl group at 150°C compared to that of the as-spun spectrum. This band showed a further decrease in intensity by raising the temperature to 200°C. These results are therefore in agreement with those obtained for the CA 15 and 17 samples previously shown in Figure 37.
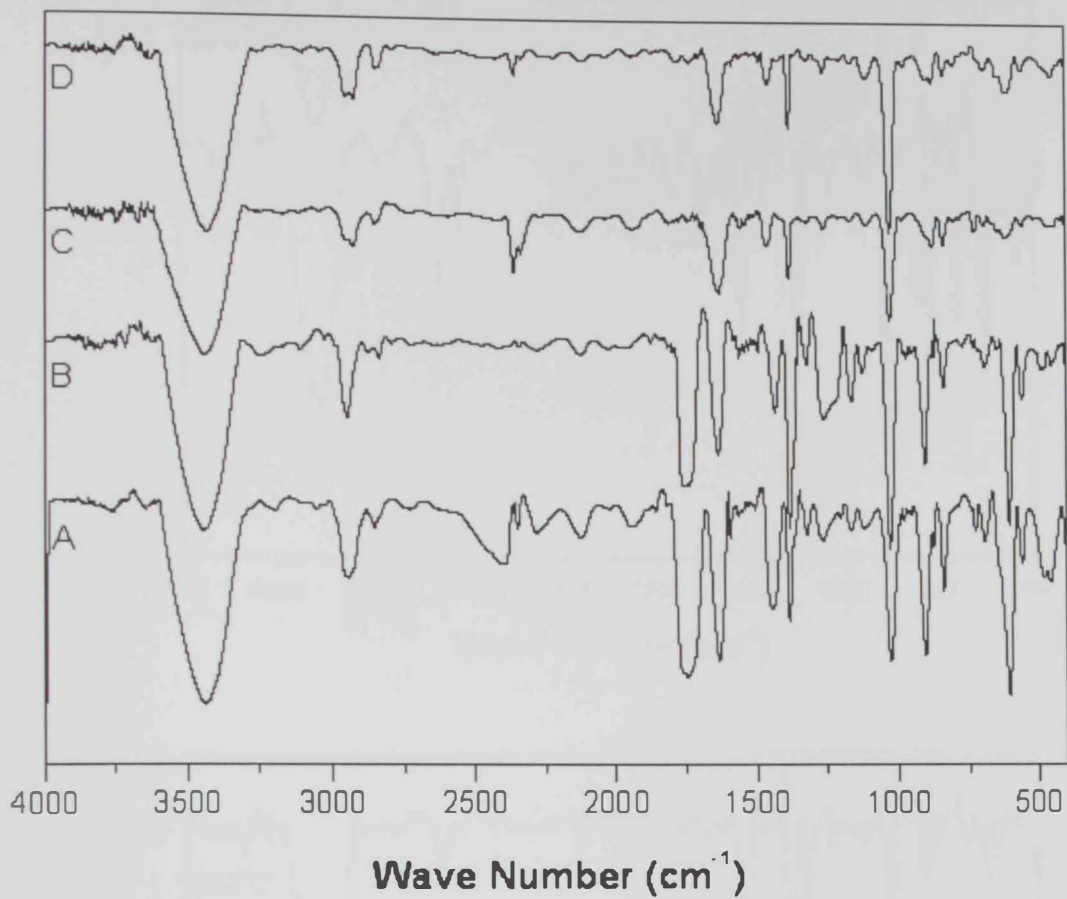
Figure 37. IR spectra of CA nanofibrous membranes containing A) 10, B) 12, C) 15 and D) 17 wt % After thermal treatment at 208°C for 1 hour
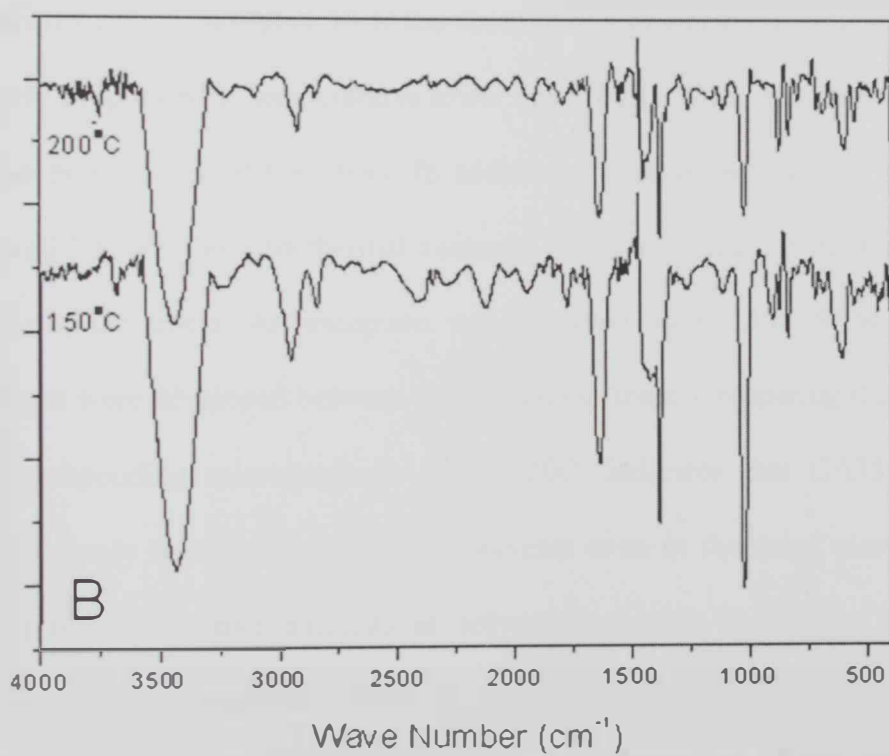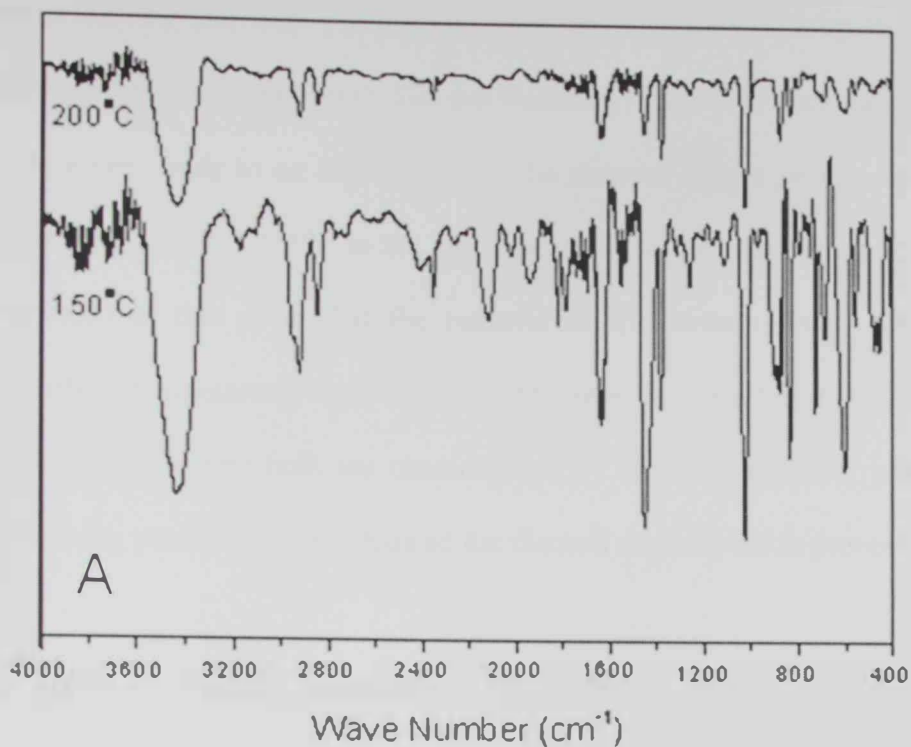
Figure 38. IR spectra of CA nanofibrous membranes made from a solution containing 12 wt% and thermally treated in A) sandwiched between Teflon sheets, and B) open Pyrex beaker at 150, 200°C for both

These findings indicate that what was known as thermal stability of CA up to 208°C [12], was most probably of thick samples (> 100 μm thickness). Careful investigation of the IR outcomes, therefore, leads to an explanation of the thermal events previously shown as endotherms at 190, 208 and 215°C in the DSC spectrum of CA nanofibers; Figure 36. It can be concluded at this point that the removal of the acetate group from the CA nanofibers starts at temperatures right below 190°C, especially in thin membranes and/or small CA nanofibers, where both are characterized by high surface area, which can be considered a strong parameter that enhanced the thermal de-acetylation process.

The effect of thermal treatment at 208°C on the morphology of CA 10-17 membranes is shown in the SEM micrographs in Figure 39. The common feature between the micrographs shown in Figure 39 is the absence of signs of remaining solvents as all solvents were evaporated at temperatures lower than 208°C. This, however, is not shown to affect the morphology of the fibers. In addition, the observed removal of the acetyl group from all CA samples after thermal treatment at 208°C, is neither shown to affect the morphology of the fibers. An exception was observed with CA15 SEM micrograph, where linkages were developed between the remaining fibers. Comparing this micrograph with its corresponding micrograph in Figure 20C, indicates that CA15 membranes contained relatively higher amounts of the solvents even in the dried membranes. The presence of these excessive amounts of solvents is highly thought to result in the formation of linkages between fibers, as observed in Figure 39C. The fiber size distribution of these micrographs is summarized in Figure 40. After removal of all solvents from the studied membranes, it is evident from Figure 40 graphs that finer fibers were obtained in membranes containing 10, 12 wt% CA compared to higher concentrations.
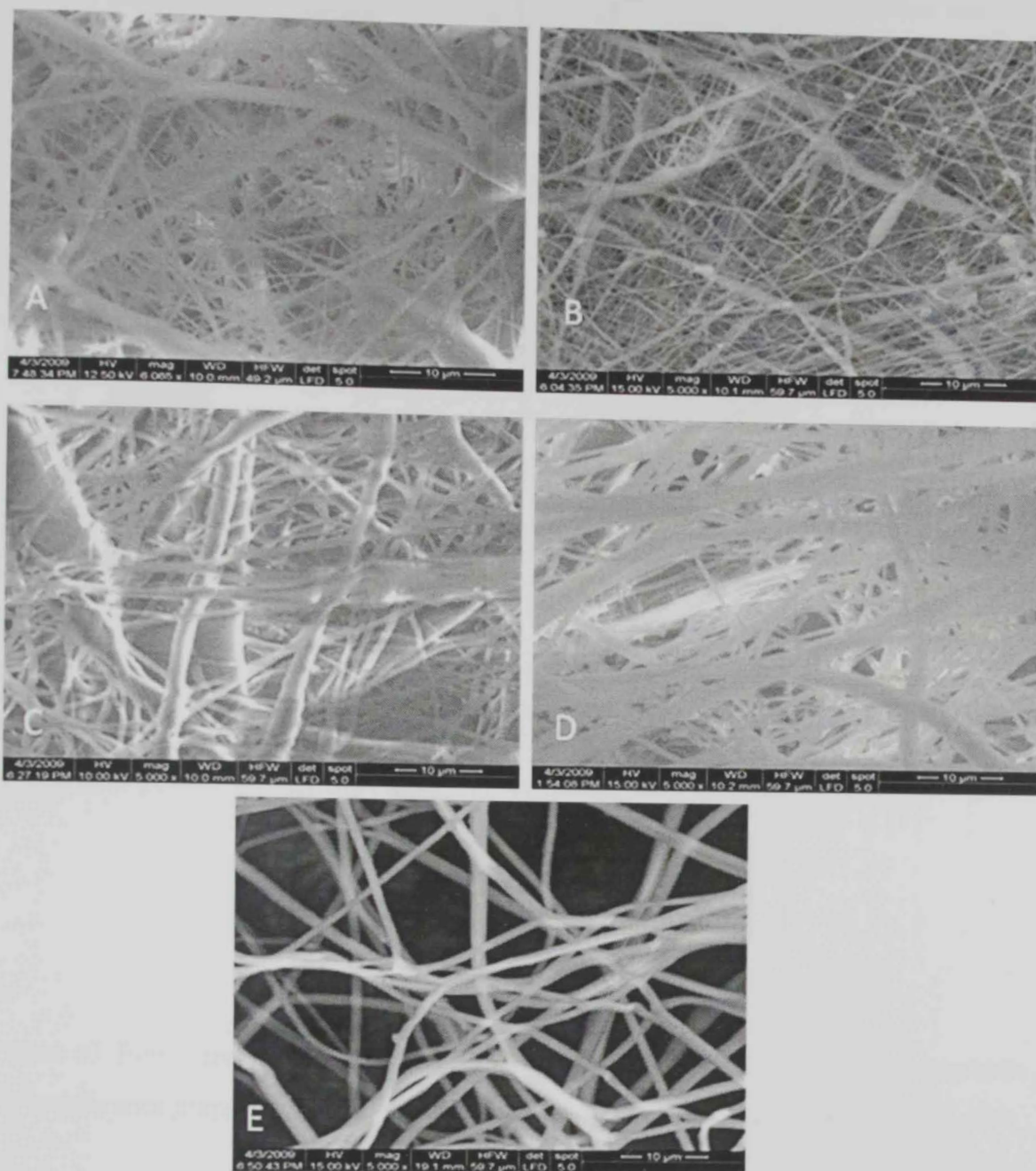
Figure 39. SEM micrographs of CA nanofibrous membranes prepared from A) 10, B) 12, C) 15, D) 17 and E) 20 wt% solutions, after thermal treatment at 208°C for 1 hour
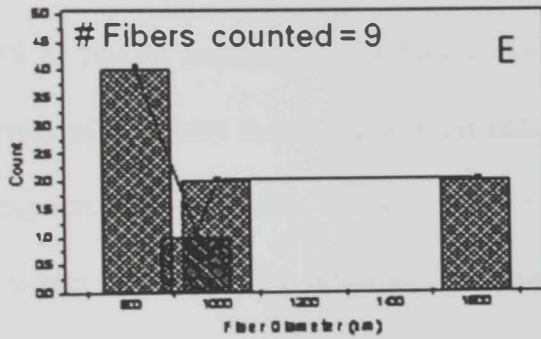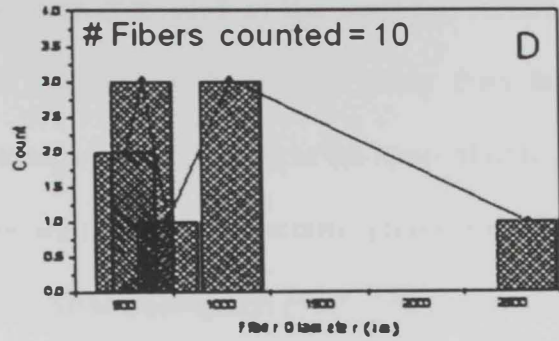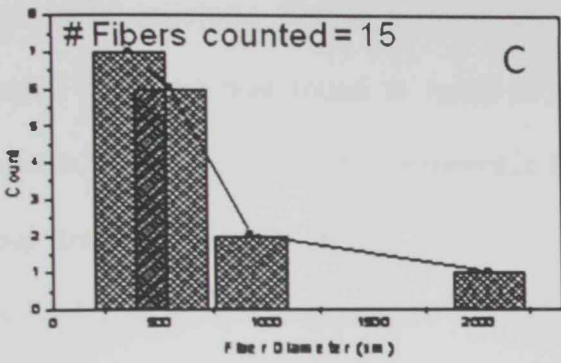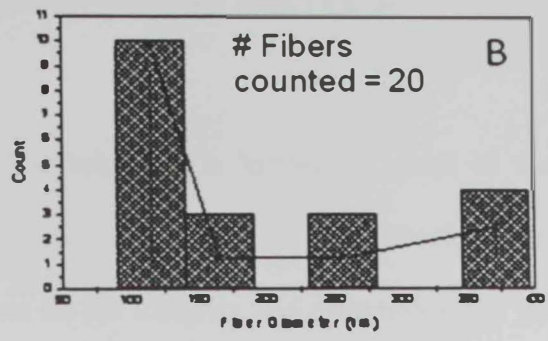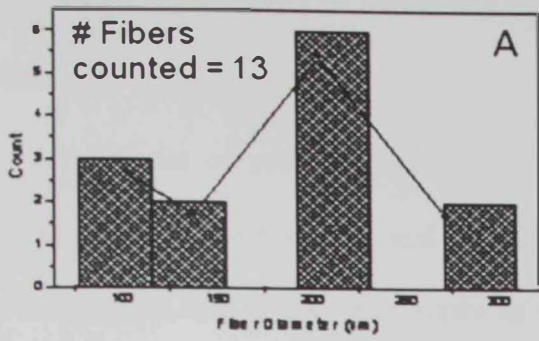
Figure 40. Fiber-size distribution obtained by an image analysis of the SEM micrographs of membranes prepared from A) 10, B) 12, C) 15, D) 17 and E) 20 wt% solutions, after thermal treatment at 208°C for 1 hour

IV.8 Alkali treatment of cellulose acetate nanofibers and regeneration of cellulose:

Treatment of cellulose acetate in alkaline solutions is known to result in the removal of the acetate groups and the regeneration of cellulose [113]. Therefore, the objective of this step was to investigate its effect on the integrity and morphology of the regenerated cellulosic fibrous membranes. As was discussed in the previous section, thermal treatment was found to result in the removal of the acetate group from the structure. Therefore, the first experiment in this regard was to confirm the removal of this group from a thermally treated membrane in which traces of acetate group was still observed in its IR spectrum. Figure 41A shows a SEM micrograph of a CA12 membrane, 100 μm thickness, that was sandwiched between Teflon sheets, thermally treated at 208°C followed by soaking in 0.5 M NaOH solution for 24 hours, then completely dried at 100°C for 24 hours. Distortion of the fibers morphology is the main observation that can be implied from the micrograph. However, this was not found to affect the structural stability of the membranes where its IR spectrum revealed the presence of cellulose as the only phase; Figure 41B.

These findings indicate that regeneration of cellulose from thermally treated may take place completely but on the expense of the quality of the fibers morphology. Based on the main objectives of the current studies, the formation of high quality cellulose fibrous membranes is the optimum goal. Therefore, regeneration of cellulose was decided to be carried out on fibrous membranes that were only dried at 100°C without further thermal treatment. As a result of the alkali treatment, the volume of un-reacted NaOH was determined by titrating the remaining NaOH against a standard 0.5M HCl solution. Figure
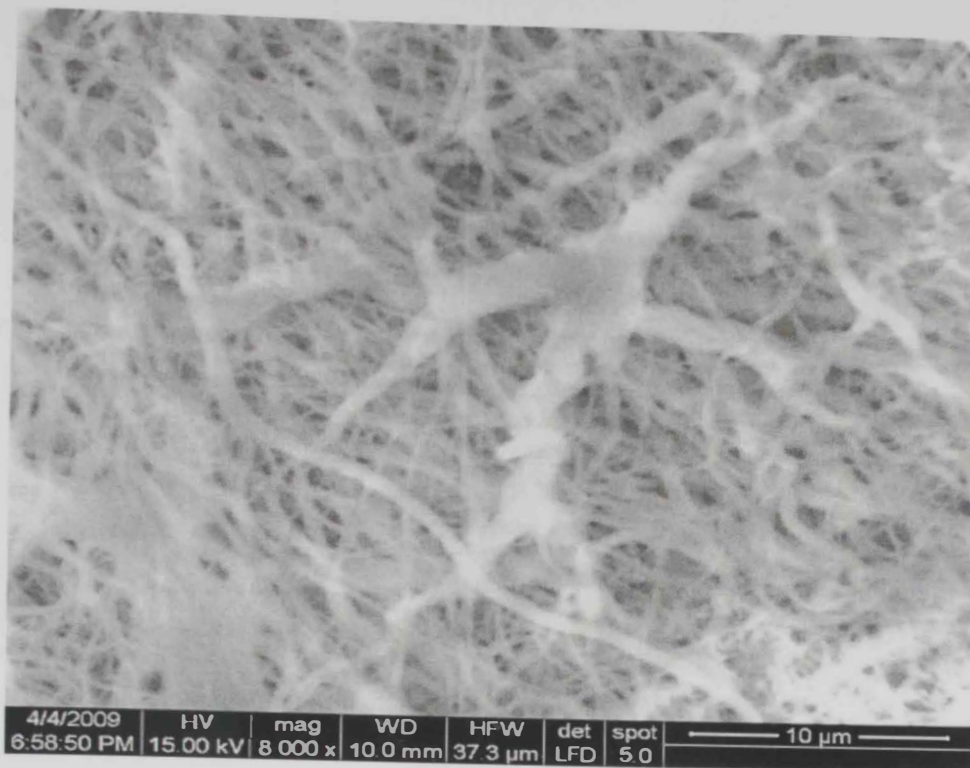
Figure 41A. SEM micrograph of a CA nanofibrous membrane made from a solution containing 12 wt% after Thermally treated at 208°C for 1 hour followed by alkali treatment in a 0.5 M NaOH solution for 24 hours
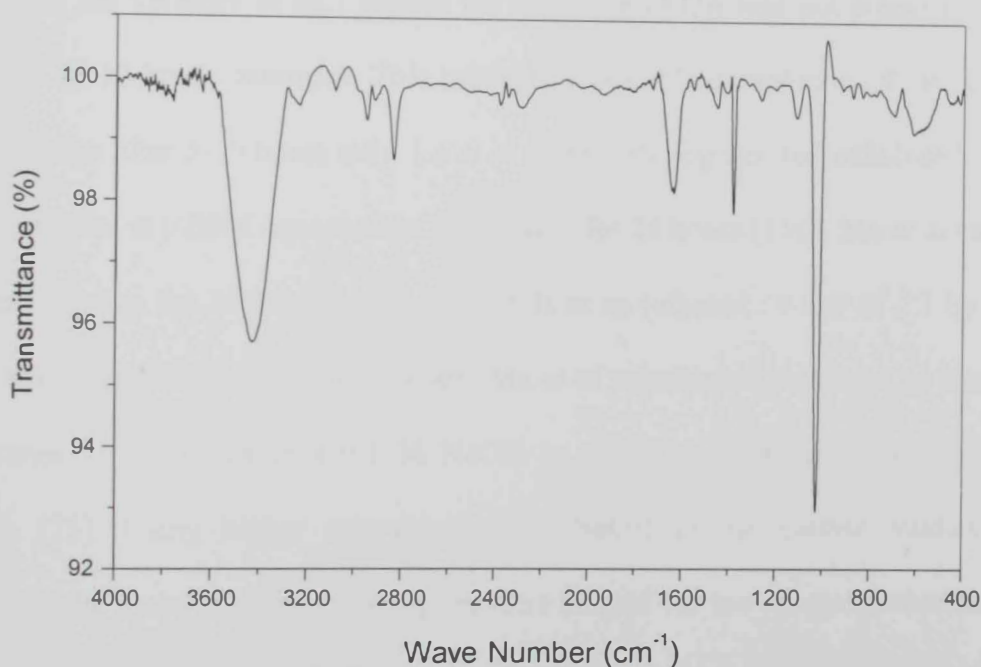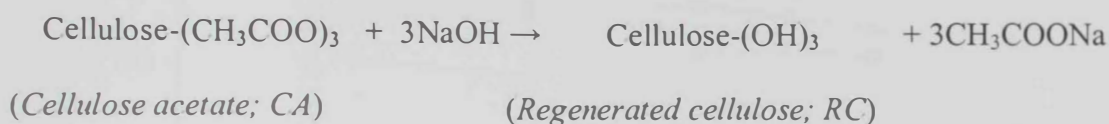

Figure 41B. IR spectrum of a CA nanofibrous membrane made from a solution containing 12 wt% after Thermally treated at 208°C for 1 hour followed by alkali treatment in a 0.5 M NaOH solution for 24 hours

42 shows the volumes of HCl needed to neutralize the un-reacted NaOH in each of the alkaline solutions after each time period of soaking the different membranes in them. All samples showed a decrease in the volume of HCl needed to neutralize the remaining NaOH compared to the standard membrane-free titrations. This decrease is attributed to the consumption of variable amounts of NaOH for the removal of acetate groups from the CA structure, and the consequent regeneration of cellulose. This takes place according to the following reaction:

$$\text{Cellulose-}(CH_3COO)_3 + 3NaOH \rightarrow \text{Cellulose-}(OH)_3 + 3CH_3COONa$$

(Cellulose acetate; CA)   *(Regenerated cellulose; RC)*

The difference in the volumes consumed between the various types of membranes may be attributed to the original difference in their weights. It should be mentioned that the variation of the volumes of HCl needed for each type of CA was not pronounced after a maximum of 10 hours treatment. This indicates a possible completion of the removal of acetate groups after 5-10 hours only. Lu *et al* previously regenerated cellulose by treating CA membranes in 0.05M aqueous NaOH solution for 24 hours [110]. Ma *et al* carried out the same reaction for 24 hours in a 0.1M NaOH in an (ethanol : water of 2:1 by volume) mixed solution [116]. In a previous study, Ma *et al* regenerated cellulose by treating CA membranes for 24 hours in a 0.1 M NaOH in an (ethanol: water of 4:1 by volume) solution [75]. Using higher concentration of NaOH in the current studies is thus considered the main cause of lowering the time needed for the de-acetylation reaction to take place. To confirm these findings, completely dried membranes were investigated by IR spectroscopy. Figures 43-46 show IR spectra of all membranes as a function of soaking time for each membrane. The IR spectra of as-spun CA and as-received cellulose
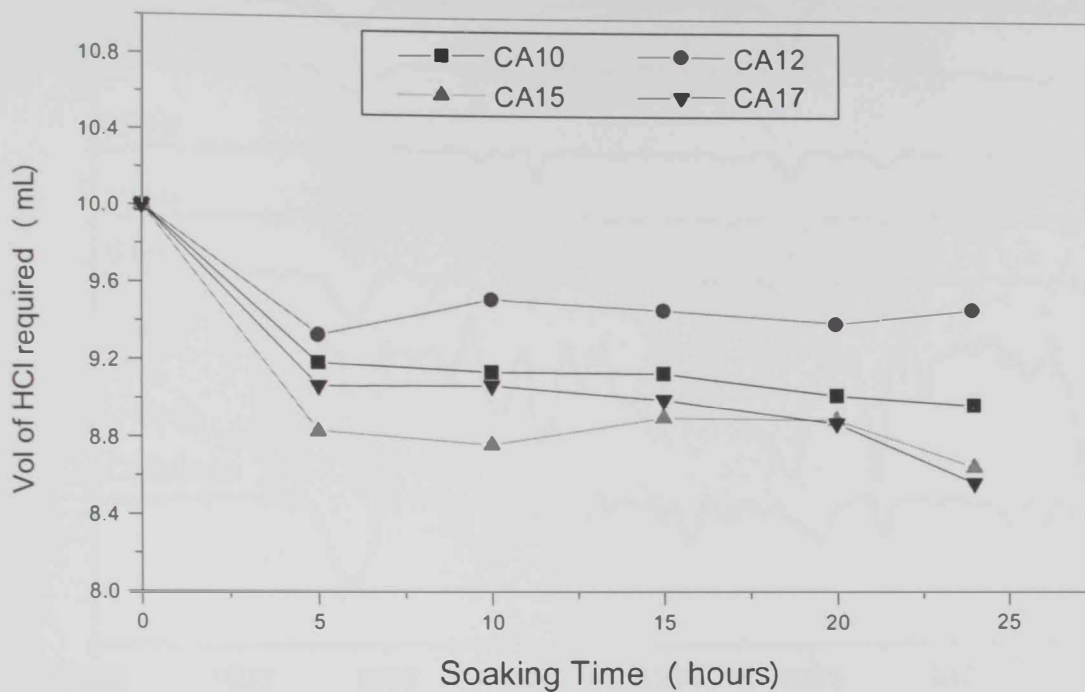
103

Figure 42. Volumes of HCl needed to neutralize the un-reacted NaOH in each of the alkaline solutions after each time period of soaking the different membranes
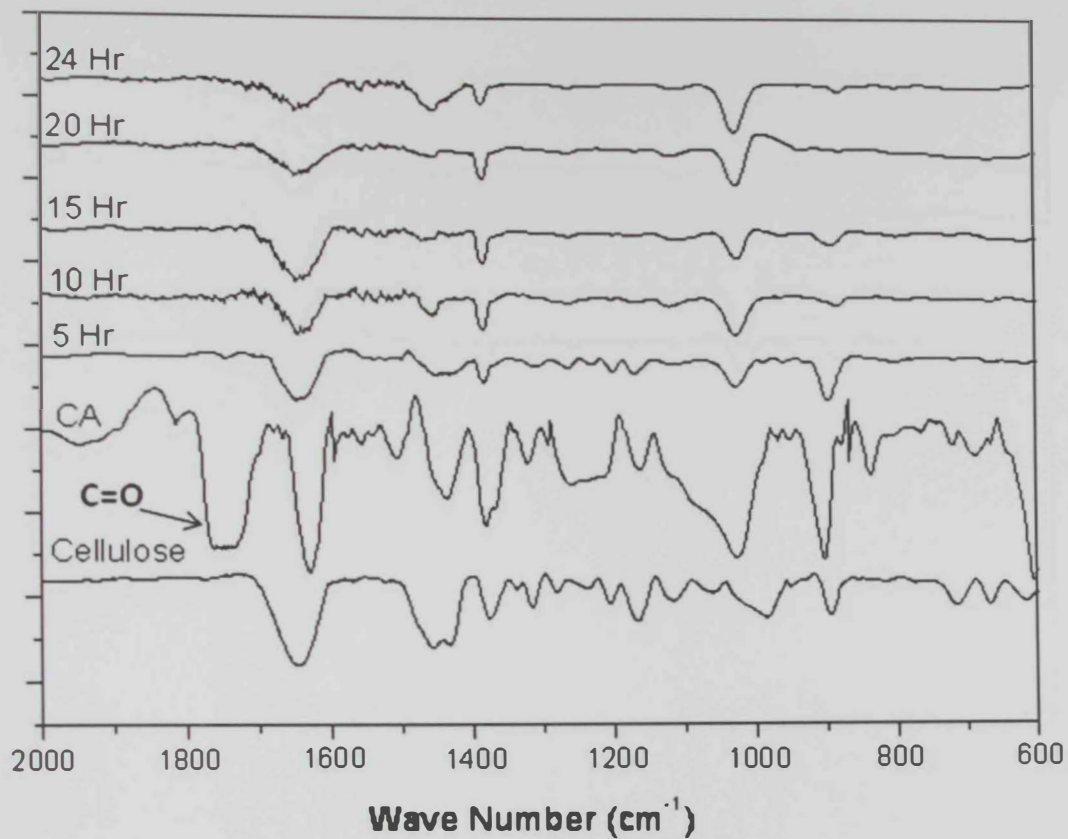
Figure 43. IR spectra of CA10 nanofibrous membranes after alkaline treatment in a 0.5 M NaOH solution for A) 5, B) 10, C) 15, D) 20 and E) 24 hours. Spectra of as spun CA and as received cellulose samples are shown for comparison

Figure 44. IR spectra of CA12 nanofibrous membranes after alkaline treatment in a 0.5 M NaOH solution for A) 5, B) 10, C) 15, D) 20 and E) 24 hours. Spectra of as spun CA and as received cellulose samples are shown for comparison

Figure 45. IR spectra of CA15 nanofibrous membranes after alkaline treatment in a 0.5 M NaOH solution for A) 5, B) 10, C) 15, D) 20 and E) 24 hours. Spectra of as spun CA and as received cellulose samples are shown for comparison
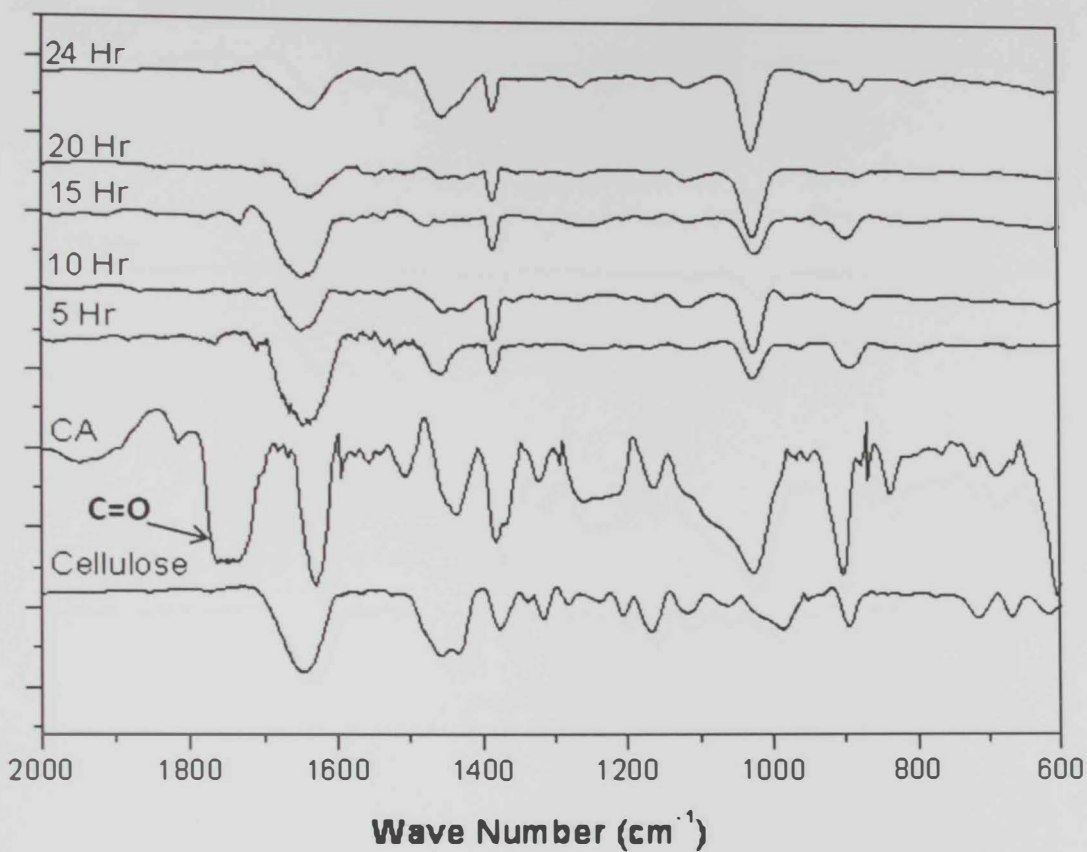
Figure 46. IR spectra of CA17 nanofibrous membranes after alkaline treatment in a 0.5 M NaOH solution for A) 5, B) 10, C) 15, D) 20 and E) 24 hours. Spectra of as spun CA and as received cellulose samples are shown for comparison
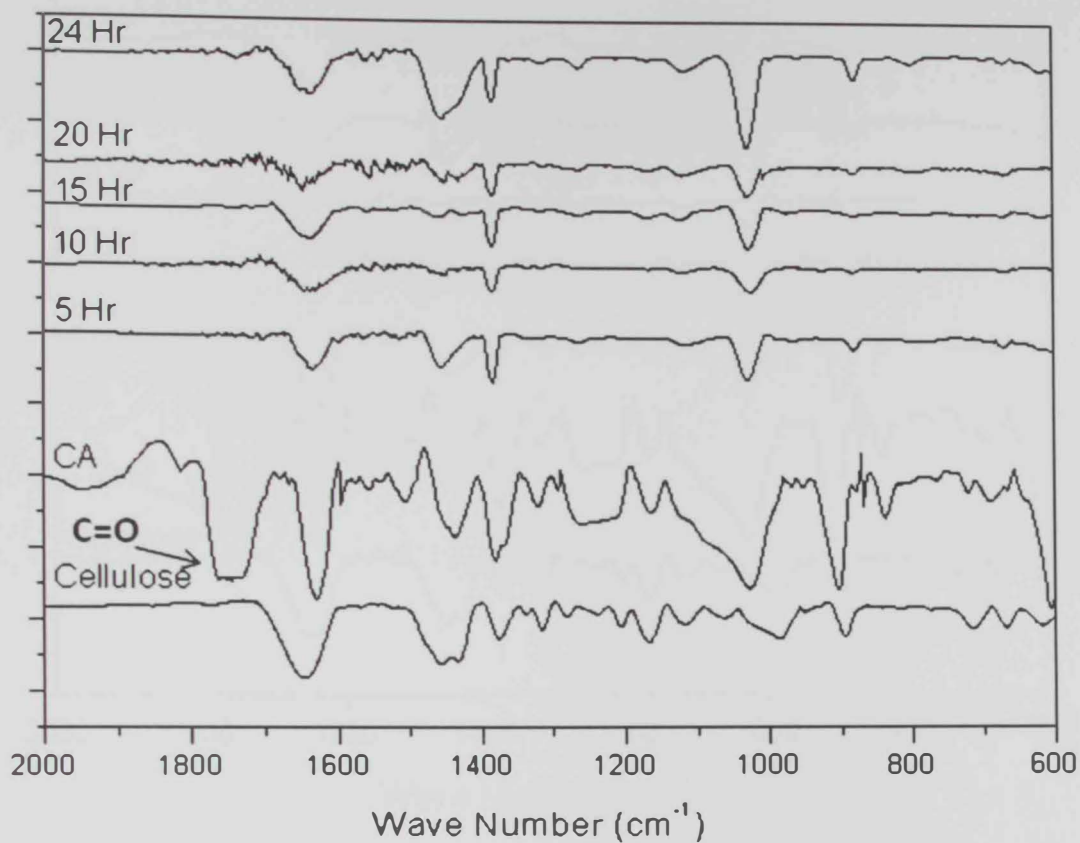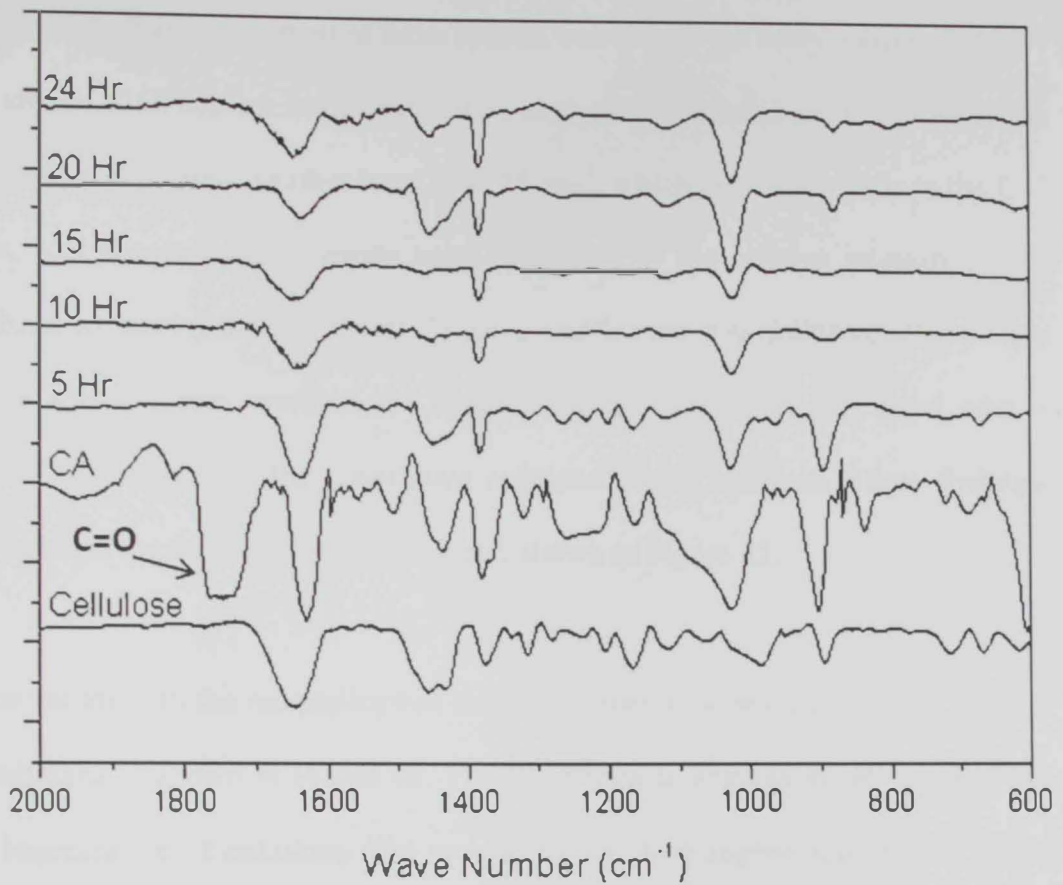
are shown in each graph for the sake of comparison with the regenerated cellulose spectra in all samples. The band of interest in these spectra was that of the acetyl carbonyl (C=O) groups at around 1750 cm^{-1}. A semi-quantitative analysis was carried out to follow up the disappearance of this band. Another band at 1375 cm^{-1}, which is characteristic to the C-C absorption, was chosen as a reference band. Variation in the relative intensity of the carbonyl band to that of the C-C band ($I_{C=O}/I_{C-C}$) with time was followed. Results are shown in Figure 47, and revealed the complete disappearance of this band after a maximum of 10 hours, and the consequent regeneration of cellulose. These findings, therefore, confirm the titration results previously shown in Figure 42.

The variation in the morphology of the membranes as a result of treating them in alkaline solutions is shown in Figure 48. The IR spectra in Figures 43-46 revealed the complete regeneration of cellulose. The process of cellulose regeneration seems not to affect the overall integrity of the fibers, where no distortion of the fibers was observed in all samples. However, comparing the fiber size distribution of these membranes, given in Figure 49, indicates a relative increase in the diameter of all fibers compared to the as spun and those thermally treated at 208°C. This could be attributed to the swelling step that was carried out to increase the spacings between the fibers to facilitate the alkaline treatment reaction.
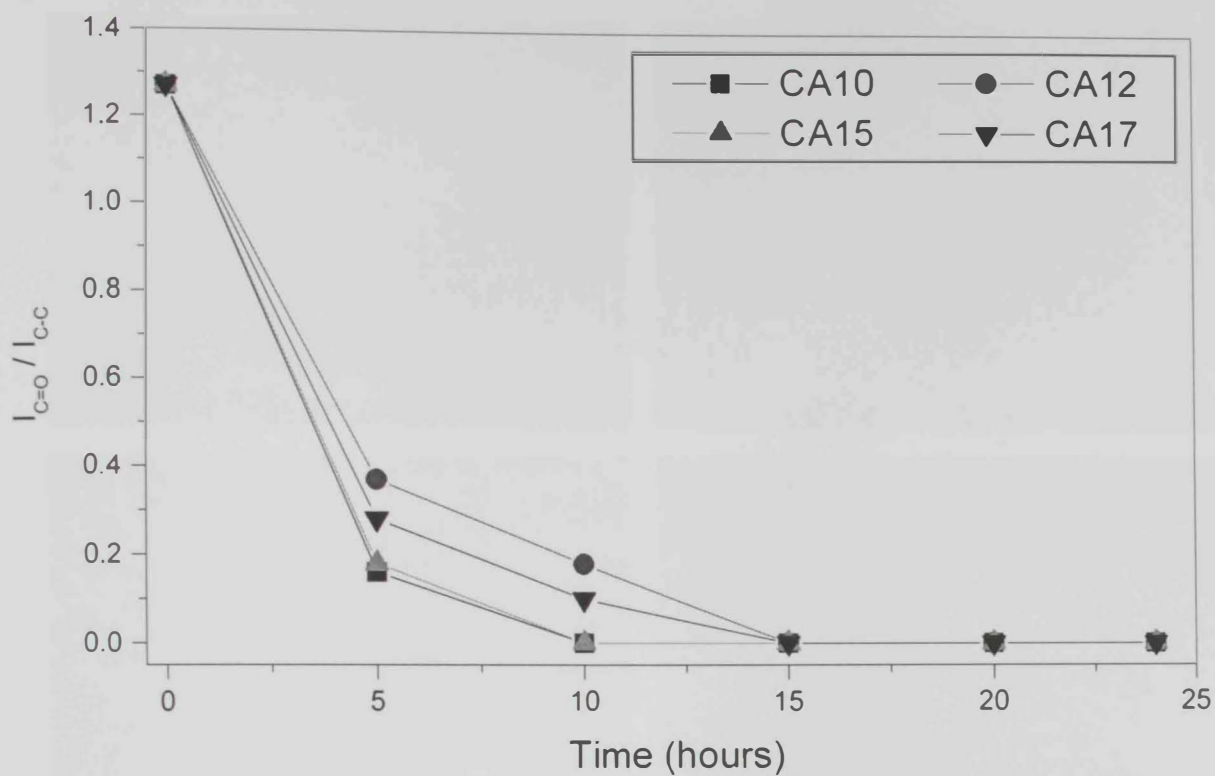
Figure 47. Relative intensity of the C=O characteristic band at 1750 cm^{-1} to the C-C characteristic band at 1375 cm^{-1} as a function of soaking time (in hours) during the alkaline treatment of CA10-17 nanofibrous membranes
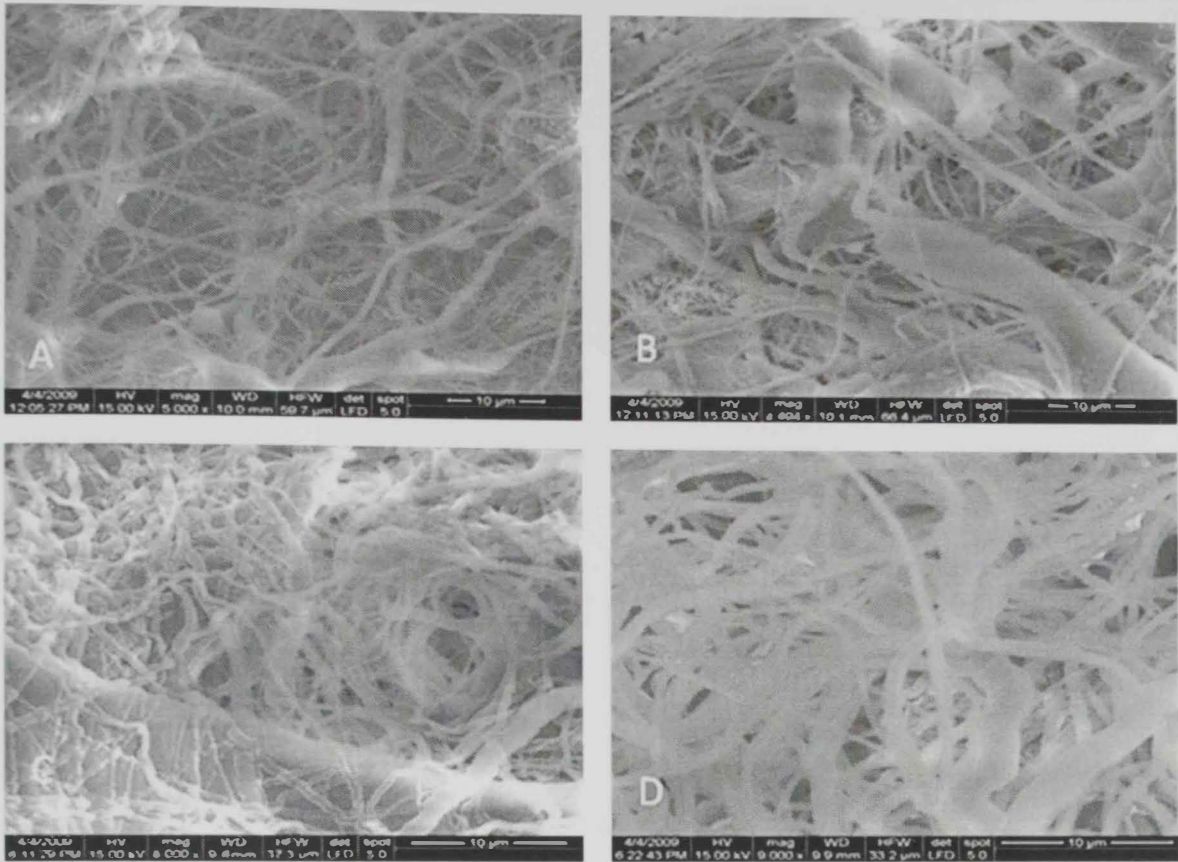
Figure 48. SEM micrographs of CA nanofibrous membranes prepared from A) 10, B) 12, C) 15, and D) 17 wt% solutions, after alkaline treatment in a 0.5 M NaOH solution for 24 hours
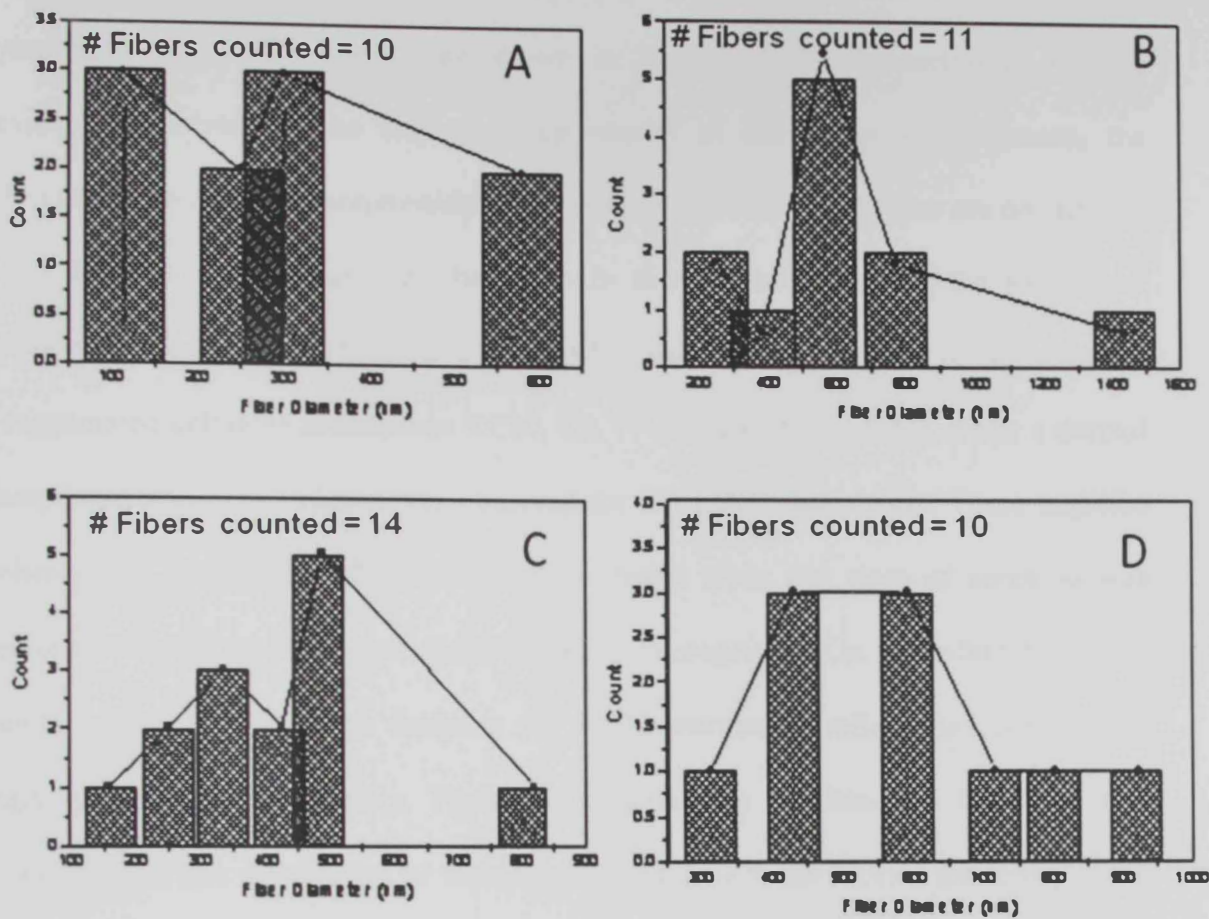
Figure 49. Fiber-size distribution obtained by an image analysis of the SEM micrographs of membranes prepared from A) 10, B) 12, C) 15, and D) 17 wt% solutions, after alkaline treatment in a 0.5 M NaOH solution for 24 hours

Measurements of the N_2-adsorption isotherms, pore size distribution, surface area, and pore volume were carried out for the alkali treated membranes after completely drying them at 100°C. Results are shown in Figures 50-53, respectively. As was previously observed in the corresponding results of the as-spun membranes, the differences between the adsorption/desorption of the different membranes are contributed to the different morphologies of the fibers in these membranes and the subsequent variations in the pore geometries. Similar step-like shapes were observed in the isotherms of regenerated cellulose membranes RC10, 15, 17 (Figures 50 A, C,D), while a normal adsorption/desorption isotherm was observed for the RC 12 membrane. These step-like isotherms are attributed to the presence of different types and sizes of pores, as was previously shown in their corresponding SEM micrographs. On the other hand, the smooth adsorption/desorption isotherm for RC12 membrane reflects the presence of singly type/size of the porosity. These results were also confirmed in Figure 51 that shows the pore size distribution of these membranes. Due to the limited sensitivity of the technique used in these experiments to pores with diameters beyond 200 nm, the BET surface area and pore volume data extracted from Figures 52, 53 of all RC membranes were only limited to a maximum pore diameter of 200 nm. Both BET surface area and pore volume results are given in Table 4.

Thermal analysis of a representative regenerated cellulose membrane; RC12, was carried out by DSC. For the sake of comparison, thermal analysis was also carried out for as-received cellulose microcrystalline powder (with an average size of 20 μm). DSC results of both samples are shown in Figure 54. The as-received cellulose sample showed the absence of glass transition (T_g) and melting (T_m) temperatures when heated up to 270°C. In contrast, the regenerated cellulose (RC12) DSC spectrum showed an average

113

Figure 50A. Adsorption-desorption isotherms of CA nanofibers made from solutions
containing 10 wt % after alkaline treatment in a 0.5 M NaOH solution for 24 hours

Figure 50B. Adsorption-desorption isotherms of CA nanofibers made from solutions
containing 12 wt % after alkaline treatment in a 0.5 M NaOH solution for 24 hours
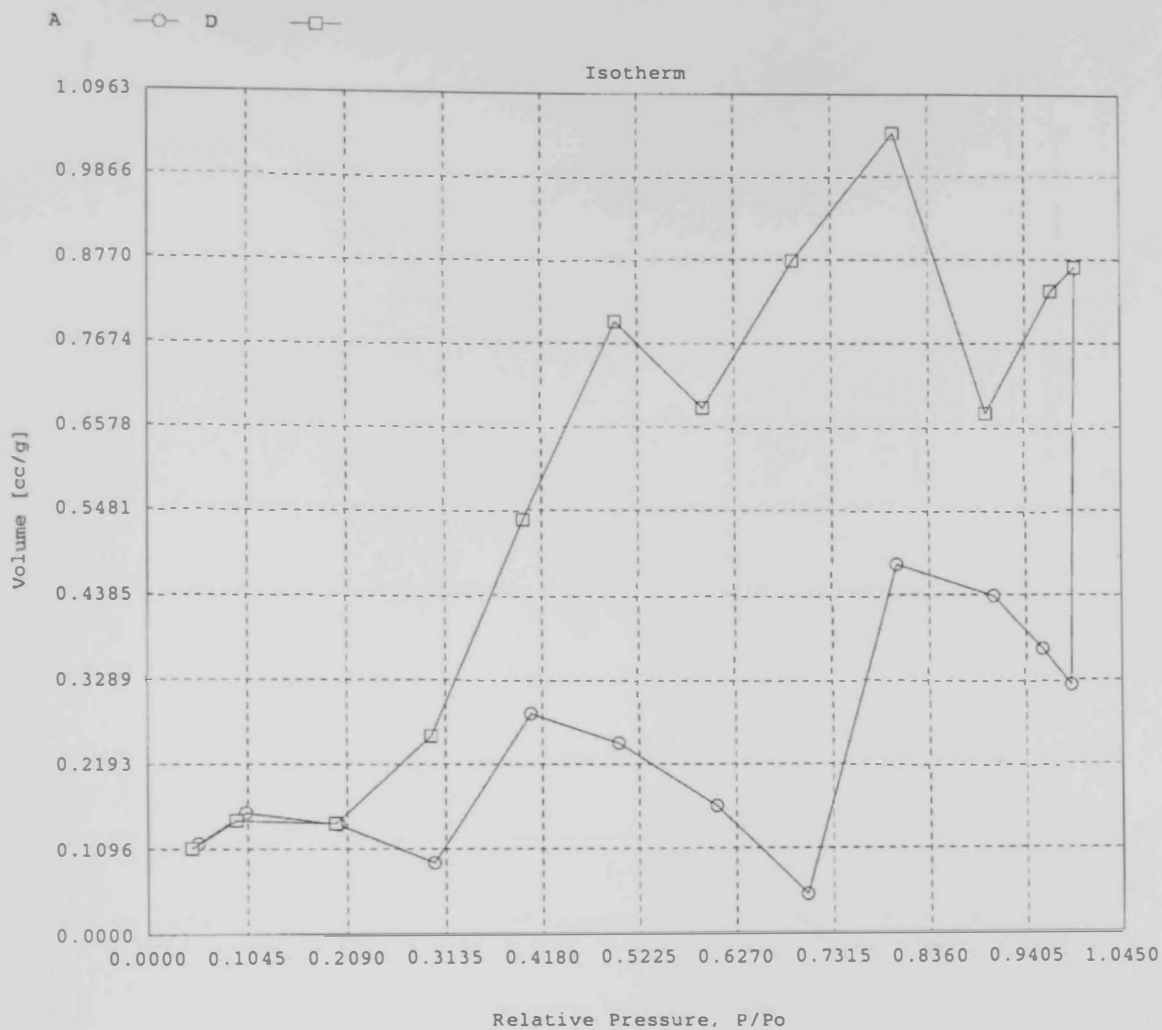
Figure 50C. Adsorption-desorption isotherms of CA nanofibers made from solutions
containing 15 wt % after alkaline treatment in a 0.5 M NaOH solution for 24 hours

Figure 50D. Adsorption-desorption isotherms of CA nanofibers made from solutions containing 17 wt % after alkaline treatment in a 0.5 M NaOH solution for 24 hours
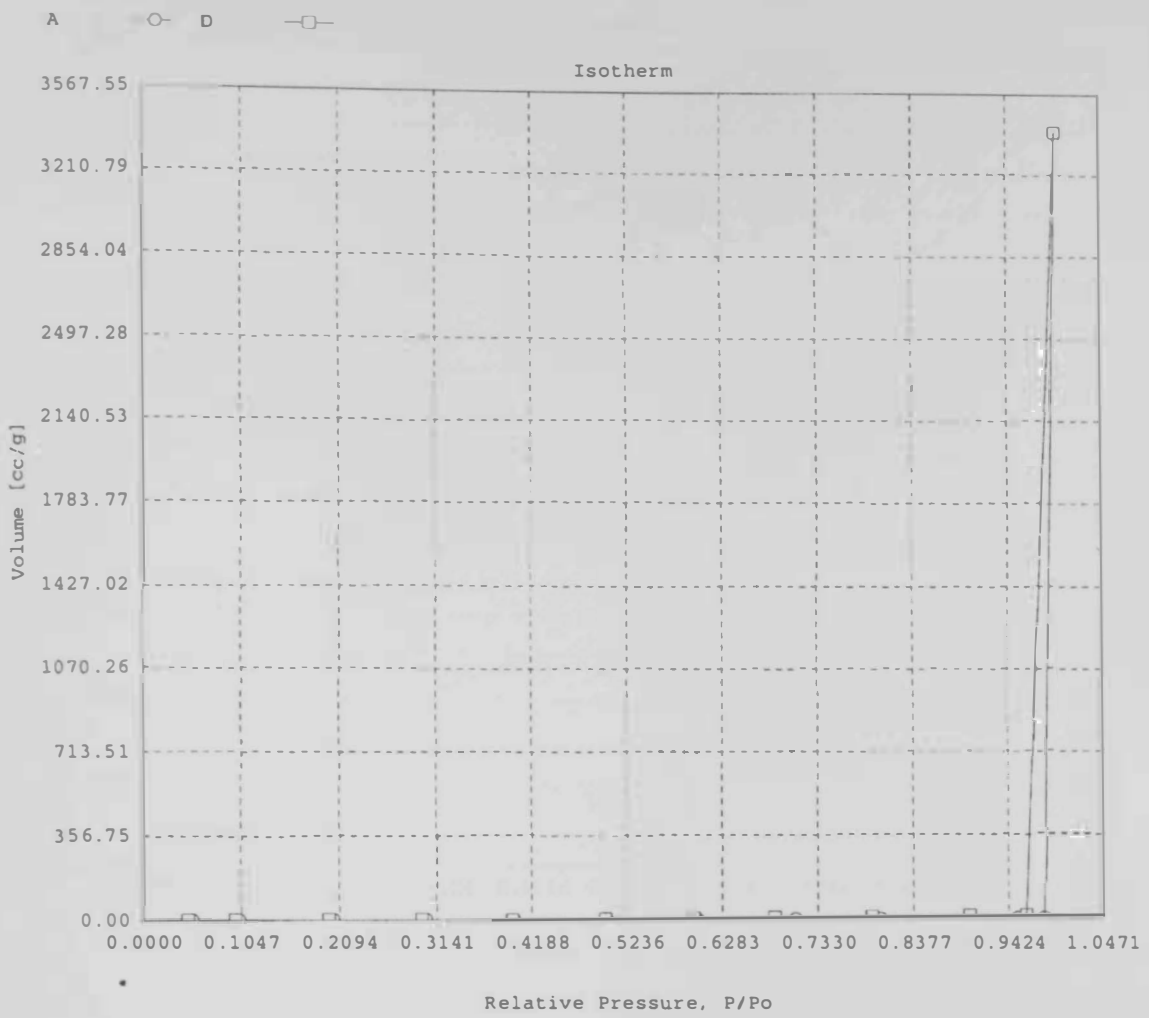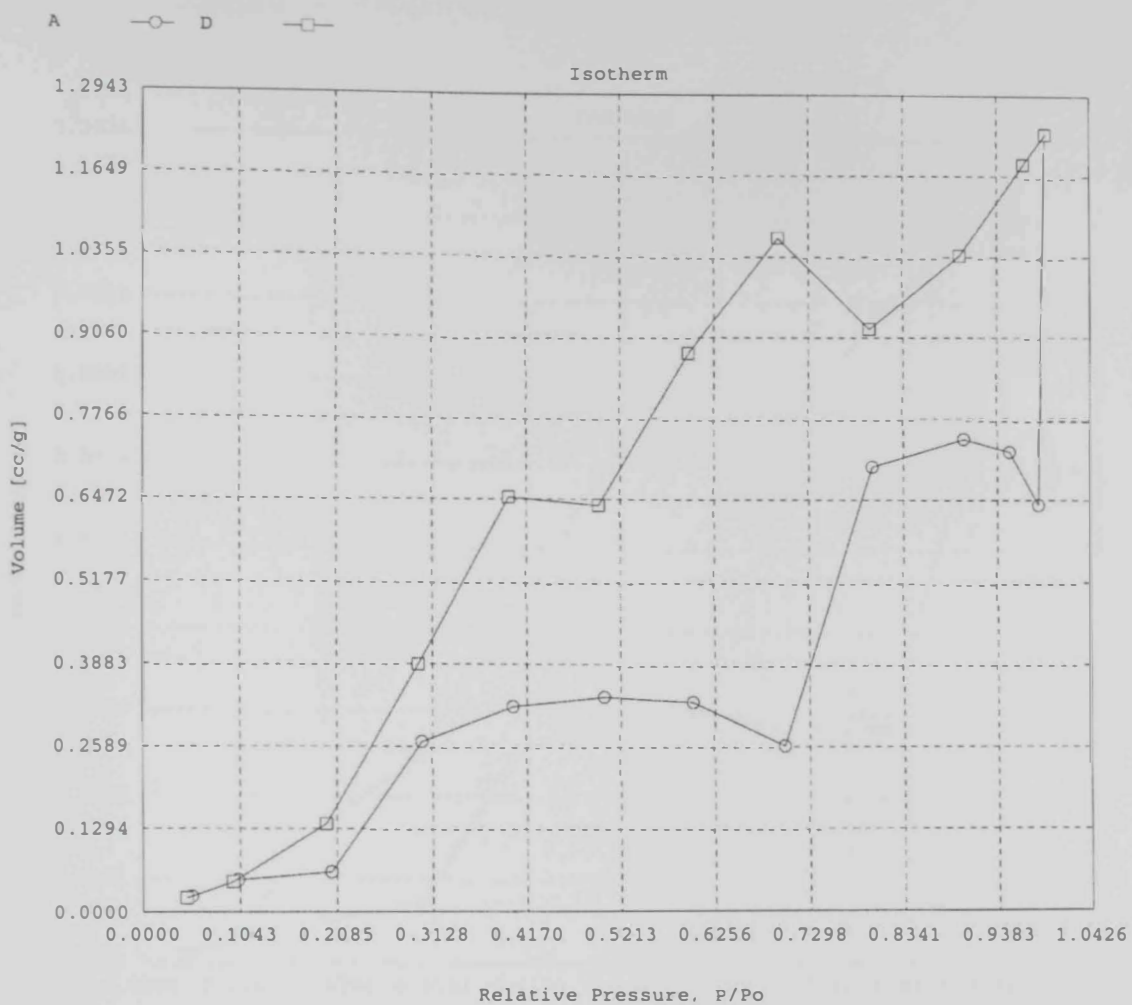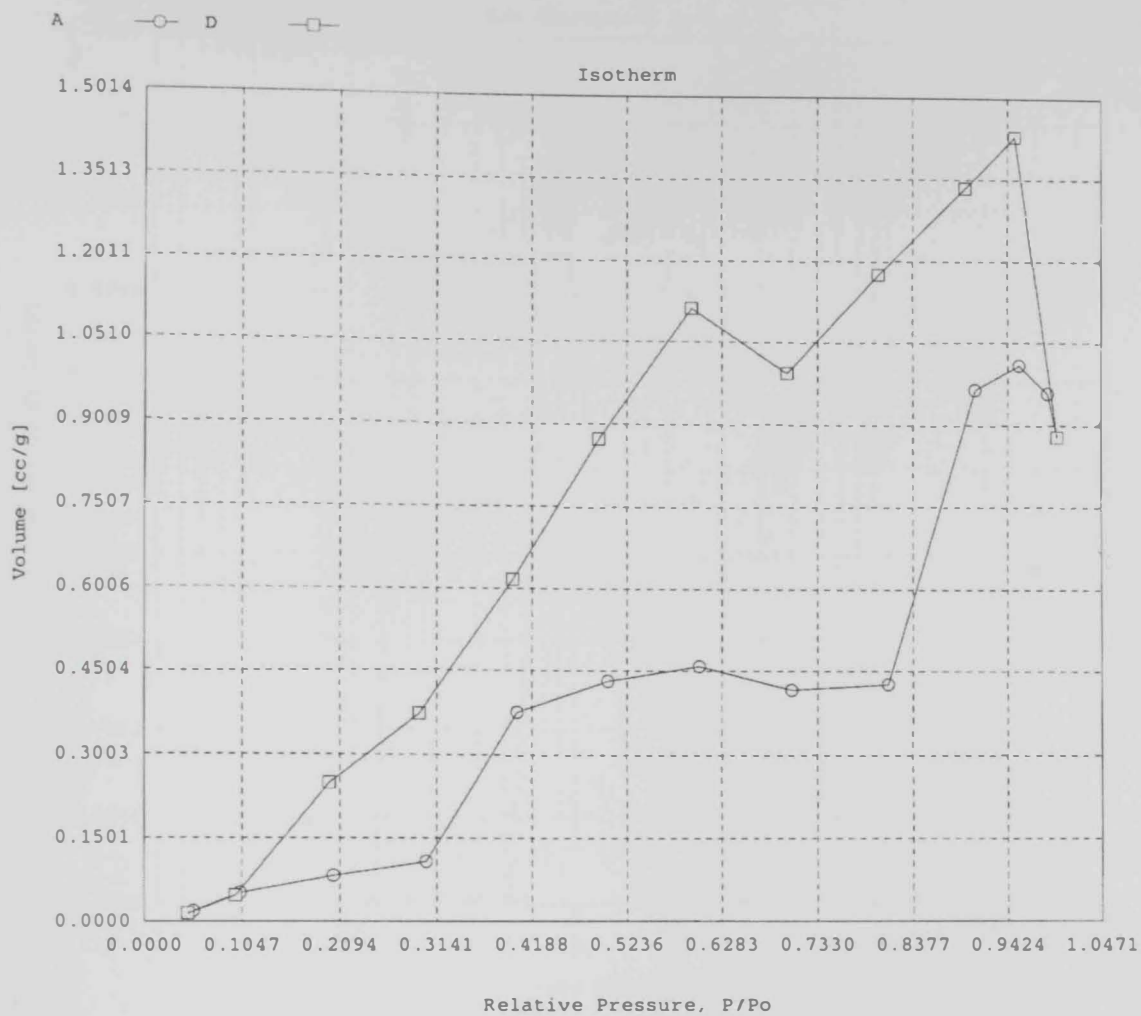
Figure 51A. Pore size distribution of CA nanofibers made from solutions containing 10 wt % after alkaline treatment in a 0.5 M NaOH solution for 24 hours

Figure 51B. Pore size distribution of CA nanofibers made from solutions containing 12 wt % after alkaline treatment in a 0.5 M NaOH solution for 24 hours
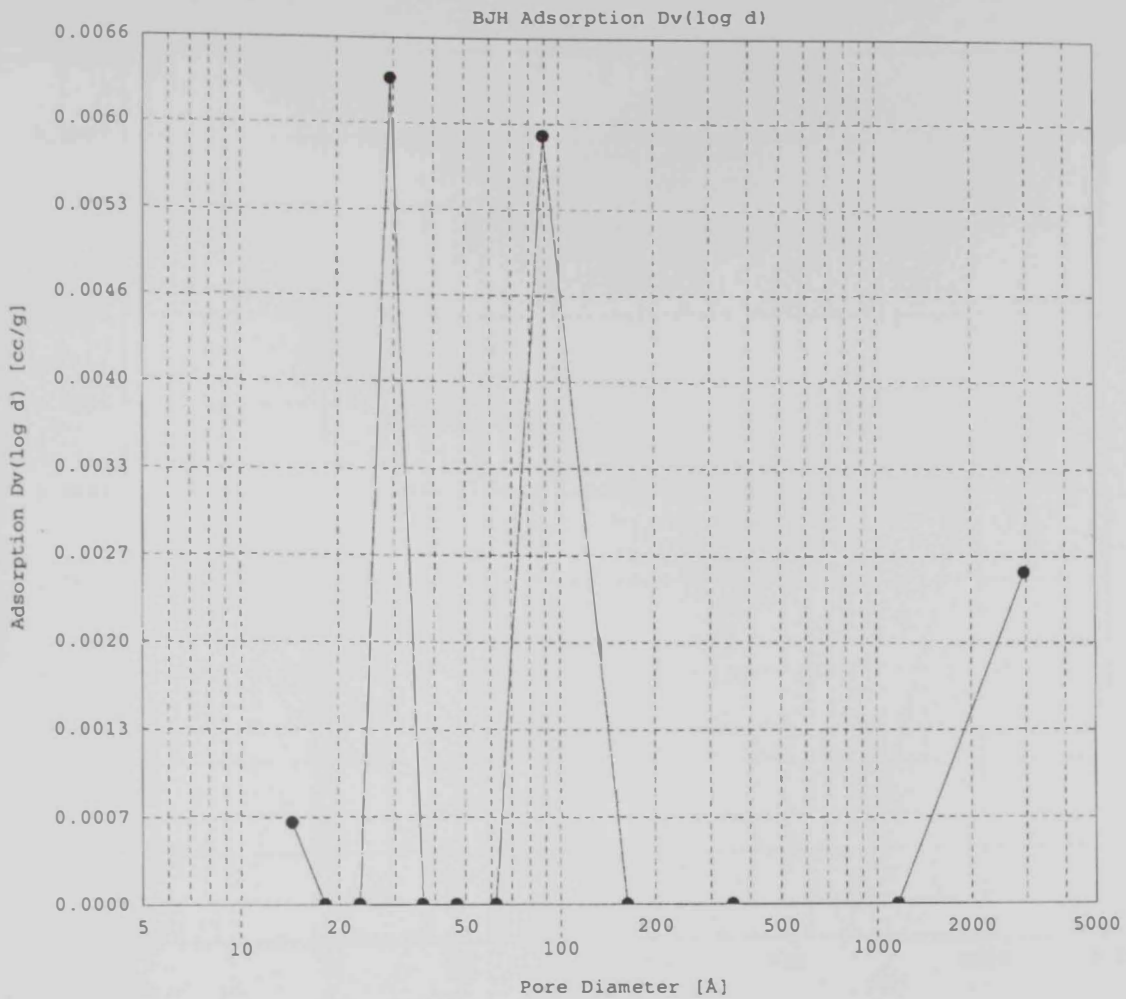
Figure 51C. Pore size distribution of CA nanofibers made from solutions containing
15 wt % after alkaline treatment in a 0.5 M NaOH solution for 24 hours
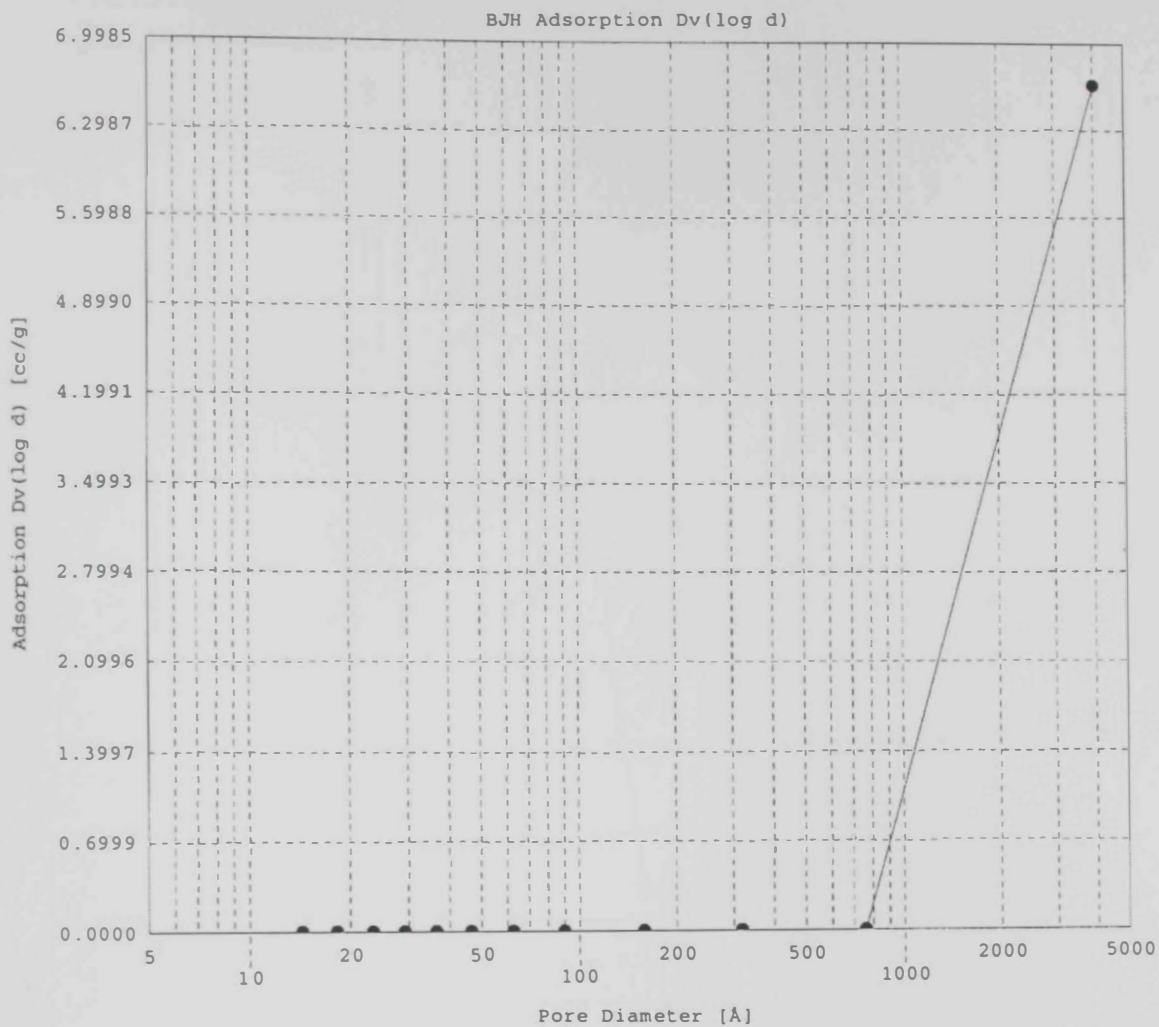
Figure 51D. Pore size distribution of CA nanofibers made from solutions containing 17 wt % after alkaline treatment in a 0.5 M NaOH solution for 24 hours

Figure 52A. BET surface area of CA nanofibers made from solutions containing
10 wt % after alkaline treatment in a 0.5 M NaOH solution for 24 hours
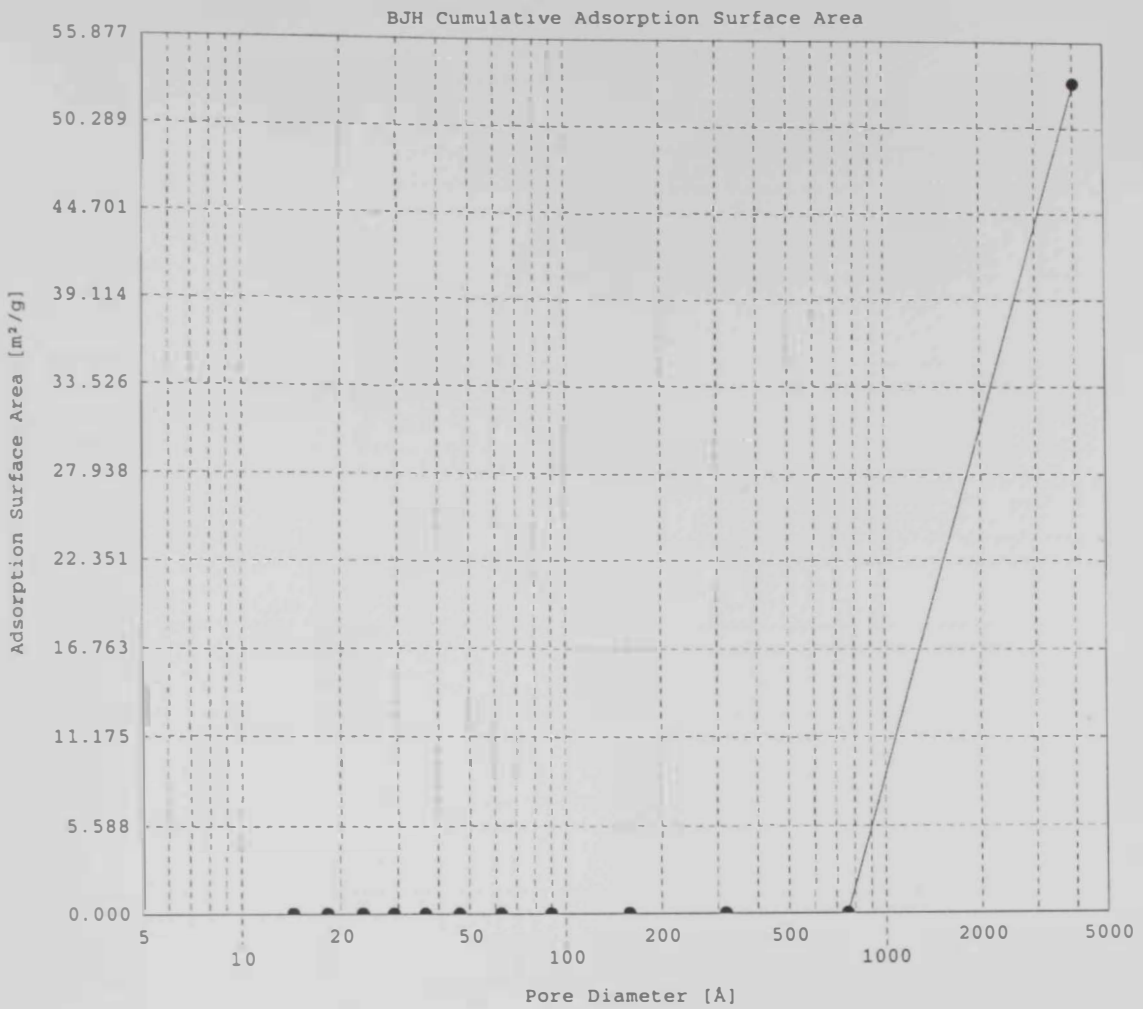
Figure 52B. BET surface area of CA nanofibers made from solutions containing 12 wt % after alkaline treatment in a 0.5 M NaOH solution for 24 hours
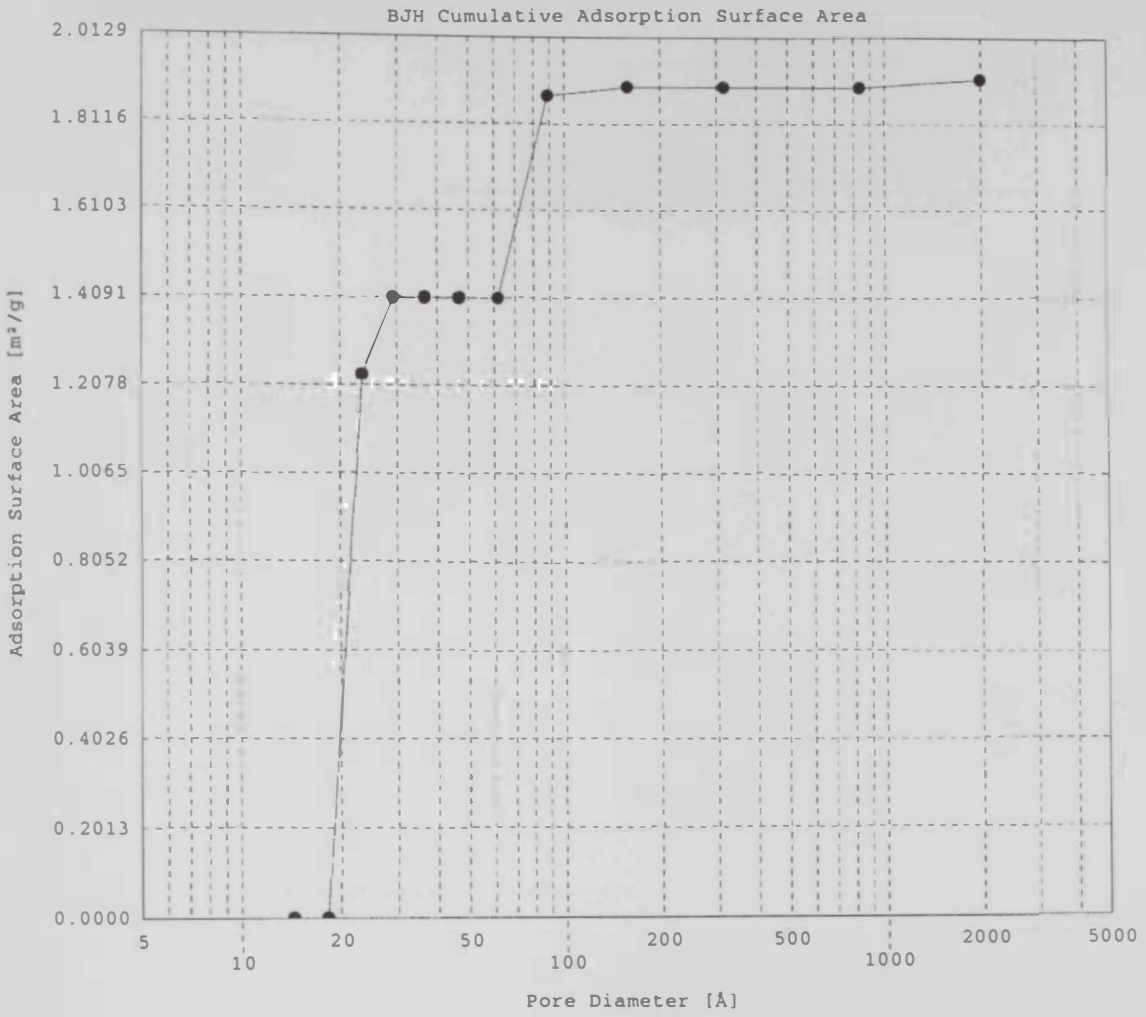
Figure 52C. BET surface area of CA nanofibers made from solutions containing
15 wt % after alkaline treatment in a 0.5 M NaOH solution for 24 hours
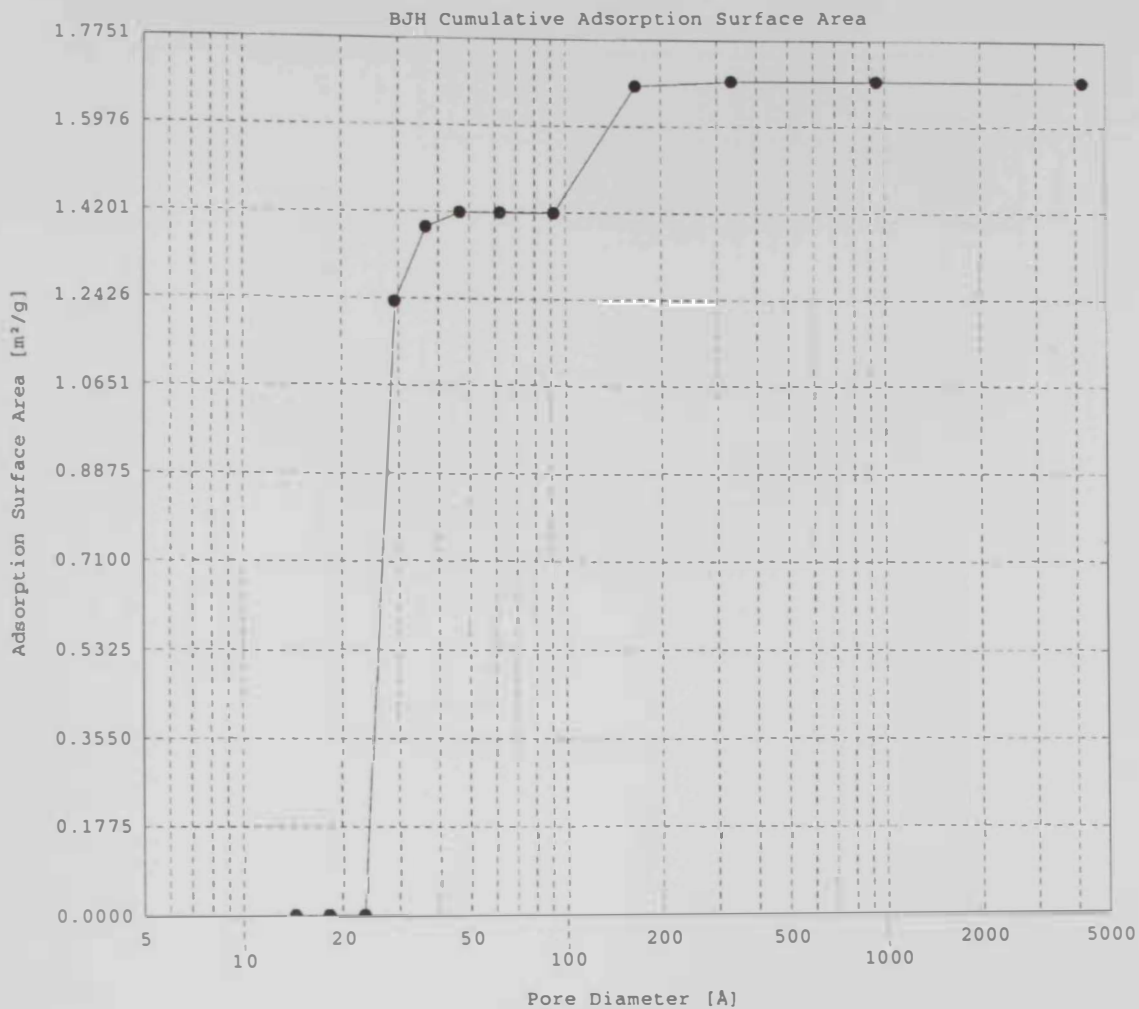
Figure 52D. BET surface area of CA nanofibers made from solutions containing 17 wt % after alkaline treatment in a 0.5 M NaOH solution for 24 hours
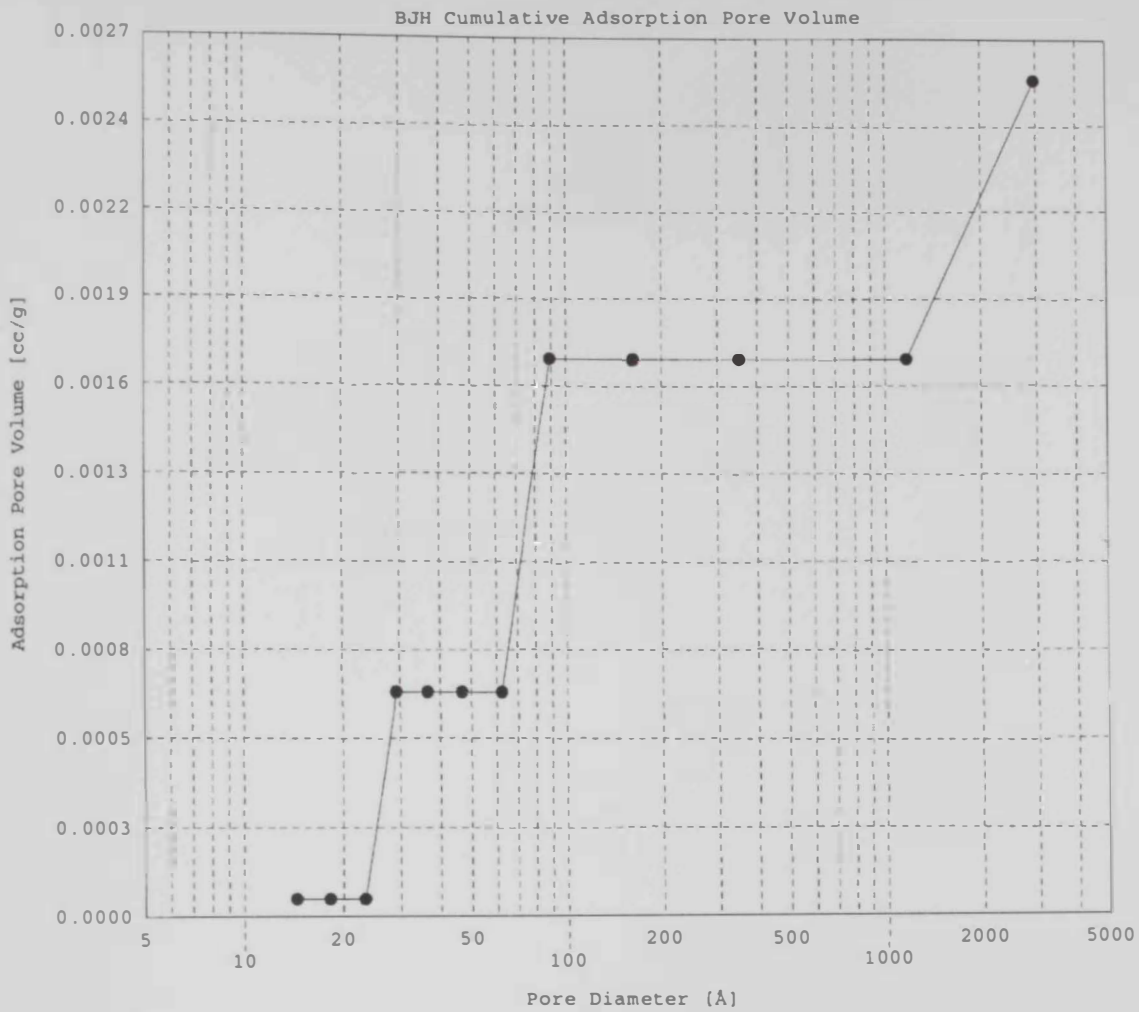
Figure 53A. Pore volume of CA nanofibers made from solutions containing
10 wt % after alkaline treatment in a 0.5 M NaOH solution for 24 hours
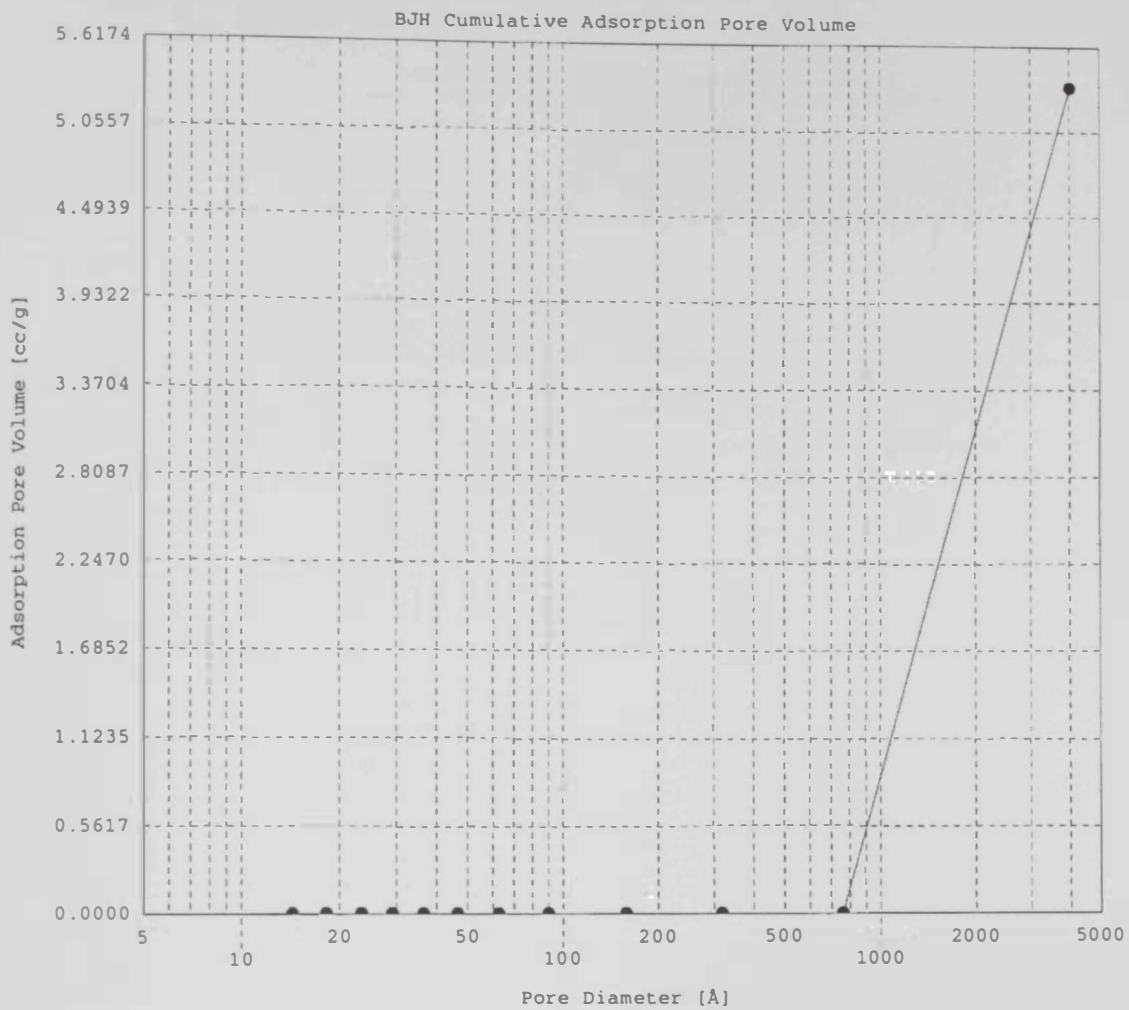
Figure 53B. Pore volume of CA nanofibers made from solutions containing
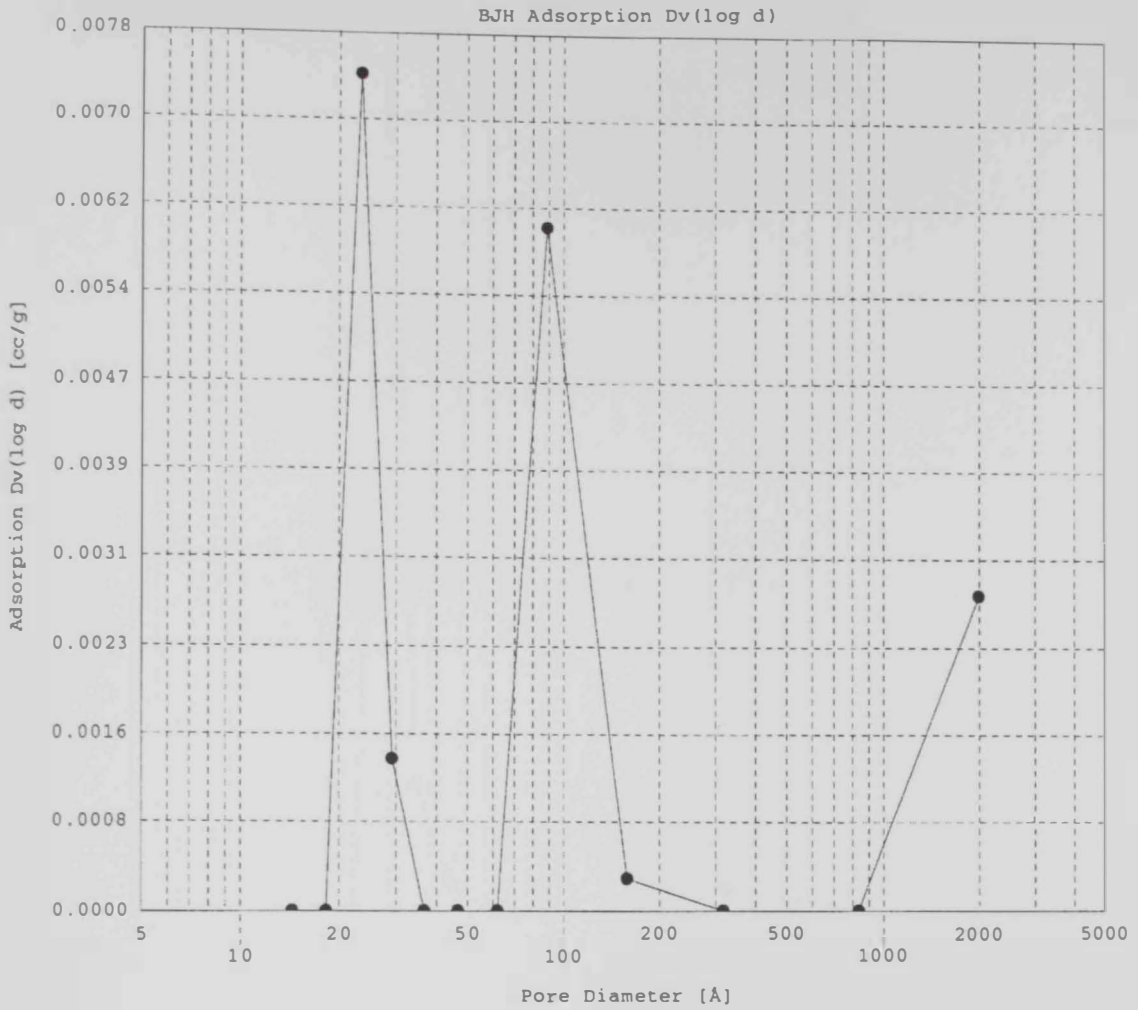12 wt % after alkaline treatment in a 0.5 M NaOH solution for 24 hours
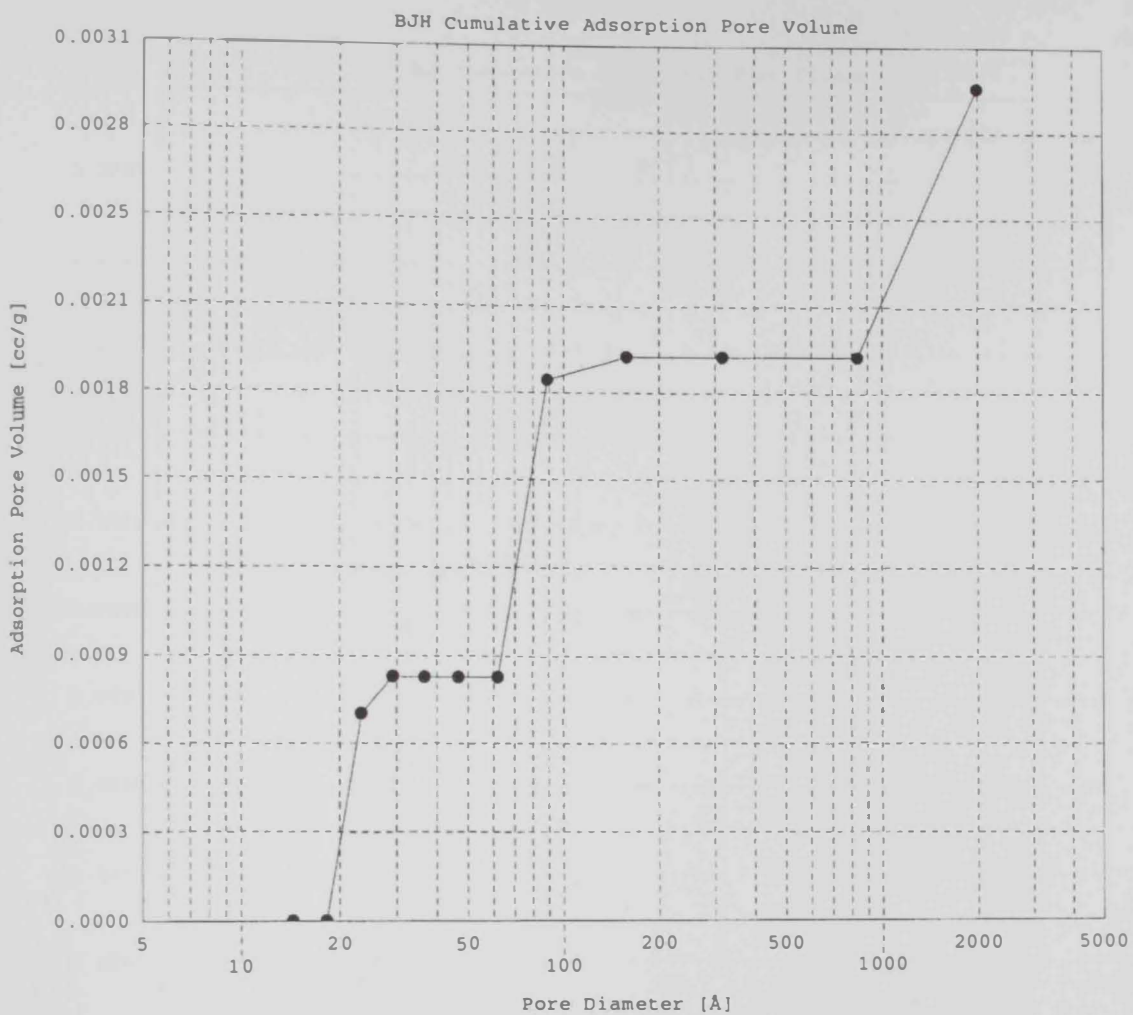
Figure 53C. Pore volume of CA nanofibers made from solutions containing
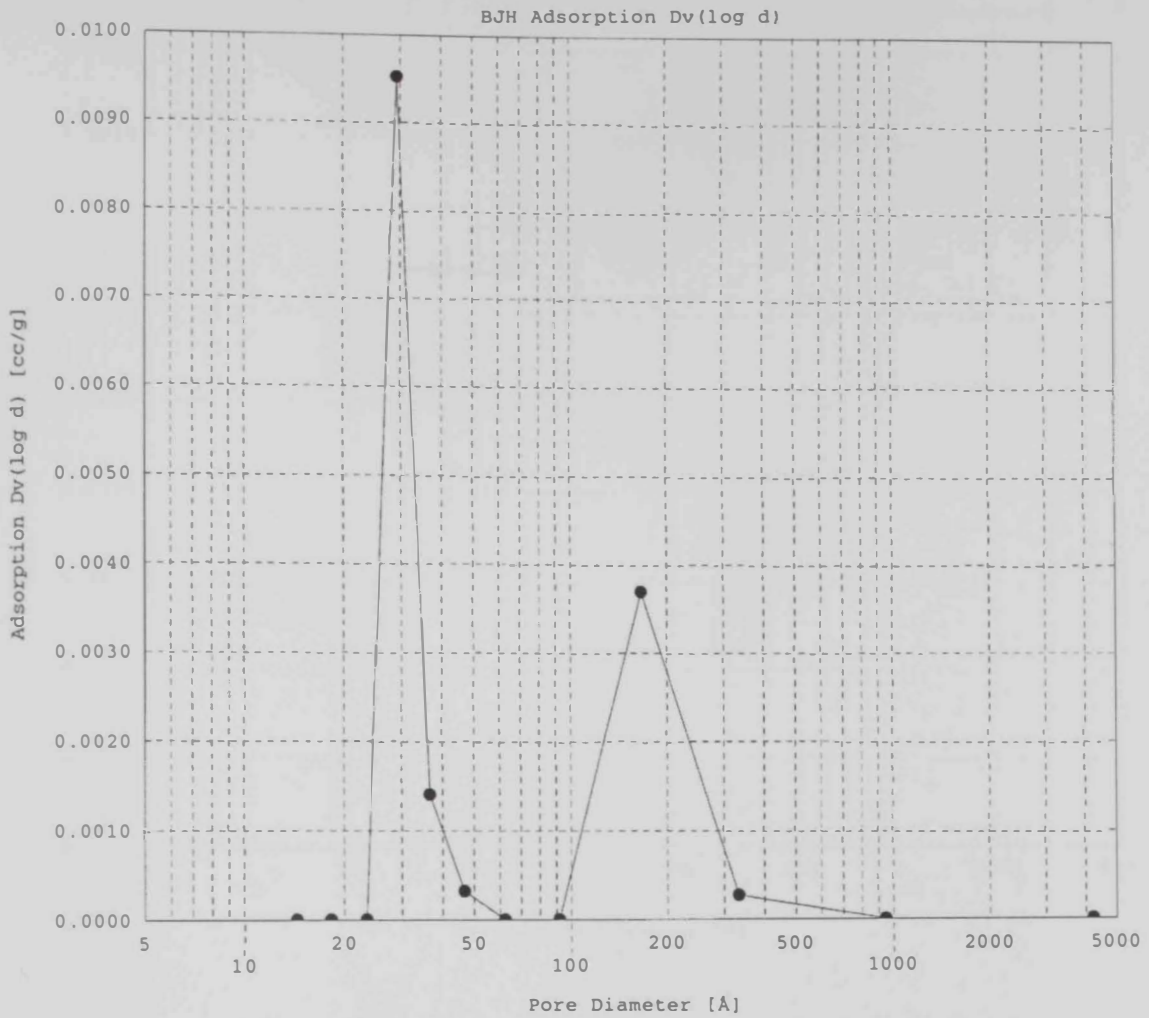15 wt % after alkaline treatment in a 0.5 M NaOH solution for 24 hours
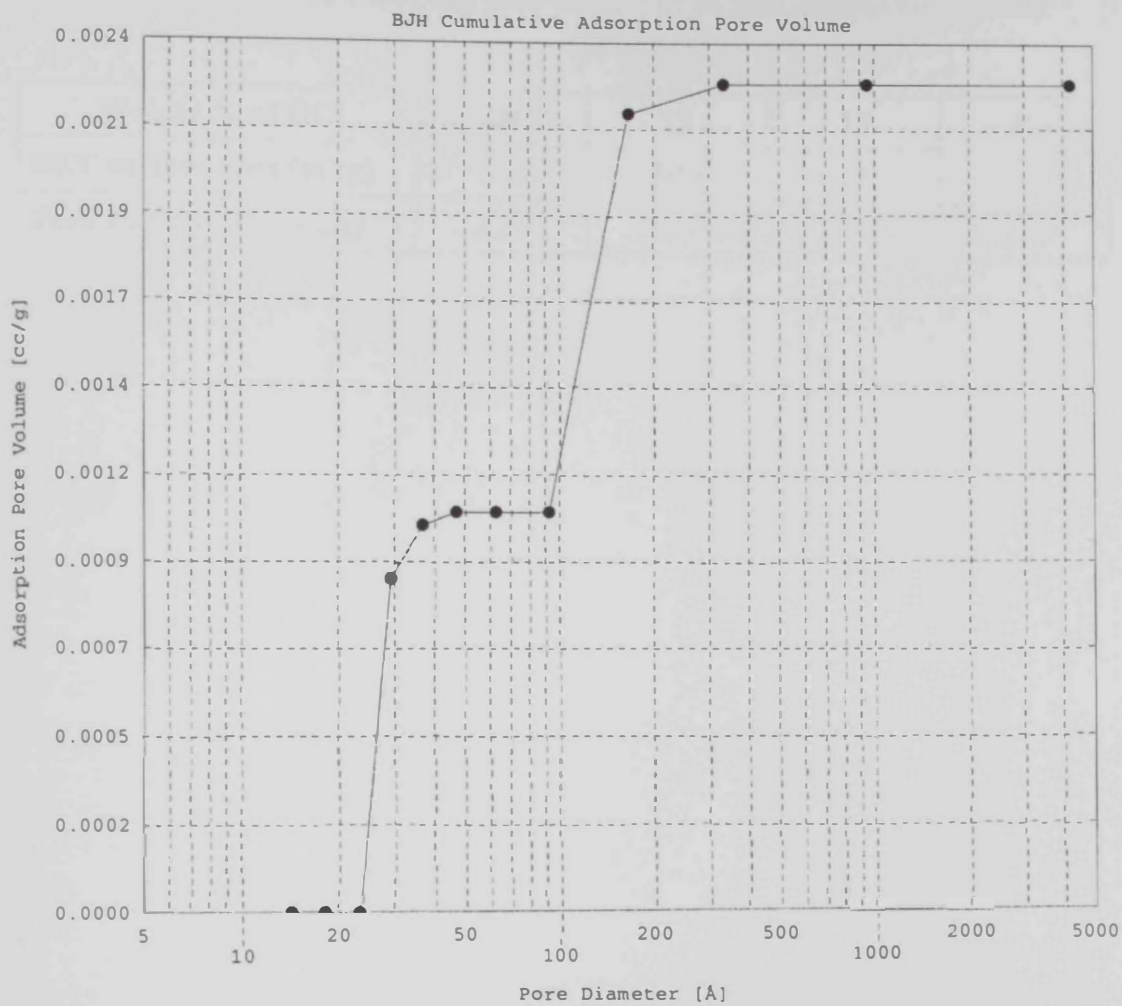
Figure 53D. Pore volume of CA nanofibers made from solutions containing

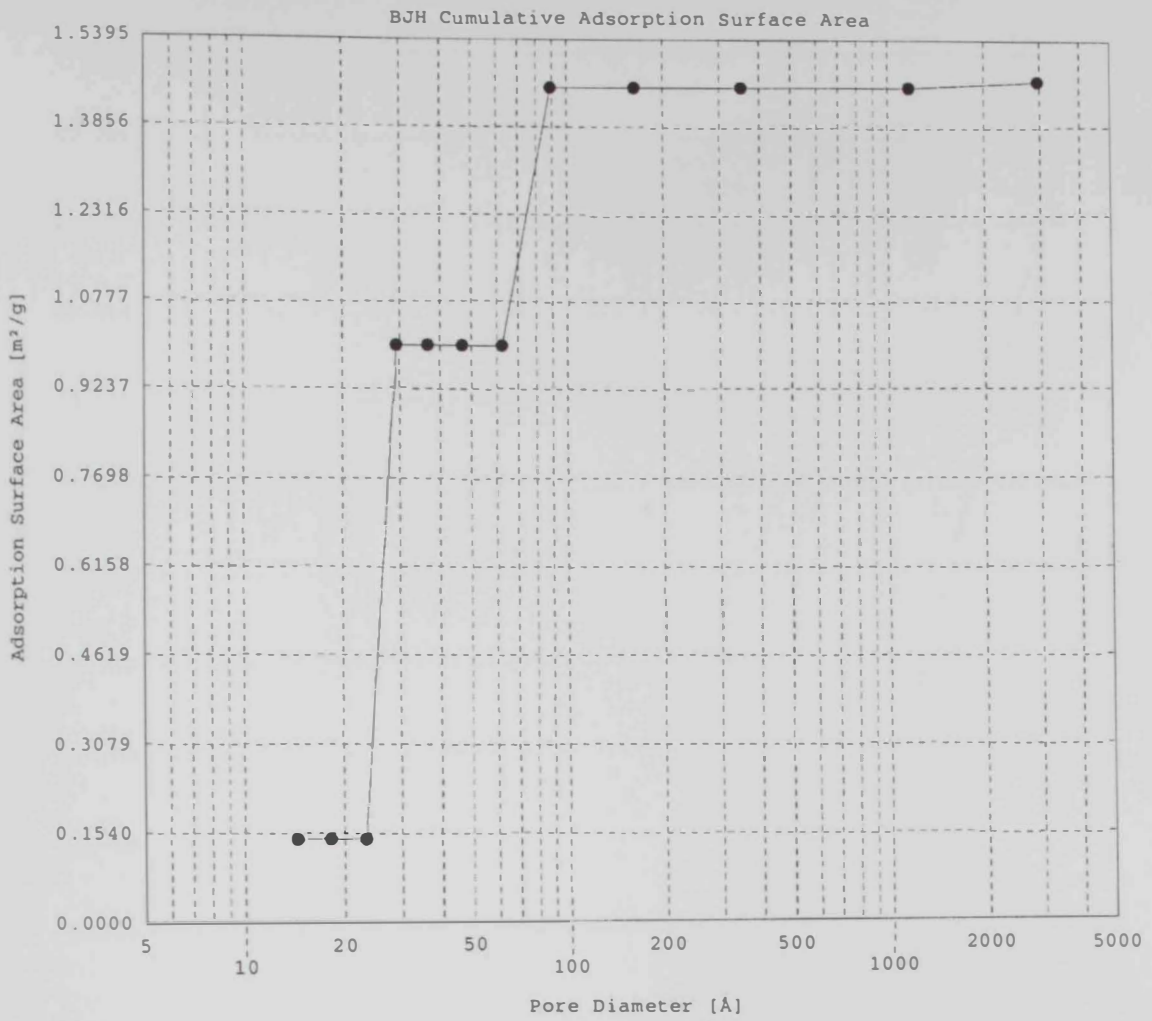17 wt % after alkaline treatment in a 0.5 M NaOH solution for 24 hours

Table 4. BET surface area and pore volume of all nanofibrous membranes:

Weight % of RC	10	12	15	17
BET surface area (m^2/g)	1.45	30.5	1.95	1.67
Pore volume ($x10^3$ cc/g)	2.25	3.10	3.00	2.28
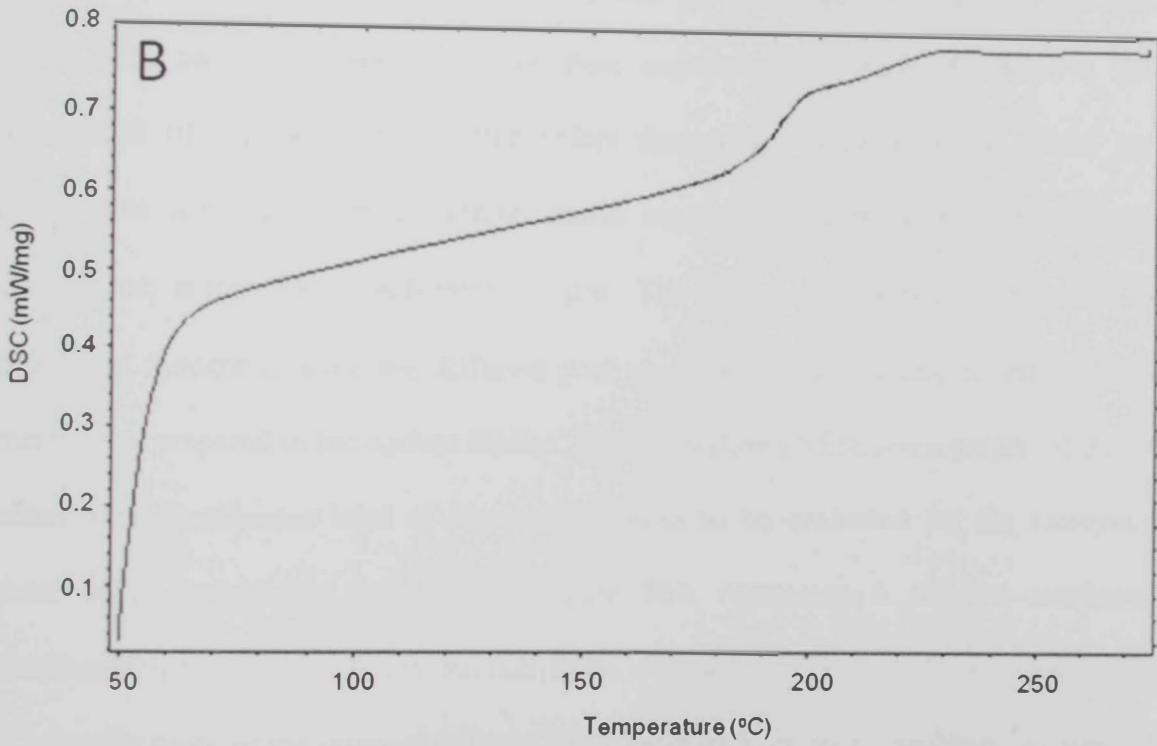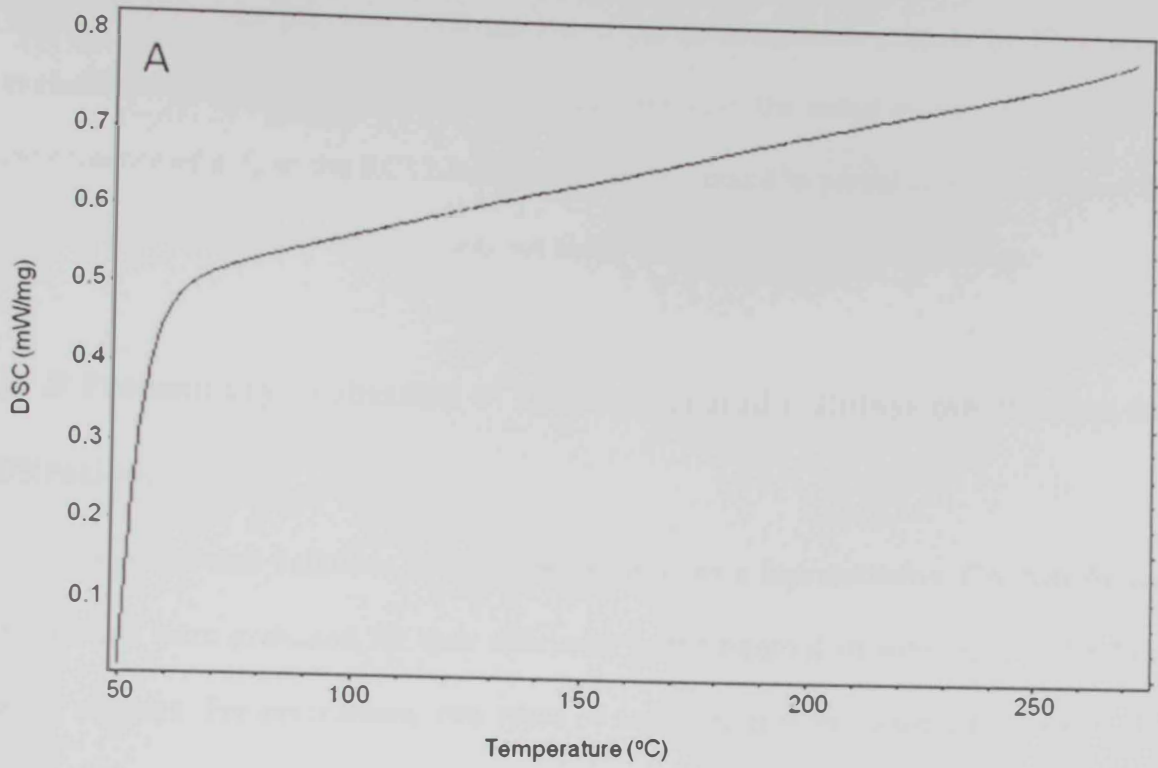
Figure 54. DSC spectrum of A) as-received versus B) regenerated cellulose

T_g of 192.1°C. The previous confirmation of the de-acetylation process by IR analysis excludes the possibility of presence of remaining CA in the tested membrane. Therefore, the presence of a T_g in the RC12 sample may be attributed to partial crystallization of the regenerated cellulose, although it was not easily identified by x-ray diffraction.

IV.9 Preliminary evaluation of the regenerated cellulose membranes for filtration:

Regenerated cellulose membranes, as well as a representative CA nanofibrous membrane, were evaluated for their efficiency in the removal of solid particulates from water samples. For comparison, two types of commercial filters were also tested in this regard. Simulated water samples containing 300 and 1000 ppm of calcium phosphate (CaP) solid particulates were used in these experiments. Figure 55 shows a SEM micrograph of CaP solid particulates before suspending them in water. These solid particulates appeared with an almost round morphology with a wide particle size distribution; in the range of sub-μm to 12 μm. The wide particle size distribution of this powder is thought to suite the different pore size distributions found in the cellulosic membranes prepared in the current studies. Figure 56 shows SEM micrographs of the two commercial membranes used as blank membranes to be evaluated for the removal of these solid particulates from water. Figure 56A represents a fibrous commercial membrane that is made of fibers and non-fibers with an average size of few microns. This is normally used for the removal of clays from water in filter press machines. Figure 55B, on the other hand, shows a highly porous commercial membrane made of polypropylene fibers, that is normally used for home water purification systems. Figures 57, 58 show

Figure 55. SEM micrograph of the CaP solid particulate sample used for the filtration experiments. Particulate sizes are shown on the graph
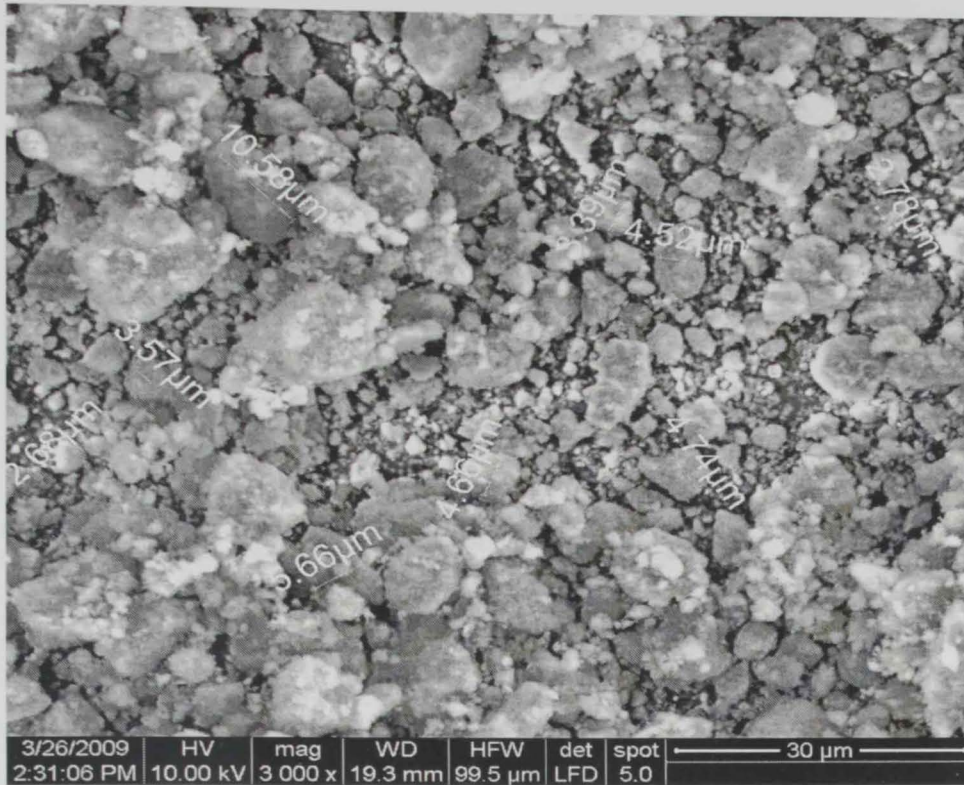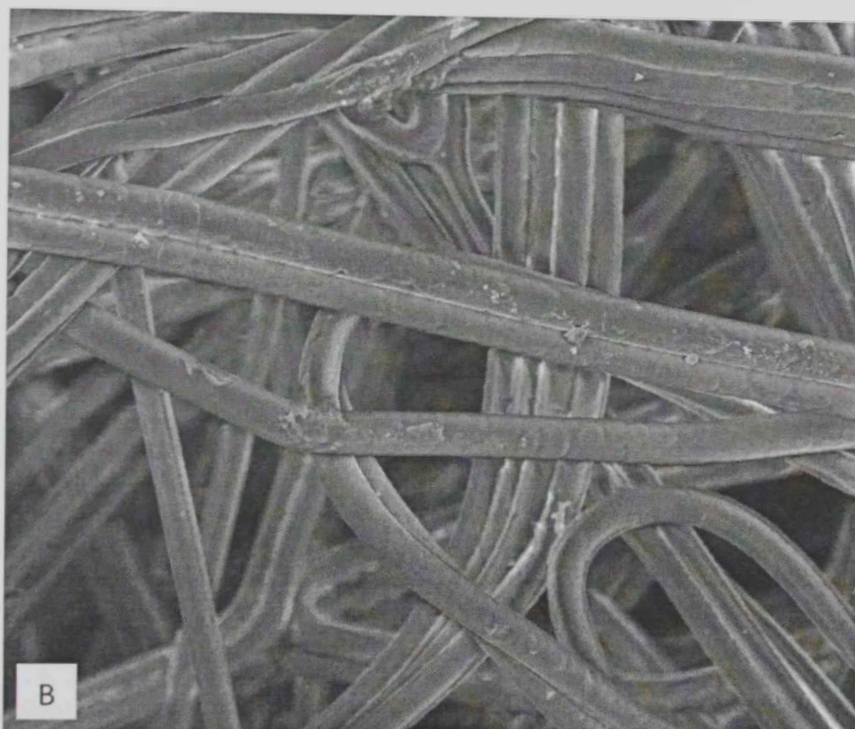
Figure 56. SEM micrographs of the commercial membranes used in this study
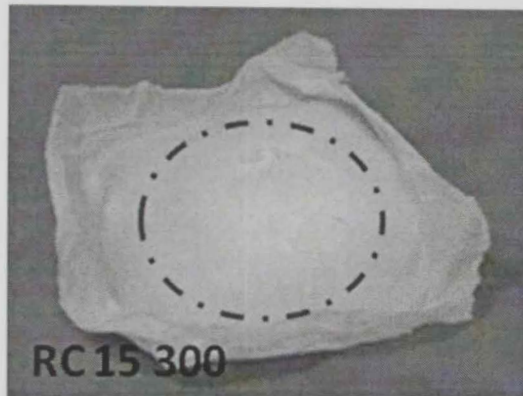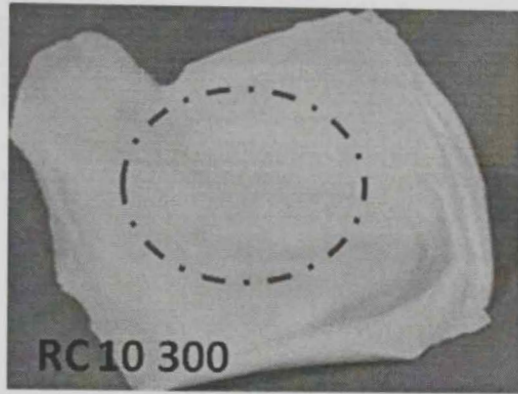
A. Commercial 1, B. commercial 2
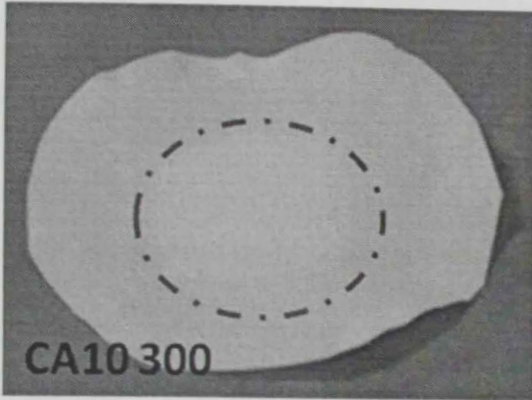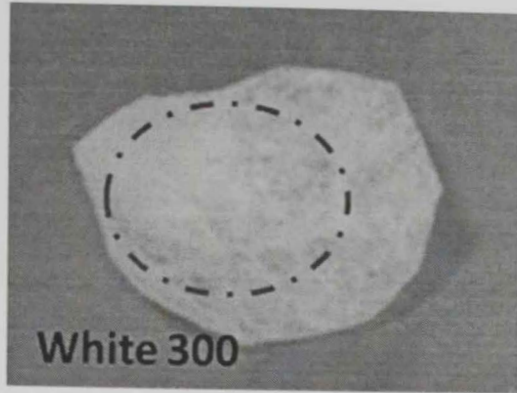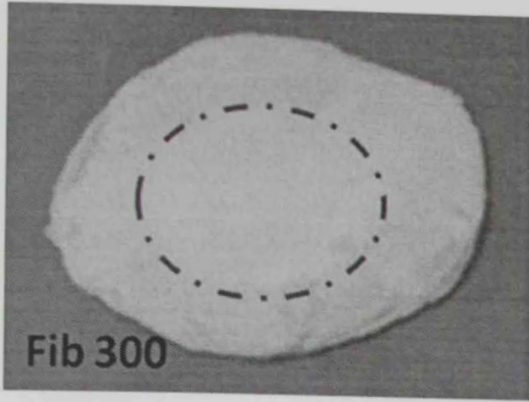
Figure 57. Photos of membranes after filtration of 300 ppm suspensions
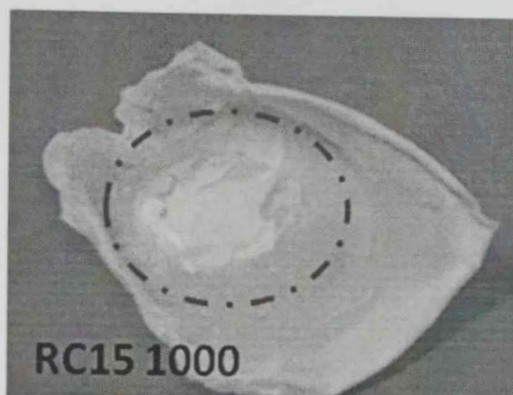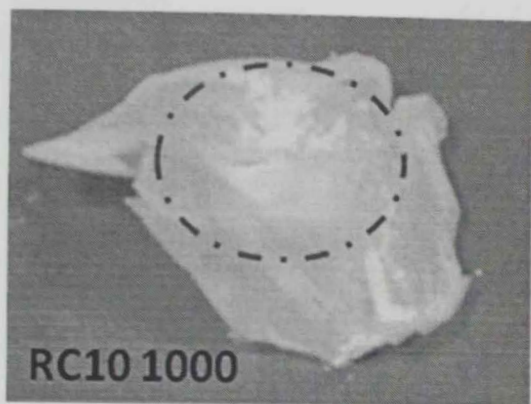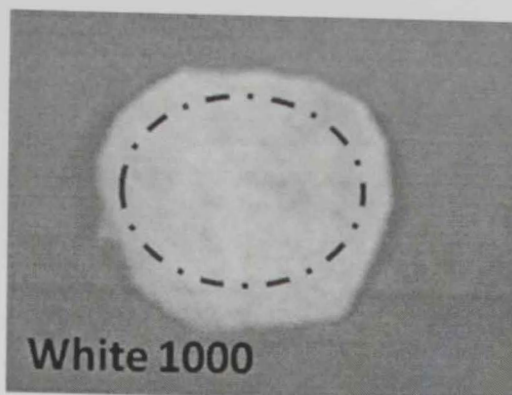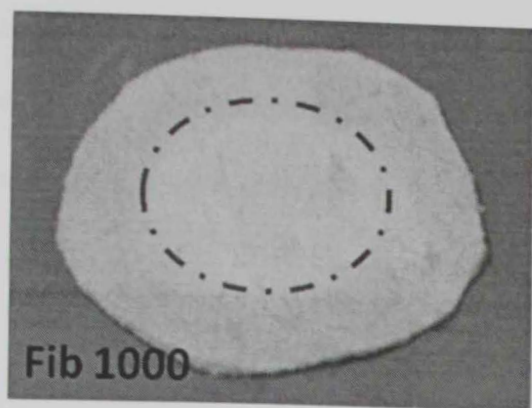
Figure 58. Photos of membranes after filtration of 1000 ppm suspensions

photos of all membranes after using them in the removal of CaP particulates from aqueous suspensions containing 300 and 1000 ppm, respectively. All membranes showed variable capabilities of removing CaP from suspensions. The polypropylene membrane showed the least amount of solid CaP separated from solution, compared with other membranes. This may be attributed to its relatively higher porosity compared to other membranes. Figures 59, 60 show SEM micrographs of these membranes, confirming the visual observations of precipitations formed on the tested membranes. These micrographs show the superiority of the interlocking of finer (nano-) fibers of both CA and RC membranes over the commercial filters in terms of dimensioning the porosities between these fibers, hence enhancing its ability to remove finer solid particles from their suspensions. On the other hand, the micro-fibrous cellulosic commercial membrane showed a close similarity to the CA and RC nanofibrous membranes. However, a closer investigation of the microstructure of this membrane reflects the compactness of its fibers as well as the presence of different morphologies of fibers and non-fibers, presumably pressed together into this membrane shape during the recycling of cellulose. An EDX analysis of the separated particulates was carried out for all membranes used with solutions containing 300 ppm of CaP particulates. Results are shown in Figure 61. All EDX spectra confirmed the identity of the separated particulates in all tested membranes. It should be mentioned that the Si peak detected in all samples is attributed to the vacuum lubricant that was used to avoid leakage during the filtration experiments.

The filtrates were analyzed for their total calcium content and compared to that of the starting solutions; 300 ppm. The total calcium content is attributed to the solid CaP particulates passed through the membranes in addition to the dissolved calcium ions in solutions. However, contribution of the dissolved calcium ions to the total calcium
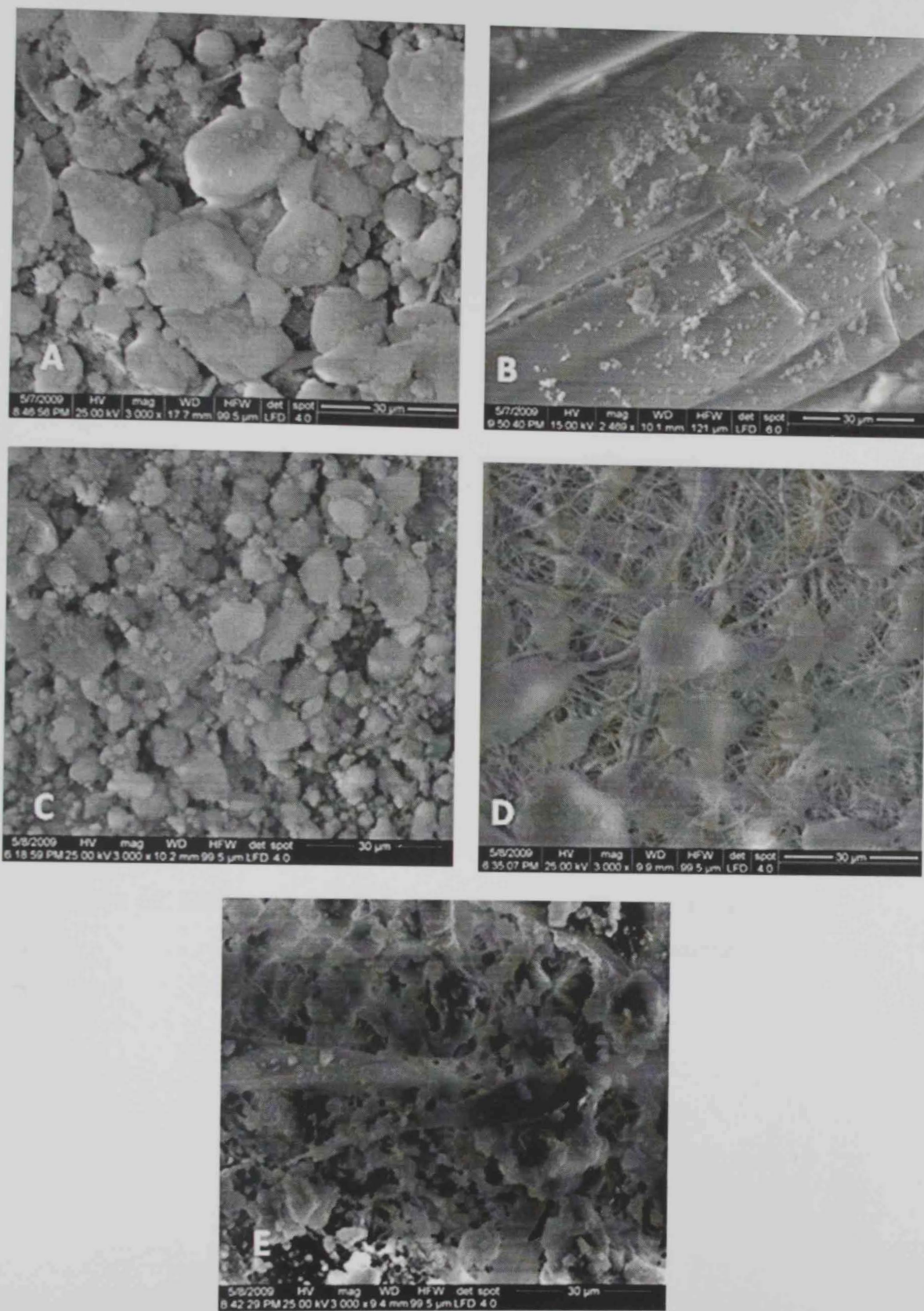
Figure 59. SEM micrographs of A) commercial 1, B) commercial 2, C) CA10, D) RC 10, and E) RC 15 membranes after filtration of 300 ppm suspensions
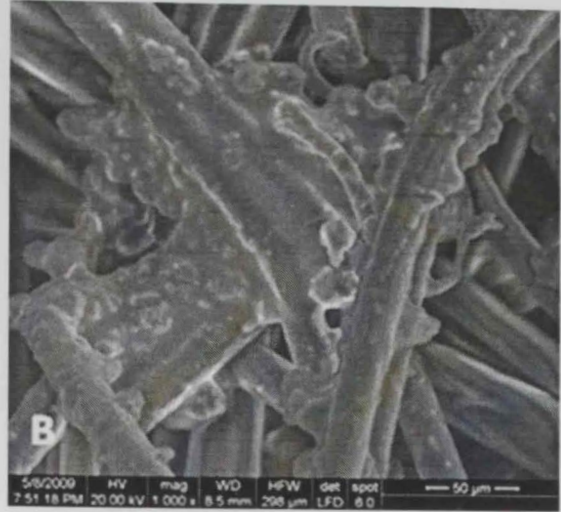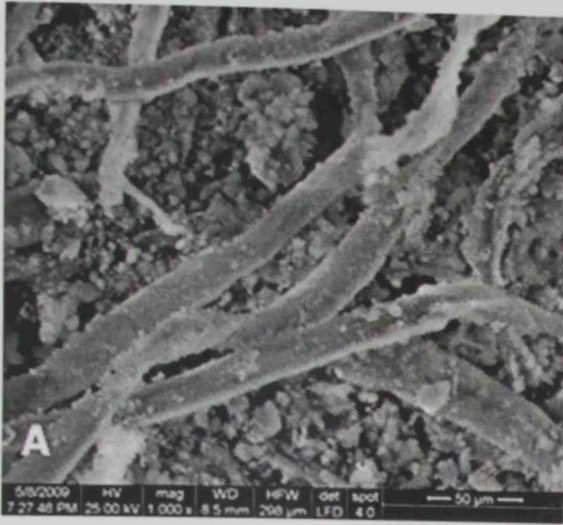
Figure 60. SEM micrographs of A) commercial 1, B) commercial 2, C) RC 10
membranes after filtration of 1000 ppm suspensions
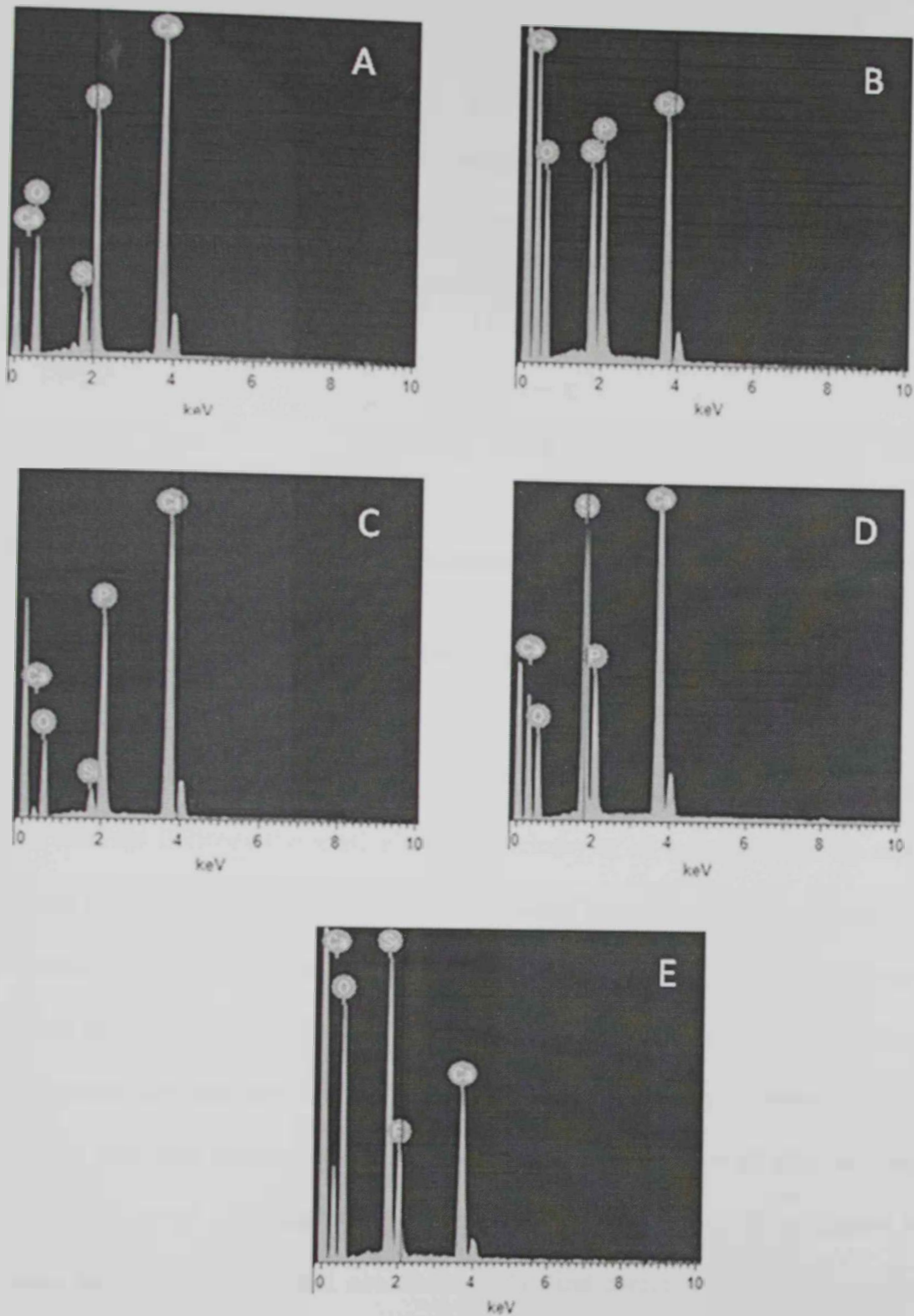
Figure 61. EDX analysis of the CaP particles trapped within the A) Commercial 1, B) commercial 2, C) CA10, D) RC10, and E) RC15 fibrous membranes after filtration of 300 ppm suspensions

concentration is expected to be minimum due to the limited solubility of the CaP in water ($K_{sp} = 6.8 \times 10^{-37}$). A clear de-ionized water sample was also analyzed as a reference.

Figure 62 shows a comparison between the different membranes in terms of the total calcium concentrations in their filtrates. The corresponding efficiencies of these membranes were calculated using the following formula:

$$Efficiency = \left(\frac{300 - x}{300} \right)$$

Where: 300 represents the total calcium content (in ppm) in the starting CaP solutions

x is the total calcium determined in each of the filtrate solutions

The efficiency results are shown in Figure 63. Combined with the results in Figure 62, these findings illustrate the relatively high efficiency of all membranes in the separation of solid particulates from aqueous media. This could be attributed to the fibrous nature of all tested membranes, and the subsequent presence of porosities with variable dimensions that are thus shown to separate different sizes of solid particulates from water. However, the variation between their efficiencies is mainly attributed to the differences in the pore size and pore size distributions in these membranes. The relatively high efficiency of filtration observed with the first commercial membrane may be attributed to the compactness of the fibers and non-fibers in the first commercial membrane, shown in Figure 56A. On the other hand, the higher porous nature of the second commercial membrane, shown in Figure 56B was reflected on its lower efficiency for filtering tiny particles from solutions. The high efficiency of the CA and RC membranes is attributed
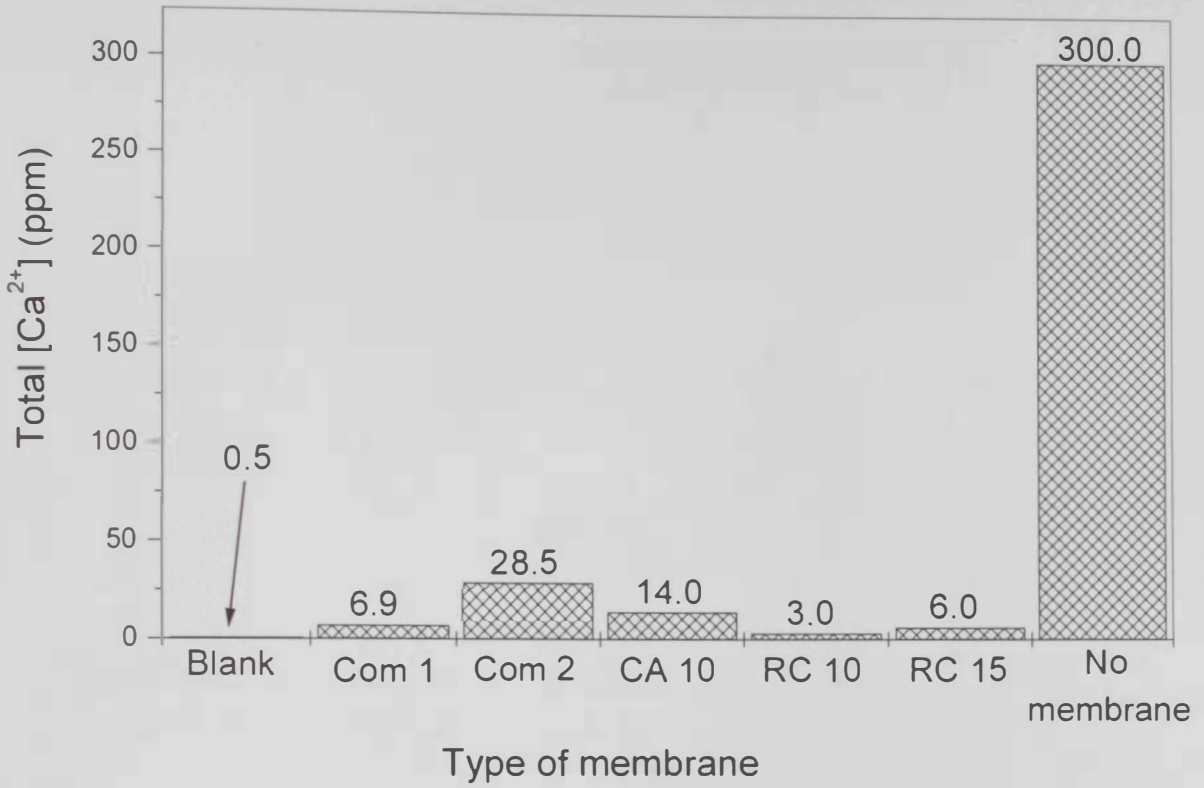
Figure 62. Total calcium in filtrates produced after using different membranes for the filtration of solutions containing 300 ppm of CaP. A blank de-ionized water sample and the concentration of the original solutions are shown for comparison
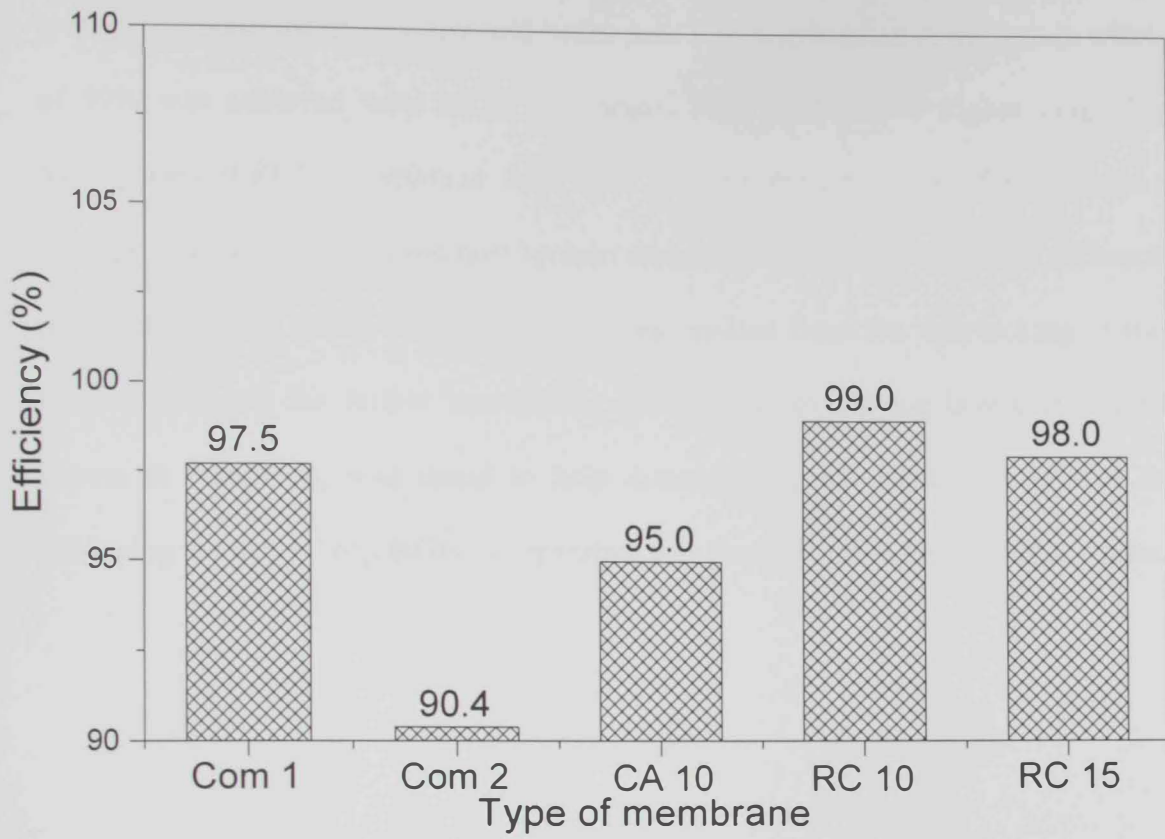
Figure 63. Efficiency of different membranes for the removal of particulates from 300 ppm solutions

to their relatively lower pore size and better pore size distribution. A maximum efficiency of 99% was achieved with RC10 membrane. Figure 64 shows higher magnification micrographs of RC10 membrane after been used in the separation of particulates from 300 ppm CaP solutions. These micrographs demonstrate the trapping of the different size particulates in the micro- and nano-size pores resulted from the interlocking of the RC fibers. Moreover, the further interlocking between the overlaying layers of nanofibers, shown in Figure 64, was found to help dimensioning the resulted pore size, hence enhancing the overall capability of separating tiny particles from their aqueous media.
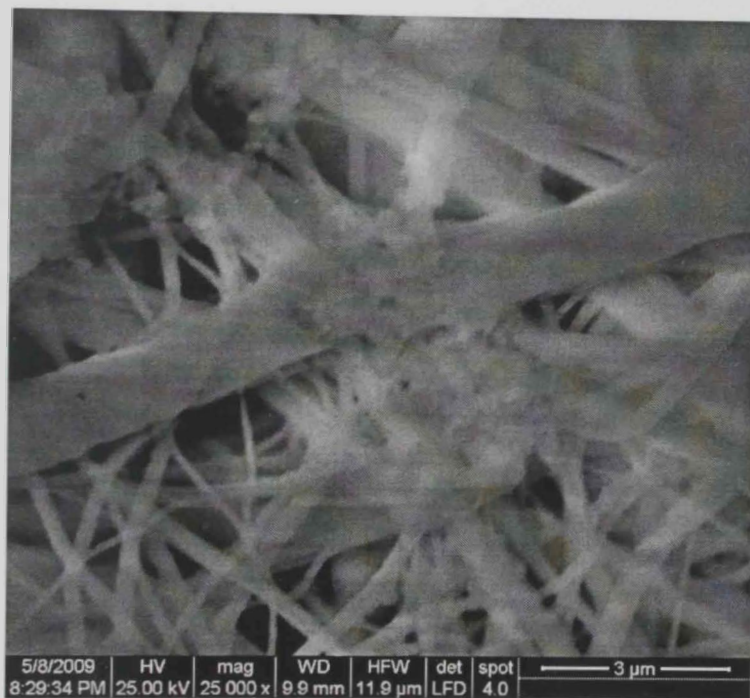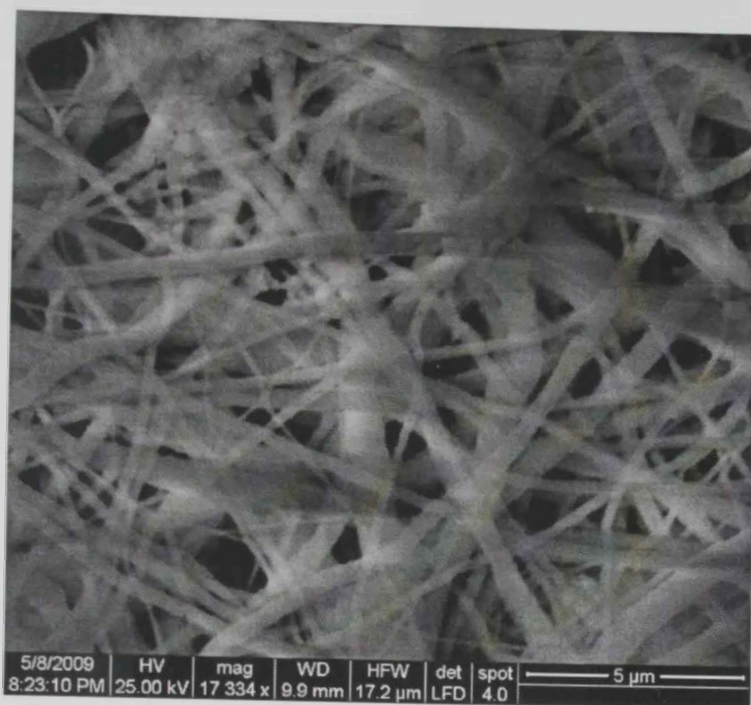
Figure 64. SEM micrographs as different magnifications of RC10 membranes after
The filtration of 300 ppm suspensions-

Chapter V
Conclusions

V. Conclusions

The current study was intended to investigate the use of an electrospinning technique to prepare nanofibrous membranes to be used for the separation of tiny solid particulates from water. Results showed the high sensitivity of the morphology of the nanofibrous membranes to slight variations in each of the electrospinning parameters. To avoid the formation of different non-fibrous morphology of the prepared membranes, the main objectives were to optimize the process parameters and follow the structure and properties of the formed fibers in order to achieve the most homogeneous fiber and pore size distribution. These two criteria were considered crucial for membranes that are intended to be used in water filtration. Variations in applied voltage (up to 20 kV), cellulose acetate concentration (up to 20 % by weight), flow rate (up to 100 mL/hr), and the distance between the nozzle and collector (for up to 20 cm) were studied in details.

Comparisons between the obtained membranes at each of these stages were carried out using two main characterization techniques: infrared spectroscopy and scanning electron microscopy. Variation in the physical properties of the optimal as-spun membranes were also followed for all membranes containing different concentrations of CA. Studies of the effect of thermal treatment on the optimal membranes structure and characteristics were also carried out. Optimization of the alkaline treatment stage to regenerate the cellulose without affecting the characteristics of the prepared membranes was also performed. Finally, the prepared membranes as well as two commercially available membranes were tested for their efficiency of separating solid calcium phosphate particulates from 300 pp solutions.

The current study investigated the formation of nanofibrous membranes, from a cellulose precursor; cellulose acetate, for water filtration. Membranes were prepared by an electrospinning technique that was based on the use of a high voltage power supply to force polymeric droplets to be sprayed in the form of fibers with different aspect ratios, depending on the process parameters. Different parameters affecting the structure, morphology and physical properties of the membranes were studied in details in order to optimize them. Characterization of the membranes was carried out at every stage of the electrospinning process by infrared spectroscopy (IR) and scanning electron microscopy (SEM). Physical properties of the membranes such as density, porosity, BET surface area, pore size distribution, viscosity and surface tension were determined. Thermal treatment effects on the structure and morphology of the membranes were studied. Regeneration of cellulose was attempted by treatment of the membranes in alkaline media. Optimization of the alkali treatment process was also reached. Preliminary evaluation of the nanofibrous membranes for removing solid particulates from simulated solutions was also carried out.

Results were compared to those obtained with two commercially available membranes. Results showed the possibility of obtaining nanofibrous membranes from solutions containing different concentrations of cellulose acetate, and showed a wide range of fiber and pore size distribution. It was found of an extreme importance to fully optimize the electrospinning conditions to achieve membranes with the highest homogeneity of both fiber and pore size distribution. Optimum conditions reached as a result of the current studies were: an operating voltage of 12 kV, a flow rate of 5 mL/hr, a distance between the nozzle and collector of 14 cm. The presence of acetone as a solvent to saturate the electrospinning chamber and the use of a shaker were also found crucial to

the morphology and homogeneity of the obtained fibrous membranes. Structure instability was observed with the thermal treatment of these membranes and was found to be dependent on the membrane thickness. Drying the electrospun membranes at a maximum temperature of $100^{o}C$ was found sufficient to remove the un-remaining solvents. Complete regeneration of cellulose was found to take place after 10 hours of immersion of the membranes in 0.5M NaOH solutions. Regeneration of cellulose was found to take place without affecting the morphology of the fibrous media. Efficiency of the nanofibrous membranes prepared in the current study showed superiority over the commercially available membranes, achieving 99% for the removal of CaP solid particulates from 300ppm simulated aqueous solutions.

Chapter VI

Recommendations

& Future work

Chapter VI: Recommendations & future work

Based on the findings of the current study the following recommendations were drawn:

1. It is was found convenient and productive to prepare nanofibers with the electrospinning technique, suggesting its future use for making nanofibers for a wide range of applications, as was also supported by the literature

2. The importance of a full optimization of all the process as well as polymer parameters, before final conclusions are to be taken for the development of nanofibrous membranes.

3. Additional types of polymers may be pre-blended with CA before spinning in order to provide extra elasticity to the membranes to avoid the effect of un-expected over-pressure of the water flow.

4. Following up the mechanical properties of the membranes are also recommended, especially after examining them for different cycles of water filtration.

5. Investigating the effect of varying the thickness of the membranes on their efficiency of purification of water from solid contaminants

Chapter VII

References

VII. References

1. Krantz D. and Kifferstein B. "Water pollution and society". http://www.umich.edu/~gs265/society/waterpollution.htm. (Last viewed April 30, 2009)

2. Pink, Daniel H. (April 19, 2006). "Investing in Tomorrow's Liquid Gold". Yahoo. http://finance.yahoo.com/columnist/article/trenddesk/3748. (Last viewed April 30, 2009)

3. West, Larry (March 26, 2006). "World Water Day: A Billion People Worldwide Lack Safe Drinking Water". http://environment.about.com/od/environmentalevents/a/waterdayqa.htm. (Last viewed April 30, 2009)

4. United States Environmental Protection Agency (EPA). Washington, DC. "The National Water Quality Inventory: Report to Congress for the 2002 Reporting Cycle – A Profile." October 2007. Fact Sheet No. EPA 841-F-07-003.

5. Alfred Z. Keller and Henry C. Wilson. Hazards to Drinking Water Supplies, London: Springer-Verlag; 1992.

6. Clean Water Act. "US code collection, 1362. Definitions". [Online]. Available: http://www.law.cornell.edu/uscode/33/1362.html. (Last viewed April 30, 2009)

7. Clean Water Act. "US code collection, 1342. National pollutant discharge elimination system ". http://www.law.cornell.edu/uscode/33/1342(p).html. (Last viewed April 30, 2009)

8. Frits van der Leeden, Fred L. Troise and David Keith Todd, The Water Encyclopedia, 2nd ed., Michigan: Lewis Publishers; 1990.

9. Nicholas P. Cheremisinoff. Handbook of Water and Wastewater Treatment Technologies, America: Butterworth- Heinemann Publications; 2002.

10. Mark J. Hammer and Mark J. Hammer Jr. Water and Wastewater Technology, 5th ed., New Jersey: Prentice-Hall; 2004.

11. Barhate RS, Ramakrishna S. J. *Membrane science.* (2007) 296: 1-8

12. Ma M., Kotaki S., Ramakrishna A. *Journal of Membrane Science* (2005) 265: 115–123

13. Ondarcuhu T, Joachim C. *Europhys. Lett.* (1998) 42: 215-220

14. Feng J. *Phys. Fluids.* (2002) 14: 3912-3926

15. Ma Z., Zhang R. J. *Biomed. Mater. Res.* (1999) 46: 60-72

16. Perez M. *US Patent 6*, 110, 588, 2000

17. Pike R. *US Patent 5*, 935, 883, 1999

18. Reneker D. *US Patent 6*, 382, 526, 2002

19. Tseng A. J. *Vac. Sci. Technol. B.* (2005) 23: 2480

20. Huie J. *Smart Mater. Struct.* (2003) 12: 264

21. Luong-Van E., Grondahl L., Chua K., Leong K., Nurcombe V., *Cool S. Biomaterials* (2006) 27: 2042

22. Ramakrishna S, Fujihara K, Teo W, Yong T, Ma Z, Ramaseshan R. *Materials Today* (2006) 9: 40-50

23. Yu Q., Shi M., Deng M., Wang M., Chen H. *Mater. Sci. Eng. B* (2008) 150: 70-76

24. Li D., Xia Y.. *Adv. Mater.* (2004) 16: 1151-70

25. Pan H., Li L., Hu L., Cui X. *Polymer* (2006) 47: 4901-4904

26. Deitzel J., Kosik W., McKnight S., Tan N., DeSimone J., Crette S. *Polymer* (2002) 43: 1025-1029

27. Deitzel J., Kleinmeyer J., Harris D., Beck T. *Polymer* (2001) 42: 261-72

28. Rutledge G., Fridrikh S. *Advanced Drug Delivery Reviews* (2007) 59: 1384-91

29. Zeleny J. *Phys. Rev.* (1914) 3, 69

30. Formhals A. (1934). *US Patent.* 1,975,504.

31. Taylor G. *Proc. R. Soc.* (1964) A 280, 383

32. Eda G, Liu J, Shivkumar S. *Materials Letters* (2007) 61: 1451-1455

33. Kenawy E, Layman J, Watkins J, Bowlin G, Matthews J, Simpson D, Wnek G. *Biomaterials* (2003) 907-913

34. Dehai L., Benjamin S. H., Benjamin C. *Advanced Drug Delivery Reviews.* (2007) 59: 1392-1412.(becomes 34)

35. Brian P. Sautter. (2005). Continuous Polymer Nanofibers Using Electrospinning. Report for the NSF-REU summer program. (2005)

36. Ramakrishna S., Fujihara K., Teo W., Lim T., Ma Z. An Introduction to Electrospinning and Nanofibers, Singapore: World Scientific Publishing Co.; 2005.

37. Frenot A., Ioannis S. Chronakis. *Current Opinion in Colloid and Interface Science*. (2003) 8: 64-75.

38. Yang E., Qin X., Wang S. *Materials Letters* (2008) 62: 3555-3557.

39. Subbiah T., Bhat G., Tock R., Parameswaran S., Ramkumar S. J. *Applied Polymer Science*. (2005) 96: 557-569

40. Matthew E. H., Kristie N. G., Joseph M. D., Norman J. W. *Polymer* (2008) 49: 2924-2936.

41. Kenneth L., Chua K., Christopherson G. T., Lim S., Mao H. *Polymer* (2007) 48: 6384-6394.

42. Reneker D. H., Yarin A. L. *Polymer* (2008) 49: 2387-2425.

43. Wu L., Yuan X., Sheng J. *Journal of Membrane Science* (2005) 250: 167-173.

44. Han T, Yarin A, Reneker D. *Polymer* (2008) 49: 1651-1658

45. Reneker D. H., Chun I. *Nanotechnology* (1996) 7: 216–223.

46. Fong H., Reneker, D.H. *Polym. Sci. Pt. B-Polym. Phys.* (1999) 37: 3488-3493.

47. Reneker D. H., Yarin A. L., Fong H. and Koombhongse S. J. *Appl. Phys.* (2000) 87: 4531-4547.

48. Chen Z., Foster M.D., Zhou W., Fong H., Reneker D.H., Resendes R. and Manners I. *Macromol.* (2001) 34: 6156-6158.

49. Suthar A. and Chase G. *Chemical Engineer* (2001) 26-28.

50. Huang Z.M., Zhang Y.Z., Kotaki M. and Ramakrishna S. *Comp. Sci. Tech.* (2003) 63: 2223-2253

51. Lim T.C., Kotaki M., Yong T.K.J., Fujihara K. and Ramakrishna S. *Mater. Technol.* (2004) 19: 20-27.

52. Yang F., Murugan R., Wang S. and Ramakrishna, S. *Biomaterials* (2005) 26: 2603-2610.

53. Park J. Y., Lee I. H., Bea G. N. *Journal of Industrial and Engineering Chemisty* (2008) 14: 707-713.

54. Xu J., Zhang J., Gao W., Liang H., Wang H., Li J. *Materials Letters* (2009) 63: 658-660.

55. Baumgarten, P. K. J. *Colloid Interf. Sci.* (1971) 36: 75-79.

56. Larrondo L., Manley R.S.J. J *Polym Sci Polym Phys Ed.* (1981) 19: 909–920.

57. Dalton P. D., Klinkhammer K., Salber J., Klee D. and Moller M. *Biomacromolecules* (2006) 7: 686-690.

58. Hajra M.G., Mehta K., Chase G.G. *Sep. Purif. Technol.* (2003) 3: 79–88.

59. Gibson P.W., Schreuder-Gibson H.L., Riven D. *AIChE* (1999) 45: 190–195.

60. Schreuder-Gibson H., Gibson P., Senecal K., Sennett M., Walker J., Yeomans W., Ziegler D., Tsai P.P. J. *Adv. Mater.* (2002) 3: 44–55.

61. Gibson P., Schreuder-Gibson H., Rivin D. *Colloids Surf. A: Physicochem. Eng. Aspects* (2001) 187–188: 469–481.

62. Wang X., Drew C., Lee S.H., Senecal K.J., Kumar J., Samuelson L.A. *Nano Lett.* (2002) 2: 1273–1275.

63. Wang X., Kim Y.G., Drew C., Ku B.C., Kumar J., Samuelson L.A. *Nano Lett.* (2004) 4: 331–334.

64. Kim J.S., Reneker D.H. *Polym. Compos.* (1999) 20: 124–131.

65. Bergshoef M.M., Vancso G.J. *Adv. Mater.* (1999) 11: 1362–1365.

66. Fong H., *Polymer* (2004) 45: 2427–2432.

67. Drew C., Wang X., Senecal K., Schreuder-Gibson H., He J., Kumar J., Samuelson L.A., Macromol J. *Sci. Pure Appl. Chem.* (2005) 39: 1085–1094.

68. Verreck G., Chun I., Rosenblatt J., Peeters J., Dijck A.V., Mensch J., Noppe M., Brewster M.E. *Controll J. Release* (2003) 92: 349–360.

69. Khil M.S., Cha D.I., Kim H.Y., Kim I.S., Bhattarai N. Biomed J. *Mater. Res. B Appl. Biomater.* (2003) 67: 675–679.

70. Matthews J.A., Wnek G.E., Simpson D.G., Bowlin G.L. *Biomacromolecules* (2002) 3: 232–238.

71. Yoshimoto H., Shin Y.M., Terai H., Vacanti J.P. *Biomaterials* (2003) 24: 2077–2082.

72. Xu C.Y., Inai R., Kotaki M., Ramakrishna S. *Biomaterials* (2004) 25: 877–886.

73. Min B.M., Lee G., Kim S.H., Nam Y.S., Lee T.S., Park W.H. *Biomaterials* (2004) 2: 1289–1297.

74. Shin M., Ishii O., Sueda T., Vacanti J. *Biomaterials* (2004) 25: 3717–3723.

75. Ma Z., Kotaki M., Ramakrishna S. *Membr J. Sci.* (2005) 265: 115–123.

76. Groitzsch D., Fahrbach E. *US Patent* 4,618,524 (1986).

77. Grafe T., Graham K. *Nonwoven Technol. Rev. INJ Spring* (2003) 51–55.

78. Wang X., Chen X., Yoon K., Fang D., Hsiao B.S., Chu B. *Environ. Sci. Technol.* (2005) 39: 7684–7691.

79. Shin C., Chase G.G. *AIChE* (2004) 50: 343–350.

80. Gopal R., Kaur S., Ma Z., Chan C., Ramakrishna S., Matsuura T., *Membr J. Sci.* (2006) 281: 581–586. [30]

81. Zhou J, Zhou M, Chen Z, Zhang Z, Chen C, Li R, Gao X, Xie E. *Surface & Coatings Technology* (2009) Available online

82. Kim I., Rothschild A., Lee B., Kim D., Jo S., Tuller H. *Nanoletters.* (2006) 6: 2009-2013

83. Taepaiboon P., Rungsardthong U., Supaphol P. European J. *Pharamceutics and Bio pharamceutics.* (2007) 67, 387-397

84. Kim K., Luuc Y.K., Chang C, Fang D., Hsiao B.S., Chua B. and Hadjiargyrou M. J. *Control. Release.* (2004) 98: 47-56.

85. Kenawy E.R., Bowlin G.L., Mansfield K., Layman J., Simpson D.G., Sanders E.H. and Wnek G.E. J. *Control. Release.* (2002) 81: 57-64.

86. Bhattarai S.R., Bhattarai N., Yi H.K., Hwang P.H., Cha D.I. and Kim H.Y. *Biomaterials.* (2004) 25: 2595-2602.

87. KM M. S., Bhattarai S. R., Kim H. Y., Kim S. Z. and Lee K. H. J. Biomed. Res. Part B: *Appl. Biomater.* (2005) 72: 117-124.

88. Smith D., Reneker D.H., Schreuder G.H., Mello C., Sennett M. and Gibson P. (2001), PCT/US00/27776.

89. Smith W.J. and Dunn M.A. *Arch. Dermatol.* (1991) 127: 1207-1213.

90. Gibson H.S. and Gibson P. U.S. Army Soldier Systems Center, AMSSB-RSS-MS(N) Natick, Massachusetts, 01760-5020 (2002).

91. Choi S.W., Jo S.M., Lee W.S., Kim Y.R. *Adv. Mater.* (2003) 15: 2027-2032.

92. Choi S. S., Lee Y. S., Joo C. W., Lee S. G., Park J. K. and Han K. S. *Electrochim Acta* (2004) 50: 338-342.

93. Choi S.W., Kim J.R, Jo S.M., Lee W.S. and Kim B.C. *Electrochim. Acta.* (2004) 50: 69-75.

94. Hong K.H., Oh K.W. and Kang T.J. J. *Appl. Poly. Sci.* (2005) 96: 983-991.

95. Suthat A., Chase G. *Chemical Engineer* (2001) 26-8.

96. Ma Z., Masaya K., Ramakrishna S. J. *Membrane Sci.* (2006) 282: 237-244

97. Roper D.K. and Lightfoot E.N. J *Chromatogra. A* (1995) 702: 3-26.

98. Klein E. J. *Membr. Sci.* (2000) 179: 1-27.

99. Gibson P., Schreuder-Gibson H. and Pentheny C. J. *Coated Fabric.* (1998) 28: 6372.

100. Steffens J., Coury J.R.. *Separation and Purification Technology.* (2007) 58: 99-105.

101. AMSOIL EaAR air filters for automobiles.
http://www.performanceoiltechnology.com/EaAR.htm (Last viewed April 30, 2009)

102. Gopal R., Kaur S., Feng C. Y., Chan C., Ramakrishna S., Tabe S., Matsuura T. *Journal of Membrane Science.* (2007) 289: 210-219.

103. Kaur S., Kotaki M., Ma Z., Gopal R., Ng S.C., Ramakrishna S. 1st Nano-Engineering and Nano-Science Congress, July7-9, 2004 Singapore.

104. Saeed K., Haider S., Oh T., Park S. *Journal of Membrane Science.* (2008) 322: 400-405.

105. Kaur S., Ma Z., Chan C., Ramakrishna S., Matsuura T. *Journal of Membrane Science.* (2006) 281: 581-586.

106. Han S., Youk J., Min K., Kang Y., Park W. *Mater. Lett.* (2008) 62: 759–762

107. Liu H., Hsieh Y. J. *Polymer Scie: Polymer Physics.* (2002) 40: 2119-2129

108. Kim C., Kim D., Kang S., Marquez M., Joo Y. *Polymer* (2006) 47: 5097-5107

109. Xu S., Zhang J., He A., Li J., Zhang H., Han C. *Polymer* (2008) 49: 2911-17

110. Lu P., Hsieh Y. J. *Membrane Sci.* (2009) 330: 288-296

111. Zhang L., Menkhaus T., Fong H. J. *Membrane Sci.* (2008) 176-84

112. Ritcharoen W., Supsphol P., Pavsdsnt P. *European Polymer J.* (2008) 44: 3963-68

113. Son W., Youk J., Lee T., Park W. J. *Polymer Sci: Polymer Phys.* (2004) 42: 5-11

114. Yoon Y., Moon H., Lyoo W., Lee T., Park W. *Carbohydrate Polymers.* (2009) 75: 246-250

115. Tang C., Liu H. *Composites: Part A* (2008) 39: 1638-1643

116. Ma Z., Ramakrishna S. J. *Membrane Sci* (2008) 319: 23-28

117. Shukla S., Brinley E., Cho H., Seal S. *Polymer* (2005) 46: 12130-12145

118. Zhang H., Nie H., Li S., White C., Zhu L. *Materials Lett.* (2009) 63: 1199-1202

119. Zhang L., Hsieh Y. *Carbohydrate Polymers* (2008) 71: 196-207

120. Chen C., Wang L., Huang Y. *Polymer* (2007) 48: 5202-5207

121. McCabe W, Smith J, Harriott P. Unit Operations of Chemical Engineering. 5th edition, 1993, McGraw Hill Inc.

122. Skoog D., Holler F. J. and Nieman T. A. Principles of Instrumental Analysis, 5th ed, USA: Thomson Learning; 1998

123. Meier M, Kanis L, Soldi V. Int. J. *Pharm.* (2004) 278: 99-110

124. Hellmann C, Belardi J, Dersch R, Greiner A, Wendorff J, Bahnmueller S. *Polymer* (2009) 50: 1197-1205

125. Tripatanasuwan S, Zhong Z, Reneker D. *Polymer 48* (2007) 5742-5746

126. Baker B, Gee A, Metter R, Nathan A, Marklein R, Burdick J, Mauck R. *Biomater. 29* (2008) 2348-2358

127. Gupta P, Wilkes G. *Polymer 44* (2003) 6353-6359

128. Huang Z, Zhang Y, Kotaki M, Ramakrishna S. *Composite Sci Tech* 63 (2003) 2223-2253

129. Megelski S, Stephens J, Chase D, Rabolt J. *Macromolecules* (2002) 35: 8456

130. Rouquerol F, Sing K. Adsorption by powders and porous solids: principles, methodology and applications. Academic Press, UK (1999)

مسام مختلفة. أدى اختيار أنسب العوامل لعملية (الالكتروسبننج) إلى الحصول على أغشية ذات مسامية عالية (تصل الى 94%) وخيوط متجانسة وتوزيع مسامات متجانس. تم ملاحظة عدم ثبات التركيب في العملية الحرارية لهذه الأغشية وقد وجد أن ذلك يعتمد على سمك الغشاء. تم الحصول على تحول كامل الى سيليلوز بعد 10 ساعات عن طريق معالجة أغشية أسيتات السيليلوز في 0.5 عياري من محلول هيدروكسيد الصوديوم. لم تؤثر هذه العملية في شكل اللدائن النانونية ولا حتى في قياسات المسام او في توزيعها. أظهرت نتائج الكفاءة لأغشية اللدائن النانونية المحضرة أفضليتها بالنسبة لأغشية الفلاتر التجارية.

Arabic Abstract

هذه الدراسة تهدف إلى دراسة أثر العامل البشري على المهارات التقنية عبر دراسة... في قطاع النفط. ويمثل قطاع النفط في مملكة... حوالي 1000 من...

ويمثل التأثير في قطاع النفط حوالي 1-10 من الإنتاجية... من التقنيات المستخدمة في قطاع النفط... إن التقنيات الحديثة في قطاع النفط... من قطاع إنتاج النفط... إذا ما تم النظر إلى كفاءة قطاع النفط من...

من التقنيات المستخدمة... على أن... من التقنيات... من التقنيات الحديثة والتقنية حوالي 0.3 من الإنتاجية... التقنيات الحديثة والتقنية، إن... إلى أن التقنية في قطاع النفط... التقنية الحديثة.

تتراوح من 1-35 مليون برميل/يوم... النفط على عدد من العوامل وكفاءة التقنية على...

إن... التقنيات التقنية من... إن التقنية... (الاستراتيجية)... إن التقنية... إلى أن التقنية... من قبل... من التقنيات... على...

من... التقنيات من (الاستراتيجية)... التقنية... إن... (الاستراتيجية)...

... التقنية الاستراتيجية إلى...

... التقنية الاستراتيجية...

...

جامعة الإمارات العربية المتحدة

كلية العلوم

برنامج ماجستير علوم البيئة

خيوط لدائن نانونية لتحسين تنقية المياه الجوفية

رسالة مقدمة من/

بثينة عبدالله محمد الشامسي

مقدمة إلى/

جامعة الإمارات العربية المتحدة

استكمالا لمتطلبات الحصول على درجة الماجستير في علوم البيئة

المشرفون

د. عيسى المطروشي	د. محمد ميتاني	د. ياسر جريش
أستاد مساعد	أستاد مساعد	أستاد مساعد
قسم الهندسة الكيميائية	قسم الكيمياء	قسم الكيمياء
كلية الهندسة	كلية العلوم	كلية العلوم
جامعة الامارات	جامعة الامارات	جامعة الامارات

2008-2009

جامعة الإمارات العربية المتحدة

كلية العلوم

برنامج ماجستير علوم البيئة

خيوط لدائن نانونية لتحسين تنقية المياه الجوفية

رسالة مقدمة من/

بثينة عبدالله محمد الشامسي

مقدمة إلى/

جامعة الإمارات العربية المتحدة

استكمالا لمتطلبات الحصول على درجة الماجستير في علوم البيئة

2009